USGS
science for a changing world

U.S. DEPARTMENT OF THE INTERIOR
U.S. GEOLOGICAL SURVEY

PRELIMINARY SCIENTIFIC RESULTS OF THE CREEDE CALDERA CONTINENTAL SCIENTIFIC DRILLING PROGRAM

P.M. Bethke, Editor

Open-File Report 94-260-E

2001

DEPOSITIONAL ENVIRONMENTS AND AUTHIGENIC MINERAL DISTRIBUTIONS IN THE OLIGOCENE CREEDE FORMATION, COLORADO, USA

By

Daniel Larsen[1]
Laura J. Crossey
University of New Mexico, Albuquerque, NM

[1]Present address:
Department of Geological Sciences,
University of Memphis, Memphis, TN 38152

ABSTRACT

The Oligocene Creede Formation represents an exceptionally well-preserved intracaldera sedimentary sequence within a large, resurgent caldera. The tuffaceous, epiclastic, and limestone deposits observed in surface exposures and Continental Scientific Drilling Program (CSDP) core provide a record of depositional and mineral-water interaction processes following caldera collapse. The sedimentology and authigenic mineral distributions also provide information regarding the role of the Creede Formation in the ancient Creede hydrothermal system.

The basal part of the Creede Formation is characterized by interbedded caldera wall-derived debris-flow breccias and ephemeral lake deposits. This unit is succeeded by deep-water lacustrine beds that constitute the bulk of the Creede Formation. Interbedded fallout tuffs from intracaldera volcanic eruptions significantly affected lacustrine sedimentation patterns and provide a means of basin-wide correlation. Carbonate minerals were deposited as travertine at spring-orifices and as suspension-fallout (micrite and micritic peloids) lamina across the bottom. The travertine accumulations circumscribe the margins of the moat basin and probably outline the structural margin of the caldera. Remains of invertebrate and fish fauna are not observed in the lake beds.

Deposition in a cool, montane climate is indicated by the presence of pseudomorphs after ikaite in the lacustrine deposits and corroborative paleofloral analyses. Distinctive lowstand and highstand facies-association distributions were deposited; the transition between which is recorded by fining-upward, alluvial-lacustrine sequences around the caldera margin and in paleovalleys. Changes in the proportion and character of lowstand versus highstand sequences imply an evolution from a narrow, deep, steep-walled basin to a broad, shallow, incised basin through time. The character of the lacustrine lamina and travertine suggests that the lake evolved into a meromictic lake with bicarbonate-rich waters. Although the basin was topographically closed, no evidence for hypersaline conditions is observed.

Most of the detrital sediment within the Creede strata was derived from reworking of Fisher Quartz Latite fallout ash and erosion of the caldera walls. Hydrolysis and dissolution of the ash are interpreted to have led to formation of smectite, clinoptilolite, erionite, potassium feldspar, and quartz during burial diagenesis. The effects of two major low-temperature hydrothermal events are superimposed on diagenesis. The Antlers Park event resulted in replacement of the smectite and zeolite diagenetic assemblage by analcime and chlorite-smectite mixed-layered clay in the northwestern part of the moat. The Creede hydrothermal event is interpreted to have produced various silica minerals, illite, and potassium feldspar observed above 400 m in the formation. In both events, the patterns of alteration indicate that faults and coarse-grained deltaic and lacustrine fan deposits served as pathways for fluid movement through the formation. The alteration associated with the Creede hydrothermal event appears to have resulted from reactions associated with conductive cooling of the hydrothermal fluid and mixing

with diagenetic fluids. The pattern of alteration suggests that the hydrothermal plume flowed laterally into the Creede Formation from the fault-controlled Creede mineral district to the north of the caldera.
Diagenetic reactions in the tuffaceous strata probably resulted in moderately saline, alkaline fluids, especially in the upper part of the formation. Initiation of faulting and hydrothermal fluid flow in the Creede hydrothermal system could have allowed diagenetic pore waters from the Creede Formation to recharge the hydrothermal flow cell. The chemical evolution of the Na-bicarbonate diagenetic fluids in the hydrothermal system has not been investigated, but is required to address the problem further.

INTRODUCTION

The Creede caldera (Fig. 1) is the best-preserved caldera within the late Tertiary San Juan volcanic field in southwestern Colorado and is a type-example of a large, resurgent caldera (Steven and Ratté, 1965; Lipman, 1984). Following caldera formation, the moat basin was filled with up to 1,000 m of intracaldera sedimentary deposits of the Creede Formation, and lava flows and domes of the Fisher Quartz Latite. Previous investigations of the Creede Formation interpreted deposition and diagenesis to have occurred in a saline, alkaline-lake environment (Steven and Ratté, 1965; Bodine and others, 1987). This interpretation was based on limited sedimentological and authigenic mineral studies of the Creede Formation. Extensive surface exposures and recently-obtained Continental Scientific Drilling Project (CSDP) cores have provided an excellent opportunity to re-evaluate the saline, alkaline-lake model.

The results are important both for understanding caldera lake processes and testing the genetic model for the Creede Ag-Pb-Zn deposits proposed by Bethke and Rye (1979) and Bethke (1987). Most available information on sedimentary processes in caldera lake environments is based on studies of recent volcanoes (Nelson, 1967; Poppe and others, 1985; Newhall and others, 1987; Giresse and others, 1991; and Nelson and others, 1994). These studies provide geologic snapshots of active processes, but provide less clear information regarding processes active through the evolution of caldera basins. The Creede Formation is also hypothesized to have been the source of saline, alkaline fluids that participated in the formation of base-metal deposits north of the Creede caldera (Bethke, 1987). A thorough understanding of the depositional and diagenetic history of the Creede Formation is necessary to test this model.

The purpose of this contribution is to (1) document the types and distributions of sedimentary facies and, by inference, depositional environments in the Creede caldera moat, (2) document the types and distributions of authigenic minerals in the strata and discuss mechanisms of formation, and (3) assess the possible role of the Creede Formation in the Creede hydrothermal system. The results show how intracaldera environments may evolve through time. They also provide an

example of the complex interplay between volcanism, tectonism, sedimentation, and hydrology that exists in volcanic settings.

METHODS OF STUDY

The distribution of sedimentary facies and structural features was mapped at a scale of 1:25,000, and 23 detailed stratigraphic sections were measured (Larsen, 1994a). Parts of CSDP cores CCM-1 and CCM-2 (Fig. 1) were described in detail. The complete stratigraphy of the cores is described in detail elsewhere (see Hulen, 1991). The sections and cores were sampled every 3 to 5 m for petrographic, X-diffraction, and geochemical analyses.

Soluble carbonate content was determined gravimetrically on 150 samples by dissolution in 1 N Na-acetate solution (buffered at pH = 5). Mole % magnesium was determined in 16 bulk carbonate samples by X-ray diffraction using the method of Goldsmith and others (1961). TOC (total organic carbon), HI (hydrogen index), and OI (oxygen index) were determined by Joel Leventhal and Ted Daws at the U. S. Geological Survey (Denver) using a Leco carbon apparatus and Rock-Eval anhydrous pyrolysis.

The authigenic mineralogy was investigated through a combination of X-ray diffraction, petrographic, scanning electron microscope, and electron microprobe analysis. The authigenic mineral composition of 270 samples was determined by X-ray diffraction analysis of semi-random glass-slide mounts of the < 20 μm (fine silt) and oriented glass-slide mounts of the < 2 μm (clay) fractions (see Larsen, 1994a). The carbonate-free, fine-silt fraction was used because volcanic rock fragments, pyrogenic crystals, and soluble carbonate dilute the proportion of authigenic mineral phases and produce peak interferences with authigenic silicates. The mounts were subjected to Cu Kα (30 to 35 mA, 45 keV) radiation using a Scintagg PAD V X-ray diffractometer. Spectra were obtained continuously through a range of 2 to 50° 2θ for the fine-silt fraction and 2 to 35° 2θ for the clay fraction. Selected clay-fraction samples were analyzed using the thermal treatment of Boles (1972) in order to assess the composition and structure of clinoptilolite.

Peak intensity data from the fine-silt fraction were used to calculate weight proportions of the constituent mineral phases by the Chung method (Chung, 1974a and 1974b). Mineral standards were prepared with corundum, and were mounted and analyzed using the same procedure as for the fine-silt fraction (see Larsen 1994a). The mineral-standard peak intensities were used to calculate reference intensity ratios (RIR) for each mineral as required by the Chung method. The precision of the analysis was determined by multiple analyses of five samples to be between ± 10 to 20 % (1 standard deviation). The accuracy of the analyses was determined using synthetic mixtures of mineral standards to be within 10 to 20 % of measured values (Larsen, 1994a).

The authigenic mineral paragenesis was determined using a combination of polarized-light and scanning electron microscopy. Approximately 150 thin sections were described; of which, 60 were point-counted using a Swift automated point

counting system. Twenty-nine samples were examined with an Hitachi S-450 scanning electron microscope equipped with a Tracor Northern energy dispersive X-ray analysis system.

The chemical composition of primary pyroclastic materials and authigenic silicates was determined by electron microprobe analysis. Six samples were analyzed using a JEOL Superprobe 733 using the following conditions: accelerating voltage, 15 keV; beam current, 10 and 20 nA; beam size, 5 to 10 μm. Following calibration to anhydrous silicate standards, analyses of appropriate mineral standards were conducted in order to insure consistent analysis quality. The quality of microprobe analyses was judged using criteria from the following sources: analcime, feldspar, biotite, and hornblende, Papike (1988); smectite, Newman and Brown (1987); and clinoptilolite, Boles and Wise (1978) and Broxton and others (1987).

GEOLOGIC BACKGROUND

The Creede caldera lies at the intersection of three older calderas (La Garita, Bachelor, and South River) in the central caldera cluster of the San Juan Mountains (Lipman and others, 1989). It formed by eruption-related collapse of a roughly circular, 12 km-diameter region and was concurrently partially filled with the dacitic Snowshoe Mountain Tuff (Steven and Ratté, 1965). The caldera was inset into a low-relief volcanic plateau capped by rhyolitic to dacitic ash-flow tuffs from previous caldera-related eruptions and intermediate-composition lava flows and domes (Steven, 1968). Following collapse, the central part of the Creede caldera was uplifted to form a resurgent dome (Steven and Ratté, 1965). The structural moat thus created was subsequently filled with intracaldera lava flows and domes of the Fisher Quartz Latite and intercalated tuffaceous, epiclastic, and limestone deposits of the Creede Formation (Fig. 1). The duration of Creede Formation sedimentation was less than 660,000 yrs based on $^{40}Ar/^{39}Ar$ dating of enclosing volcanic units (Lanphere, 1994). Faulting followed Creede Formation deposition and created two major graben systems, the Rio Grande and Clear Creek grabens (Steven and Lipman, 1976). Faulting is also interpreted to have initiated development of the ancient Creede hydrothermal system, ultimately resulting in the epithermal Ag-Pb-Zn deposits for which the region is well-known (Steven and Eaton, 1975; Bethke, 1987).

Paleofloral studies of the well-preserved leaf fossils within the lacustrine beds have reached differing interpretations regarding the paleoclimate. Using a floristic approach, Axelrod (1987) interpreted the paleoclimate within the moat basin to have been warm and semi-arid. Wolfe and Schorn (1989), applying a physiognomic analysis of Axelrod's data, interpreted the paleoclimate to have been similar to the cool, montane climate within the region today. Further, Wolfe and Schorn suggested that the floral data represent conditions experienced at the caldera rim rather than those within the basin. Sedimentological data presented in this contribution and evidence for the former presence of ikaite (Larsen, 1994b), a cold-water carbonate mineral, are most consistent with the paleoclimatic interpretations of Wolfe and Schorn (1989).

STRATIGRAPHY AND STRUCTURE OF THE CREEDE FORMATION

Although exposures of the Creede Formation are found throughout the caldera moat, no more than 100 m of section is exposed at any location. Furthermore, extensive faulting (Fig. 1) commonly prohibits correlation across major drainages. Cores CCM-1 and CCM-2 provide the most complete sections of Creede Formation. Correlation between the cores (Fig. 2) was accomplished using a combination of lithostratigraphy, tephrostratigraphy, and borehole geophysical data (Nelson and Kibler, Chapter P, the Open-File Report). Core-to-surface correlation was completed using lithological and mineralogical characteristics of the fallout tuffs (labeled A through M2 in Fig. 2) and lithologic characteristics of the depositional and early diagenetic carbonates (Larsen, 1994a). The base of the Creede Formation in core CCM-2 is chosen as a datum because of the great thickness represented by this core. Assuming that no fault exists between the CCM-2 site and measured sections 0.5 km to the north, approximately 700 m of Creede Formation are present in the north-central part of the moat.

The Rio Grande graben structure is particularly well-developed where it coincides with the apical graben of the Bachelor caldera (Steven and Ratté, 1965). Significant displacements (up to 200 m) are also present in the Creede Formation to the south, as indicated by surface mapping and the correlation in Figure 2. Travertine accumulations are observed around the margins of the moat basin, but also commonly follow the trace of faults. The moat-margin travertine distribution does not correspond to a lithologic discontinuity or a specific elevation, but rather probably reflects the position of the caldera ring-fracture system (Heiken and Krier, 1987) and pre-existing structures (Larsen, 1994a). Evidence for syndepositional movement (buried scarps, travertine talus, etc.) is not observed. Thus, many of the present-day faults with associated travertine accumulations may have existed as fractures or faults of minimal displacement during Creede Formation deposition.

FACIES AND FACIES ASSOCIATIONS

Stratified Sedimentary Facies

The stratified sedimentary facies include lamina and beds composed of pyroclastic and epiclastic detritus, depositional carbonate, intraclasts, and minor organic material (Table 1). Low-magnesium calcite is the only carbonate mineral identified by X-ray diffraction of bulk samples (Table 2). Carbonized organic material is commonly preserved along partings, especially in laminated facies. Impressions of conifer needles, shrub leaves, and deciduous tree leaves are common; insect impressions are rare. Remains of shelly or vertebrate fauna are nearly absent in the beds; gastropod shells have been reported (E. Evanoff, personal communication, 1993) and diatoms are present in some travertine deposits (P. M. Bethke, personal communication, 1994).

The bulk of the formation is composed of interbedded suspension laminae and sediment-gravity-flow deposits (Fig. 3)(Table 1). The alternating carbonate and detrital lamina are similar to seasonal lamina observed by Ludlam (1969) and Kelts and Hsü (1978). The discrete nature and relative purity of the carbonate lamina is consistent with such an origin; however, compositionally-distinct laminations may also form at other periodicities (e.g., Halfman and Johnson, 1988). The carbonate lamina are interpreted to have formed through organic processes based on the presence of the elongate peloids, significant organic carbon content, and hydrogen-rich, lacustrine-aquatic kerogen composition (Table 2). The characteristics of the peloids are most consistent with lacustrine shrimp fecal pellets (e.g., Eardley, 1938).

The calcareous pseudomorphs show grain morphologies (Fig. 4A), replacement textures (Fig. 4B), and chemical characteristics diagnostic of pseudomorphs after ikaite (Larsen, 1994b; Shearman and Smith, 1985). Ikaite, $CaCO_3 \cdot 6H_2O$, is metastable with respect to calcite at near-surface conditions (Marland, 1975), but is observed in numerous modern cold-water marine and lacustrine settings. Formation of ikaite requires: a solution supersaturated with respect to calcite, water temperatures of 0-3°C, and presence of a chemical component in solution to inhibit growth of anhydrous carbonates (Shearman and others, 1989; Bischoff and others, 1993a).

The graded tuffaceous sandstones have characteristics of lacustrine turbidites (Fig. 3B)(Table 1). The absence of internal structure may reflect synchronous deposition from two flows separated along a density boundary within a lake: a high-density underflow and a low-density interflow (e.g., Sturm and Matter, 1978). Many of the coarser-grained, graded, massive sandstones and conglomerates interbedded with the laminated strata, however, share characteristics with deposits of both debris-flow and turbidity current depositional processes (Table 1). For example, the distribution of intraclasts within matrix-supported beds (Fig. 5A) is highly variable; this observation may reflect bouyant rise of the clasts within flows (Nelson and Nilsen, 1984; Ballance and Gregory, 1991) or a flow transformation (Fisher, 1983; Smith and Lowe, 1991). Distribution-normal grading and crude bedding observed in the upper parts of these coarse-grained beds are consistent with laminar-to-turbulent flow transformations (Fisher, 1983; Lowe, 1982). Similar relationships between subaqueous debris-flows and turbidites have been documented in modern settings (Weirich, 1989). Thus, subaqueous sediment-gravity-flow strata in the Creede Formation reflect a continuum of process, rather than simple end-members.

Wave-rippled and horizontal laminated sandstones (Table 1) are found in core near the base of the Creede Formation and sporadically in surface exposures around the margin of the moat basin. Using the approach of Komar (1974) with maximum orbital velocity data from Allen (1984), the wave-rippled beds could have formed at maximum water depths ranging from 1.0 to 9.0 m (Larsen, 1994a). A similar approach can be applied to estimate the maximum water depth permitted for formation of the pinch-and-swell cross-laminated sandstone (Table 1). Using some reasonable values for storm characteristics in the Creede moat basin (8 to 16 km fetch, 48 to 64 km/hr winds, 1 to 2 hr storm duration), waves with periods between 3.5 to 5.0 seconds could produce orbital velocities of 12 cm/s (data from Komar,

1976). Considering these conditions, the threshold for movement of 0.1 millimeter-size quartz grains would occur between 11 and 25 m water depth. Given the uncertainties in some terms, these values provide a rough estimate of maximum water depths in which these structures could have formed.

Large-scale cross-bedded calcareous sandstones and conglomerates (Fig. 5B)(Table 1) are interpreted to represent wave-formed-terrace foresets based on the (1) winnowing of all fine-grained detritus, (2) abundance of grains with calcareous coatings, commonly in the form of ooids, and (3) moderate or bimodal sorting of the grains. Similar facies have been documented by Swirydczuk and others (1980) and are observed in wave-formed terraces at numerous lakes in the western Great Basin, U.S.A. Although this facies is rare in the Creede Formation, intraclasts and individual grains with the characteristics described above are common in subaqueous, sediment-gravity-flow deposits. Thus, despite the paucity of wave-formed-terrace facies, these observations suggest that the foreshore was an active zone of sediment modification that supplied offshore depositional environments.

Facies reflecting deposition by uni-directional currents are primarily found adjacent to the margin of the moat basin. The overall character of the pebbly, horizontal-bedded and low-angle cross-bedded facies (Table 1) and rare channel structures suggests deposition by sheetfloods and shallow, braided streams (Fig. 5C). Many of the interbedded sediment-gravity-flow beds are sheet-like, implying broad active depositional surfaces. Evidence for subaerial exposure is commonly lacking; thus, the distinction between purely alluvial versus shallow, lacustrine deposits is not always obvious.

Primary Pyroclastic Facies

Light-colored, fine-grained, massive and laminated beds (Fig. 5D) within the lacustrine strata are interpreted as pyroclastic fallout based on the pure vitric-ash composition, fine grain-size, and moderate sorting characteristics (Fisher and Schmincke, 1984). Rapid fallout of the ash is indicated by extensive convolution and disruption of the silty upper parts of beds. Poorly sorted, pumice-rich, lapilli-tuff beds are interpreted as deposits of pumiceous pyroclastic flows or debris-flows derived therefrom. Beds of this variety are rare in the Creede Formation. Features observed in units in the southeastern part of the moat provide evidence for hot emplacement: (1) radially-fractured Fisher Quartz Latite lava clasts indicating deposition prior to cooling (e.g., Smith and Lowe, 1991) and (2) partial welding within the middle of a 13+ m thick unit.

Fisher Quartz Latite volcanoes are believed to have been the sources of the tuffs based on: (1) mineralogical similarity of the tuffs to the Fisher Quartz Latite lavas (Larsen, 1994a), (2) the proximity of the tuffs to lava domes, and (3) contemporary emplacement of the Fisher Quartz Latite and Creede Formation. It is not clear that all of the tuffs originated within the caldera; Fisher Quartz Latite lavas are also present north of the Creede caldera (Steven and Ratté, 1965). Furthermore, a number of the tuffs in the upper part of the lacustrine sequence (tuffs I through K, Fig. 2) contain significantly less hornblende and more pyroxene than the others

(Larsen, 1994a), consistent with the mineralogy of lavas found north of the caldera (Ratté and Steven, 1967).

Travertine Facies

The travertine mounds (Fig. 5E) are predominantly composed of massive, laminated, and stromatolitic travertine facies, although travertine-cemented clastic facies are also present (Table 1). Freshly broken travertine surfaces usually emit a strong petroliferous odor, presumably due to the escape of organic gases. Detailed analysis of the travertine is hampered by degradation of depositional fabric due to weathering and post-depositional alteration (recrystallization to sparry calcite and replacement by quartz, chalcedony, and opal). X-ray diffraction of bulk samples indicates that travertine facies are composed chiefly of low-magnesium calcite (Table 2) with minor silica phases.

Micritic, clumped-micritic, and radial-fibrous varieties of calcite (Fig. 5F) all contain abundant organic inclusions and filaments suggesting that microbial and/or algal processes were instrumental in the formation of travertine (Table 1). Stromatolitic travertine is interpreted to have formed in association with similar processes (Table 1). Although oncolitic structures are regarded to form exclusively in nearshore environments (Tucker and Wright, 1990), other stromatolitic forms are known to form at as much as 50 m water depth (Cohen and Thouin, 1987). Pseudomorphs after ikaite are also observed in travertine, either as (1) monoclinic prisms in disorganized nests or weakly radiating clusters and (2) pseudotetragonal prisms in radiating (Fig. 4A) and aligned arrangements (Larsen, 1994a). The pseudomorphs are intergrown with massive and laminated travertine facies.

Facies Associations

The facies associations represent commonly observed combinations of the depositional facies and relate to specific depositional environments (Table 3). Because aquatic fauna are absent and structures indicative of subaerial exposure are rare, lacustrine facies associations are identified by the presence of finely laminated facies. The lacustrine-margin facies associations contain a variety of wave- and uni-directional-current-worked, sandy and pebbly strata interbedded with laminated beds. The alluvial facies contain a variety of uni-directional-current-worked strata, little or no laminated strata, and evidence for subaerial exposure.

Lacustrine-profundal facies association.

This facies association (Table 3) is volumetrically the most abundant in the Creede Formation. Similar associations of facies are commonly recognized in deep-water environments (greater than 20 to 30 m) of temperate lakes (Ludlam, 1969; Kelts and Hsü, 1978), crater lakes, and small caldera lakes (Poppe and others, 1985; Nelson and others, 1986; Giresse and others, 1991). The association probably represents lacustrine-slope environments where it is dominated by laminated facies and slump structures (Fig. 6A). Lamina-dominated sections lacking slump

structures but containing intraclast-rich debris-flows probably represent basinal settings isolated from sources of sandy detritus.

Turbidites and debris-flows are interbedded with the laminated facies in a random manner (Fig. 6B), although meter-scale, fining-upward and coarsening-upward cycles are locally present. The lack of organization of dominantly turbiditic sections is characteristic of base-of-slope aprons of nonchannelized turbidites described by Nelson and others (1986) in Crater Lake, Oregon. These turbiditic systems develop basinward of debris chutes in the walls of the Crater Lake caldera; similar chutes likely existed along the walls of the Creede caldera. Pinch-and-swell cross-laminated facies are locally present and interpreted to reflect periods of decreased water depth or stronger storm activity.

Slump intervals show complete gradation from tight, recumbent folds (Fig. 6A) to tabular beds with high concentrations of bedding-parallel platy and folded intraclasts. The thickest slump interval is at least 29 m thick and provides an estimate for the water depth of the profundal facies. The slumped beds are composed of and overlain by lacustrine profundal facies that show no indication of wave-reworking. Assuming that the slump deposit filled topography on the bottom of the lake, the lake depth prior to slumping must have exceeded at least 40 to 54 m.

Lacustrine-fan facies association.

This facies association is predominantly composed of pebbly sediment-gravity-flow beds with subordinate sandy turbidites and cross-stratified facies (Table 3). Individual packages of fan strata are 9 to 30 m thick and lenticular in shape (Fig. 7). The fan packages grade basinward over hundreds of meters into strata composed of suspension-lamina and sandy turbiditic beds. Fan channels are relatively uncommon. Where observed, channels are filled with crudely-bedded or cross-bedded pebble conglomerate that fines upward into sandy turbiditic facies.

Exposure patterns of lacustrine-fan facies suggest a fan-like geometry with pronounced basinward decrease in grain size and bed thickness. The association is clearly interbedded with and enclosed by profundal associations. These characteristics are typical of subaqueous fan deposits (Nelson and Nilsen, 1984); facies can readily be categorized according to inner-fan-channel, middle-fan, and outer-fan-lobe environments. Interbedded fan packages, such as those shown in Figure 7, are found basinward of present-day canyons and paleovalleys in the caldera walls. This type of fan deposition appears to have been directly related to the subaerial drainage system. Thinner, less complex intervals of fan deposits are observed to overlie thick fallout tuffs and are not necessarily found basinward of paleo-drainages. These deposits are hypothesized to have resulted from eruption-related sediment progradation. Although the Creede lacustrine-fan deposits are analogous to their marine counterparts, they are much coarser grained and contain few well-defined channels. These differences may be due to a number of factors: (1) the abundance of coarse-grained sediment, (2) high sedimentation rate, and (3) abrupt transition from steep to shallow slopes in the Creede basin.

Lacustrine-travertine facies association.

This facies association includes linear (fissure-ridge) and domical mounds with both concordant and discordant relationships to stratified lacustrine facies. Concordant bedding relationships to lacustrine facies and abundance of pseudomorphs after ikaite imply a subaqueous origin. Considering the close association with faults, the lacustrine travertine deposits are interpreted to have formed where effluent from fracture systems entered into the lake. The textural observations in travertine facies and presence of organic material suggest, however, that much of the travertine production was associated with the activity of microorganisms in the spring environment. The lack of circumscribing aprons of debris and paucity of travertine blocks in sediment-gravity-flow beds indicate that the travertine mounds had little topographic expression (possibly 5 m or less) during formation.

Debris-apron facies association.

These deposits are dominated by tabular, lithic-rich, debris-flow beds with intervening finer-grained facies (Fig. 8)(Table 3). This association is found only around the margin of the basin and grades basinward into lacustrine-profundal facies. These deposits are analogous to basin-margin debris-apron deposits described at Crater Lake, Oregon (Nelson and others, 1986). At Crater Lake, coarse-grained sediment derived from the caldera walls is transported by sediment-gravity-flows along subaerial debris chutes into the lake and deposited as nonchannelized debris-flow beds near the basin margin.

Ephemeral-lake facies association.

This association contains laminated, wave-rippled, and current-formed facies but also contains abundant desiccation cracks (Table 3). It is found only near the base of the Creede Formation, and is especially prominent in core CCM-2. This association is interpreted to represent deposition in early ephemeral lakes that occupied the moat following high discharge hydrologic events. Infiltration and evaporation, possibly accentuated by high heat flow, caused the lakes to desiccate soon after formation.

Nearshore facies association.

This association is typified by moderately-sorted, wave-rippled, planar-cross-laminated, and horizontal-laminated sandstone, but also includes sandstone-siltstone couplets related to flood or turbidity current activity (Table 3). The facies are not organized into vertical sequences and are commonly interbedded with lacustrine-profundal or other lacustrine-margin associations (Fig. 9A). This association represents nearshore environments with water depths up to approximately 9 m.

Shoreline facies association.

This association includes wave-worked-terrace foresets and associated calcareous bottomset beds (Table 3). These deposits generally lie between nearshore facies and stream-worked facies (Fig. 10), and are interpreted to record the position of the paleo-shoreline. Although this association is interpreted to have existed around the margin of the lake at all times, it is preserved only in proximity to the alluvial-fan/fan-delta association.

Gilbert-type-delta facies association.

This association is composed of inclined beds of pebbly sandstone and conglomerate (foresets) overlain by horizontal-bedded, pebbly sandstone and conglomerate (topsets). Fine-grained lamina commonly intervene between foresets and represent deposition during periods of low-flow or temporary abandonment. This association is relatively rare and is observed only in proximity to nearshore or alluvial-fan/fan-delta associations.

Alluvial-fan/fan-delta facies association.

This association forms vertical sequences that grade from debris-flow- to sheetflood-dominated deposits, capped by one of the shallow-water, lacustrine-margin associations (nearshore, shoreline, or Gilbert-type delta) and braided-stream deposits (Fig. 9)(Table 3). Laminated facies are uncommon or absent, and evidence for subaerial exposure is rarely present. Facies in the lower part of the sequences are similar to either sediment-gravity-flow-dominated portions of volcaniclastic alluvial-fans (e.g., Waresback and Turbeville, 1990) or sheetflood-dominated portions of alluvial fans (Bull, 1972; Blair and MacPherson, 1994). These sections are interpreted as proximal alluvial fan deposits. The stream and Gilbert-type deltaic deposits reflect sedimentation from small streams that incised the fan. The alluvial-fan and stream deposits grade laterally and vertically into shoreline and nearshore deposits.

Thick sequences dominated by sheetflood deposits and capped by braided-stream and shallow-water lacustrine deposits (Fig. 9B) are found basinward of major paleocanyons. These sequences are interpreted to represent fans produced by major perennial streams entering the moat basin. Thinner sequences dominated by lithic-rich, sediment-gravity-flow deposits capped by thin intervals of stream or wave-worked deposits (Fig. 9A) are believed to represent fans draining smaller canyons with minor or ephemeral streams. The vertical facies relationships are interpreted to reflect variable discharge characteristics of the paleodrainage systems and their response to rising lake level. During lake-level rise, stream and shallow-water lacustrine deposits aggraded extensively outboard of the major paleocanyons. Fans outboard from smaller canyons aggraded only minimal thicknesses of shallow-water deposits prior to being drowned.

Alluvial-valley facies association.

Fining-upward sequences are also present in the fill of paleovalleys that were incised within the caldera walls. The most prominent paleovalley, the Bachelor paleovalley (Fig. 1), drained into the Creede caldera from the north. Sequences in the Bachelor paleovalley fill comprise colluvial breccia and conglomerate that grade upward into channel-fill conglomerate, sandstone, and cumulic paleosols (Fig. 11). These facies are capped by nearshore and profundal-lacustrine deposits. Unlike the fan sequences, the character of the alluvial-valley sequences does not vary appreciably down-gradient (Rice, 1984). The confinement of these deposits to the paleovalleys, predominance of channelized facies, vertical facies distributions, and valley-parallel channel orientations (Fig. 11) are most consistent with deposits of a braided stream that aggraded its valley. The capping lacustrine facies extend one to two km up the valley, indicating that lake levels rose high enough to flood the valley.

Talus and landslide facies association.

These deposits are dominated by colluvial and landslide breccias (Table 3) with crude bedding orientations that approach the angle of repose. They are found only around the margin of the basin and along paleovalley walls. They generally lack laminated facies and are interpreted to represent subaerial or subaqueous, talus and landslide deposits.

Lacustrine-margin-travertine facies association.

Travertine facies are also found in association with alluvial-fan/fan-delta and talus deposits (Table 3). These facies usually lack pseudomorphs after ikaite, but locally possess mudcracks and borings.

DEPOSITIONAL MODEL AND HISTORY

Distribution of Facies Associations and Depositional Model

Lacustrine deposits are exposed throughout most of the basin. Deltaic and lacustrine-fan deposits are observed outboard of identified and hypothesized (on the basis of present-day geomorphology) paleovalleys. Two end-member facies association distributions are distinguished based on the interpreted lake-level (Fig. 12); however, distributions intermediate between these are also present.

The highstand distribution represents periods in which lacustrine-profundal, lacustrine-fan, lacustrine-travertine, and debris-apron deposits were laid down across the entire moat basin (Fig. 12A). The best modern analogy for this condition is probably Crater Lake, Oregon (Nelson, 1967; Nelson and others, 1986); although, caldera-margin paleovalleys and associated depositional packages are noticeably missing at Crater Lake. Shoreline deposits existed in a narrow strand at the intersection of the water surface and the caldera margin. Most of the coarse-grained detritus was deposited in either (1) debris-apron settings fed by debris chutes around the basin margin or (2) lacustrine-fan environments basinward of paleovalleys.

Progradation of lacustrine-fan deposits is interpreted to have been initiated through a fall in lake level or disturbance of the drainage basin (eruption-related defoliation and fallout, fire, etc.). Turbidites were deposited from dilute, stream-related turbidity currents and flow transformation products of debris-flows across the basin floor. Carbonate sediment precipitated in the photic zone and fine-grained detrital sediment rained out of the water column to form seasonal laminations. Travertine deposits formed both around the basin margin and in basinal settings along fracture/fault systems. Ikaite precipitated in silty sediments across the entire lake basin and in all but the most marginal travertine deposits.

The lowstand distribution represents periods in which alluvial-fan/fan-delta deposits and associated shallow-water, lacustrine-margin deposits extended well into the basin (Fig. 12B). Many modern and ancient lake systems have this distribution of facies associations (Reading, 1986), but Pyramid Lake, Nevada and Mono Lake, California are most pertinent because they also have extensive tufa with pseudomorphs after ikaite (Shearman and others, 1989). Lowered base-level in the basin enhanced incision and canyon-cutting around the caldera margin and resurgent dome. Upon stabilization or rise in lake level, fan deltas prograded into the lake basin from the mouths of canyons and smaller drainages. Braided stream and deltaic deposits were laid down in distal-fan environments by perennial and ephemeral streams incised into the fans. Wave-formed terraces were deposited around the margin of the lake and prograded into the lake on the tops of major deltaic systems. Sediment-gravity-flow and suspension deposition occurred in the basinal lacustrine settings, much as it would during highstand conditions. Because the water-depth gradient near the lake margin was much reduced during lowstands, however, nearshore facies formed a more prominent zone than present during highstand conditions. Travertine activity was reduced in the caldera wall areas and more focused in the basinal settings. Ikaite precipitation in silty sediments was confined to more basinal settings; however, ikaite precipitated in travertine adjacent to nearshore environments.

Periods of lake-level rise are evident from correlative fining-upward, transgressive sequences composed of alluvial and lacustrine-margin deposits, such as those shown in Figures 9 and 11. Evidence for deepening is not obvious in the lacustrine-profundal deposits. This is not surprising considering the lack of organization in most of the turbidite deposits and narrow, deep morphology of the basin. Conversely, periods of lake-level fall are usually indicated by erosional surfaces in basin-margin deposits. Aggradation in basin-margin settings may have occurred during minor lake-level falls, especially in deltaic environments. In most cases, however, shallow- to deep-water lacustrine facies are truncated and overlain by alluvial or lacustrine-margin facies. Indications of possible lake-level fall in lacustrine-profundal deposits include: (1) increased abundance of pinch-and-swell sandstones, (2) sediment-gravity-flow beds composed predominantly of carbonate-coated shoreline-association sands, and (3) progradation of lacustrine-fan deposits.

Depositional History of the Creede Moat Basin

Using the facies association relationships discussed above, the sedimentological and hydrological history of the basin was reconstructed from core and outcrop observations (Fig. 13). The early caldera environment was dominated by erosional processes on the unstable caldera walls and deposition of lithic-rich debris-flow and debris-avalanche breccias. Beds of caldera-wall-derived breccia were tilted 20 to 30° to the west during resurgence of the central core of the caldera (Steven and Ratté, 1965). Sediment-gravity-flow deposition was punctuated by periods in which ephemeral lakes occupied the center of the newly-formed moat. As the caldera walls stabilized, fewer debris-flows inundated the caldera floor giving way to an ephemeral lake surrounded by an alluvial-dominated lacustrine-margin environment. Organic material is rare in these deposits suggesting that vegetation was not yet fully established; however, rooting and bioturbation are observed in a few of the fine-grained beds.

At some point, water accumulated in the basin to form a permanent lake, informally named Lake Creede. Lake level rose without a significant fall to form a relatively deep lake by the time of the C tuff (Figs. 2 and 13). Fallout of the B tuff signifies the beginning of an active period of intracaldera volcanism that contributed greatly to sedimentation in the lake. The most vigorous period of volcanism (B through G tuffs) also corresponds to a relative highstand of the lake as evidenced by the domination of turbiditic and suspension deposition. Abundant fossilized plant debris in this and all overlying lake beds indicate that vegetation around the caldera was firmly established.

Strata in both cores and surface sections show evidence for shallowing between the G and H tuffs. Lacustrine-fan deposits are first observed above the H tuff in core CCM-1 and correlative strata at sections AP-1 and WC-1. The pre-H-tuff lake-level fall was likely instrumental in enhancing development of canyons around the caldera margin. These canyons would have provided flow confinement and sediment focusing necessary for lacustrine-fan development.

The extent of lacustrine-profundal deposits near the margin of the basin indicates that highstand conditions prevailed following fallout of the H through J tuffs. Lacustrine-fan progradation during this period is attributed to minor lake-level falls and eruption-related sediment-loading. Carbonate sedimentation also became an important process during this period; first predominated by suspension laminations but progressively replaced by ikaite precipitation through time.

A slow, but progressive, lake-level fall commenced following fallout of the J tuff. As a result, extensive alluvial-fan/fan-delta sedimentation occurred around the margin of the moat basin during and following fallout of the L tuffs. The Bachelor paleovalley was incised down to at least the 2,683 m (8,800 ft) level (Heiken and Krier, 1987), which roughly corresponds to the level of post-L1 tuff erosion at exposures in the town of Creede. Slightly higher levels of incision (approximately 2,805 m or 9,200 ft) are found in paleovalleys along Farmers Creek and the southwestern side of the resurgent dome. The higher levels, however, probably reflect post-depositional structural offset from the central Rio Grande graben. Lake-

level rebounded following the L-tuff lowstand, but continued to fluctuate between high and intermediate levels through the time of the M tuffs. Lacustrine-fan and deltaic deposits are more widespread above the L tuff, suggesting increased sediment load from canyon drainages.

The subsequent depositional history of the moat is more speculative because it is based largely on data from the paleovalley-fill sequences. Importantly, beds above the M tuffs in the southeastern moat are capped by Fisher Quartz Latite lava, indicating that volcanism continued through most if not all of Creede Formation deposition. Three lacustrine incursions are preserved in the Bachelor paleovalley deposits. Thus, the cycle of lake level highstands and lowstands continued until the basin was filled. Paleovalley-fill deposits are found on the resurgent dome and caldera walls at elevations up to 3,232 m. Assuming a 5% grade between the aggraded paleovalley fill and the center of the moat (152 m of relief), the Creede moat must have filled to a present-day elevation of at least 3,080 m (approximately 10,100 ft). Accounting for the 5 % grade, the thickness of the Creede Formation in the center of the moat basin was 1,017 m.

SEDIMENT COMPOSITION AND ALTERATION

Framework Grain Composition

The Creede strata are composed of five major detrital and chemical components: lithic fragments, vitric fragments, mineral fragments, matrix (detrital and carbonate), and cements. Altered and replaced grains were counted as the original framework constituent during modal analysis, if positive identification could be made. The lithic fragments are chiefly comprised of clasts of devitrified, non-welded to welded ash-flow tuffs (Fig. 14A) and andesitic to dacitic lavas. Pyroclasts include tricuspate to blocky shards and coarsely vesicular to pipe-vesicle pumice (Fig. 14B) with phenocrysts of plagioclase, biotite, hornblende, Fe-Ti oxide, pyroxene, and sanidine. In most cases, glassy pyroclasts have been replaced by clay minerals and zeolites that faithfully preserve the vesicular pyroclastic textures. The mineral fragments observed include the following, in order of decreasing abundance: plagioclase, biotite, sanidine, hornblende, Fe-Ti oxide, clinopyroxene, quartz, and accessories.

Sediment Composition and Sources

Most lacustrine tuffs and turbidites have vitric- and crystal-rich compositions, whereas basin-margin facies tend to be more crystal-and lithic-rich (Fig. 15A). Despite the lithic-vitric-crystal variability, the mineralogical composition is dominated by plagioclase, with lesser quantities of mafic minerals and minor sanidine and quartz (Fig. 15B).

The major sources for detrital sediment in the Creede Formation are: 1) ash-flow tuffs and lavas that compose the caldera walls and surrounding volcanic plateau, 2) non-welded to densely welded Snowshoe Mountain tuff of the resurgent dome, 3) Fisher Quartz Latite (FQL) lavas, and 4) pyroclastic materials erupted from FQL

dome volcanoes (Steven and Ratté, 1965; Ratté and Steven, 1967). Preliminary petrographic results suggest that the ash-flow tuff lithic composition commonly reflects the composition of caldera-wall lithologies along the adjacent basin margins. Crystal-poor tuffs, however, are consistently more common than crystal-rich tuffs. Lava fragments are dominated by intermediate composition fragments that cannot be unambiguously assigned to a given geologic unit.

The crystal fragment compositions of Creede Formation samples are plotted in Figure 15C with those of local volcanic source rocks so as to distinguish potential provenance lithologies. The bulk of the samples plot along or close to a mixing line between the FQL pyroclastics and various crystal-poor ash-flow tuffs (Carpenter Ridge Tuff). In most cases, it is possible that the small quantity of pyroxene present could have been derived from either lavas, FQL pyroclastics, or crystal-rich, dacitic ash-flow tuffs. Diagenetic removal of pyroxene is unlikely to have shifted results toward the (P+B+H)-5*S join because pyroxene dissolution is readily identifiable by blocky, apatite-rich pores. The outlined group of samples with high pyroxene contents contains four carbonate-coated, foreshore sands; this type of sediment might be expected to be enriched in dense mineral components.

In summary, the petrographic composition of the Creede Formation strata vary in an expected manner with lithic-rich compositions along the basin margin and tuffaceous compositions in the basin interior. The mineral fragment composition was largely derived from FQL pyroclastic and crystal-poor Carpenter Ridge Tuff sources, with variable contributions from other volcanic units. In terms of labile sedimentary components, the FQL pyroclastics are interpreted to have contributed nearly all of the chemically reactive, glassy materials and much of the plagioclase feldspar, hornblende, and biotite. Considering this relationship, FQL glass and phenocryst compositions provide a useful proxy for the chemical compositions of materials affected by diagenesis and alteration in the Creede Formation.

Authigenic Mineralogy and Mineral Paragenesis

The authigenic phases are described in the apparent order of formation based on growth relationships observed with polarized-light and scanning electron microscopy. The relative timing of diagenetic and alteration events is shown diagramatically in Figure 16. The diagram is divided into groups that distinguish the varying types of alteration across the basin and within specific stratigraphic intervals.

The earliest authigenic phases are ooilitic coatings and micritic cements (Fig. 14A) in foreshore sandstones and lacustrine sediment-gravity-flow beds derived therefrom. They are composed of low-magnesium calcite with < 2.5 mole % trace elements (mostly Mg, Fe, and Mn) as determined by microprobe analysis (Larsen, 1994a). The cements are interpreted to have formed in the beach environment where low-ionic strength stream waters mixed with bicarbonate-rich lake water (e.g., Popp and Wilkinson, 1983). These cements and similar depositional calcite in travertine are partially recrystallized to rhombic and "gothic-arch" calcite (Figs. 14A and 17A). Pyrite is also interpreted to have in part precipitated early in the

diagenetic history near the sediment-water interface (Table 1), but formed at other times during the alteration history as well.

Early smectite is present as a 1 to 10 μm rim on framework grains and as honeycomb-textured cement. The grain rims are interpreted to represent the earliest authigenic silicate phase (Fig. 17B and 17C); however, where smectite is intergrown with zeolitic phases the timing is less clear. X-ray diffraction patterns of smectite range from showing a single, broad peak at 17.0 to 18.0Å (001) to showing a sharper (001) peak and well-defined peaks at higher orders (Fig. 18A). The positions of the (060) peaks between 1.495 and 1.505Å indicates that the smectites are dioctahedral. A few samples also show a peak at 1.520Å, indicating a trioctahedral smectite component. The smectite also contains as much as 30 % interstratified illite (Fig. 19A), as determined using the method of Moore and Reynolds (1989). The morphology of clays with 30 % interstratified illite is no different than that of completely expandable smectites; thus, the mixed-layered illite-smectite is interpreted to have formed from a smectitic precursor. The amount of interstratified illite increases with depth in the northeastern and northwestern parts of the moat, but increases upward in the north-central part of the moat. The breadth of the (001) smectite peak provides some information regarding crystallite size (e.g., Kisch, 1983), provided samples with significant amounts of mixed-layering (in this case > 15% illite) are avoided. In all three areas (Fig. 19B) the breadth of the (001) peak increases upward reflecting a decrease in the size of diffracting domains, as expected from Ostwald ripening at higher burial temperatures. The results of limited microprobe analysis are consistent with a dioctahedral, aluminous montmorillonite (Larsen, 1994a).

Clinoptilolite and heulandite are present as 1 to 50 μm coffin-shaped euhedra that line pores and partially fill shard and pumice dissolution cavities (Fig. 17C). The results of optical and X-ray diffraction techniques on samples from surface exposures indicate that a spectrum of compositions are present in the Creede strata (Fig. 18B). Most samples contain either a mixture of crystals with differing thermal behaviors or a single, silica-poor, K-Na-Ca-Mg clinoptilolite composition. Limited microprobe analyses performed by Larsen (1994a) and more extensive analyses of core samples by Finkelstein and others (1994) confirm the compositional variety suggested by X-ray diffraction results. Some samples are heulandite as indicated using Boles' (1972) definition of heulandite (Si/Al < 4.0). McCrink (1982) also noted heulandite from samples in the northeastern part of the moat. No spatial patterns in the clinoptilolite/heulandite composition are apparent, although the surface samples appear to be much more calcic than those from the core (Finkelstein and others, 1994). Finkelstein and others (1994) also report that the thermal stability of clinoptilolite decreases downsection in core CCM-2, reflecting the transition from Na-K clinoptilolite to Ca-clinoptilolite.

Erionite is present as fine fibers, as much as 30 μm long, that are included in and overlie clinoptilolite crystals (Fig. 17D). Although other workers have interpreted similar fibers as mordenite (McCrink, 1982; Heiken and Krier, 1987), mordenite peaks are rarely observed whereas erionite peaks are fairly common (Fig. 18B).

Erionite formation was contemporaneous with clinoptilolite, but distinctly later than smectite. A fibrous zeolite that post-dates cristobalite precipitation is present in a few samples, but it is not possible to determine whether it is mordenite or erionite.

Silica phases either overlie (Fig. 17E) or show reaction relationships (Fig. 20A) to clinoptilolite. Extensive silica precipitation is evident in both the stratified and travertine facies (Fig. 17A). In most cases, the cristobalite-tridymite X-ray diffraction peak doublet indicative of opal C-T (Jones and Segnit, 1972) is not observed. Rather, the patterns resemble those of low cristobalite described by Mitsui and Taguchi (1977). The two-theta position of the cristobalite (101) peak was determined by correcting the peak positions using an external quartz standard. Because of sample displacement and peak interferences, the numbers are offset toward lower values by as much as 0.02Å and have errors of ±0.01Å. Nevertheless, the results reveal a decrease in the d-spacing with increasing depth, consistent with the effects of increased diagenetic recrystallization (Mizutani, 1970; Mitsui and Taguchi, 1977). Larger d-spacings are generally found in samples with greater proportions of silica phases, presumably reflecting kinetic inhibition of the mineral transformation due to silica abundance (e.g., Isaacs, 1982).

Clay minerals that overlie or replace early smectite and clinoptilolite include: smectite(Fig. 20B), chlorite, chlorite-smectite mixed-layered clay, illite (Fig. 17H), and kaolinite. These phases are only present locally and generally in low abundance. Mn-rich smectite or illite are present in samples above 400 m in the section, whereas chlorite minerals are generally found at greater depth. The Mn-rich smectite is indistinct from the early smectite in X-ray diffraction patterns and is only identified through SEM observations. Kaolinite is present in two tuffs from the top of the Antlers Park section (AP-1) where it replaces plagioclase, early smectite, and clinoptilolite. Jarosite is also present in these samples and replaces biotite. Chlorite-smectite mixed-layered clays range from randomly interstratification with approximately 20 to 90 % chlorite layers to ordered interstratification with 50 % chlorite layers (corrensite)(Fig. 18.

Analcime is present as poikilotopic pore-fill and replacement of clinoptilolite (Fig. 17F). It usually is present along with chlorite-smectite mixed-layered clay or chlorite in samples from the Antlers Park area (section AP-1 and core CCM-1). The silicon to aluminum ratio of 2.3 (Larsen, 1994a) is consistent with that of analcime formed from clinoptilolite under hydrothermal conditions (Boles, 1971).

Authigenic potassium feldspar and quartz are present as 1 to 10 μm crystals that line shard cavities beneath clinoptilolite (Figs. 17C and 17G) and, near the base of the formation, analcime. They clearly preceded poikilotopic calcite cement, but may have both preceded and superseded cristobalite. The abundance of potassium feldspar and quartz generally increase with depth; however, potassium feldspar alone increases upward in core CCM-2 and nearby sections from a low value at approximately 400 m.

Detrital feldspar, hornblende, and pyroxene grain show extensive dissolution and replacement by secondary phases. Dissolution porosity is commonly lined with clinoptilolite, cristobalite, or late clay minerals (Fig. 17H), but is generally filled by

poikilotopic calcite. Biotite is commonly expanded parallel to the c-axis with interleaved calcite or altered to smectite and pyrite.

Poikilotopic calcite fills pores, replaces pore-fringing clinoptilolite, and abuts against euhedral analcime. It is present across the entire basin, irrespective of height in the formation. Qualitative microprobe analyses and X-ray diffraction data suggest a low-magnesium composition.

Gypsum and hematitic oxides are observed exclusively in surface exposures. They are present as pore-fill and fracture-fill. Notably, they replace all other secondary phases, including calcite. Both are attributed to precipitation following chemical weathering of pyrite, calcite, and silicate phases in the lacustrine beds.

Rock-eval analysis was performed on selected samples (Table 2) and provides information regarding the degree of organic maturation (Waples, 1985). The high HI values of the calcite-rich extracts not only indicate an algal-dominated kerogen type but also suggest a relatively low thermal maturity. The higher OI values of the surface samples (DLCR-20, WR-1-11, DLCR-31, and CW-O-2) probably reflect partial oxidation of the organic material; thus the results from these samples are not useful diagenetic indicators. T_{max} represents the temperature at which the maximum amount of pyrolysis products are generated; T_{max} values < 420°C reflect immature kerogens with respect to oil generation, T_{max} values > 460°C reflect overmaturity. T_{max} values from samples listed in Table 2 and other Creede core data provided by Dr. Joel Leventhal are plotted in Figure 21. Values from core CCM-1 increase with depth and are overall greater than those core CCM-2, reflecting a higher degree of thermal maturity and diagenesis. The values from CCM-2 are greatest at the base and the top, with low values present between 400 and 520 m. High T_{max} excursions probably reflect local zones that experienced higher temperatures, presumably related to interaction with hot fluids. Other organic analyses also suggest that localized hydrothermal fluid flow affected the lower parts of the stratigraphy (Leventhal and others, 1994).

Authigenic Mineral Associations and Alteration Mechanisms

Authigenic mineral associations represent commonly observed combinations of minerals and follow directly from the paragenetic sequence (Fig. 16). Six regional authigenic mineral associations are apparent: 1) glass-smectite, 2) smectite-clinoptilolite-erionite, 3) smectite-potassium feldspar-quartz-clinoptilolite, 4) chlorite/smectite-chlorite-analcime-quartz-potassium feldspar, 5) cristobalite/opal C-T-illite-potassium feldspar, and 6) late calcite. The distributions of mineral associations 1 through 5 are shown in Figures 22 and 23. The glass-smectite association is observed in the uppermost beds of the Creede Formation along the eastern flank of Snowshoe Mountain and in an isolated exposure in the southwestern part of the moat. Evidence of the smectite-clinoptilolite-erionite association is observed across the entire moat basin. The smectite-potassium feldspar-clinoptilolite-quartz association appears to supplant association 2 with depth and locally along the basin margin. The chlorite/smectite-analcime-quartz-potassium feldspar association is observed only in the northwestern part of the

moat, in the vicinity of Antlers Park, where it replaces association 3 with depth. Whereas the first three associations represent successive replacement, the cristobalite/opal C-T-illite-potassium feldspar shows both replacive and superposition relationships to association 2. It is generally distributed above 400 m in the stratigraphy across the north-central part and eastern half of the moat (Figs. 22 and 23). Late calcite is distributed across the entire moat, irrespective of depth, and represents the youngest paragenetically constrained phase.

The lateral and vertical variations in mineral associations imply a complex series of diagenetic and alteration events. The authigenic mineral distributions cross-cut stratigraphic zones and depositional environments. The strong relationship between authigenic mineralogy and depositional environments observed in saline, alkaline-lake settings (Hay, 1966; Surdam and Sheppard, 1978) is not evident at Creede. Deposition in a lacustrine environment, however, precludes alteration mechanisms involving processes in a thick, vadose zone. The scale and distribution of authigenic mineral variations, types of authigenic minerals present, and geologic setting are most consistent with authigenesis related to a combination of burial diagenesis and hydrothermal alteration. Thus, the authigenic history of the Creede Formation is interpreted in terms of burial diagenesis with superimposed hydrothermal alteration events (Antlers Park and Creede hydrothermal events).

Burial diagenesis.

The presence of smectite, clinoptilolite, and erionite on all framework grain surfaces indicates that they precipitated on these surfaces from ions in solution (or gel dissolution). Textural relationships between pyroclasts and these phases suggest that the chemical constituents released during glass hydration and dissolution lead to authigenic mineral precipitation. This process is evident from observations in other volcaniclastic deposits (Hay, 1963; Sheppard and Gude, 1968; Mariner and Surdam, 1970; Khoury and Eberl, 1979) and from hydrothermal experiments (Höller and Wirsching, 1978; Hawkins and others, 1978). Zeolites are metastable with respect to quartz and feldspars, and react upon heating or prolonged burial to form the more stable phases (Hay, 1966; Iijima, 1978; Dibble and Tiller, 1981; Bowers and Burns, 1990). Observations within the Creede strata suggest that potassium feldspar and quartz replaced clinoptilolite with increasing depth of burial. Finer crystals along shard margins show the most extensive evidence for replacement (Fig. 17C and 17F), although large clinoptilolite crystals were also replaced. Such observations are consistent with greater reactivity of smaller crystals with larger surface areas per unit mass.

The transition from glass-smectite to smectite-clinoptilolite-erionite associations is largely related to depth in the southeastern part of the caldera. The transition from smectite-clinoptilolite-erionite to smectite-potassium feldspar-clinoptilolite-quartz associations occurs both laterally and with depth. Other diagenetic indicators, such as the crystallinity of the smectite, degree of mixed-layering in illite-smectite, T_{max} pyrolysis temperatures, and changes in the composition of clinoptilolite (Finkelstein and others, 1994), suggest increasing diagenetic grade with depth,

especially below 400 m in the formation. Authigenic minerals in burial diagenetic zones I and II of Iijima (1978) are nearly identical to the Creede mineral associations (1, 2, and 3), excluding the presence of erionite at Creede versus mordenite in the Japan systems. The presence of erionite may be related to the more alkalic glass composition of the Fisher Quartz Latite pyroclastics in comparison to calc-alkaline glass compositions found in sequences in Japan. The average maximum temperature associated with zone II is 86°C, found at depths between 1.5 and 3.5 km depth of burial (Iijima, 1985). The lack of ordered illite-smectite clays and minor degrees of random interstratification in the Creede Formation are consistent with this upper temperature limit (Pollastro, 1993). Assuming a maximum thickness of 1 km for the Creede Formation, the mineralogical variations in core CCM-2 correspond well with burial diagenesis under a high geothermal gradient (as much as 71 to 81°C/km, using surface temperatures of 15 and 5°C). The presence of association 3 around the margin of the caldera is probably related to thinner sequences of more permeable facies that were susceptible to hydrothermal fluid flow, either in association with volcanism in the southeastern part of the moat or one of the hydrothermal events to be discussed.

Antlers Park hydrothermal event.

The smectite-clinoptilolite-erionite association is replaced by association 3 and the chlorite/smectite-analcime-quartz-potassium feldspar association (association 4) in the northwestern part of the moat. The authigenic mineral patterns are also influenced by sedimentary facies: 1) corrensite or chlorite/smectite mixed-layered clay and analcime are present in the upper part of the section mainly in coarse-grained sediment-gravity-flow beds in the lacustrine-fan lobes; 2) clinoptilolite is preserved mostly in fine-grained turbidites; and 3) quartz and potassium feldspar are most abundant in silt to very fine-grained turbidites, suspension laminations, and tuffs. Kaolinite and jarosite are present in massive and laminated tuffs at the top of section AP-1.

Authigenic mineral association 4 and the circumscribing distribution of authigenic mineral association 3 are interpreted to have resulted from localized hydrothermal alteration, which we term the Antlers Park hydrothermal event, superimposed on burial diagenesis. Although the chlorite/smectite-analcime-quartz-potassium feldspar association is documented to form during burial diagenesis of tuffaceous strata (Iijima, 1978; Bish and Aronson, 1993), several lines of evidence suggest hydrothermal interaction. The degree of alteration increases toward the CCM-1 core site (Fig. 23), consistent with reactions induced by localized hydrothermal fluid flow. The highest degree of alteration is focused in the highly permeable, pyroclast-poor lacustrine-fan beds in core CCM-1, an expected result for hydrothermal circulation but unlikely for burial diagenesis. These beds are characterized by extensive framework grain replacement and complete matrix replacement by analcime and corrensite, suggesting extensive mass transfer. Assuming a maximum temperature for diagenetic zone II of Iijima (1985) of 86°C, stratigraphic relationships in the northwestern part of the moat would require a

geothermal gradient of 122 to 139°C/km (using surface temperatures of 15 and 5°C). Geothermal gradients this high are uncharacteristic of shallow burial diagenesis, but are common in geothermal fields (Henley and Ellis, 1983) and inferred from hydrothermal alteration (Utada, 1985). The coexistence of analcime and quartz indicates that temperatures never rose to 200°C (Liou, 1971).

Similar types of authigenic mineral relationships are evident in Japan, where burial diagenesis is superimposed on Kuroko-type mineralization areas (Utada, 1985). One possible explanation for the mineralogical variations in the Antlers Park area is illustrated in Figure 24. Hydrothermal fluids were focused into coarse-grained deltaic and lacustrine-fan deposits from vein systems around the margin of the caldera, causing localized alteration within and above the highly permeable beds. The zone of kaolinite and jarosite overlying the highly permeable beds may have resulted from acid sulfate alteration associated with condensation and oxidation of H_2S exsolved from the hydrothermal fluids. Similar reactions are described at the Wairakei hydrothermal system in New Zealand (Steiner, 1968). Beds below the lacustrine-fan deposits experienced overall higher temperatures than beds at CCM-2 due to leakage from the hydrothermal input and thermal blanketing of the coarse-grained beds. The hydrothermal event probably lasted <10,000 years as indicated by the coexistence of randomly interstratified illite-smectite and mixed-layered chlorite-smectite minerals with smectite (Finkelstein and others, 1994).

Creede hydrothermal event.

The cristobalite/opal C-T-illite-potassium feldspar association is present above approximately 400 m in the section across most of the moat (Fig. 22). It is most often manifest as silica phases and illite overlying minerals of authigenic mineral association 2. Illitization of early smectite is suggested by SEM observations and an upsection increase in illite proportions of mixed-layered clay in the north-central part of the moat (Fig. 19A). The most intense effects are observed in beds west of Creede where potassium feldspar and illite are both present in association with replacive cristobalite. T_{max} values obtained from organic pyrolysis of CCM-2 core samples follow the mineralogical trends and suggest that a thermal event affected the upper part of the section. The distribution of samples that contain > 10 weight % cristobalite fall along trend with the Creede structural graben (Fig. 23), although a few high values are also present in the western part of the moat. The high cristobalite contents in beds west of Creede abut against quartz-silicified Creede beds that were altered during formation of the Creede Pb-Zn-Ag deposits (Rice, 1984). Spatial relationships indicate that formation of cristobalite post-dates faulting.

Cristobalite and opal C-T are commonly abundant in the upper parts of tuffaceous sequences subjected to burial diagenesis (Iijima, 1978; Broxton and others, 1987). The close association of illite and potassium feldspar with cristobalite, relative timing of cristobalite formation, and relationship between mineral association 5 and quartz silicification in the Creede mineral district, however, are not consistent with such an interpretation. These observations and the pyrolysis data provide strong

evidence for formation of mineral association 5 during movement of hydrothermal fluids from the Creede hydrothermal system into the Creede Formation. The close correspondence of the distribution of abundant cristobalite to the Rio Grande graben structure suggests that the faults acted as conduits for silica-saturated fluids.

Larsen (1994a) used chemical and mineralogical data to investigate silica gain and loss in the strata. The method involves calculating the amount of cristobalite and/or quartz that would result from closed system diagenesis of the tuffaceous strata. Reactions were written using microprobe analyses of Fisher Quartz Latite glass and diagenetic smectite and clinoptilolite, and by assuming conservation of aluminum in the solid phases. The results of the semi-quantitative mineralogical analyses were compared to the calculated closed-system values to assess silica gain or loss. In general, the strata show significant silica gain, especially for samples containing greater than 15 to 20 wt. % silica phases. Using bulk rock chemistry of tuffs in core CCM-2, Finkelstein and others (1994) also showed consistent gain in potassium and silica associated with sodium, magnesium, manganese, and iron loss.

DISCUSSION

Evolution of the Basin and Caldera Lake

Despite its 26.8 Ma age, the morphology of the Creede caldera is exceptionally well preserved (Fig. 1). The morphology of the basin is regarded to have evolved from narrow and steep-sided, similar to the Crater Lake basin, to broad and gentle-sided, similar to the Valles and Long Valley caldera moat basins. This change in basin morphology is interpreted to have resulted in greater lake surface area, and therefore surface evaporation, through time. The sedimentary facies support this interpretation and record an evolution from a narrow, deep lake to a broader and shallower lake through time. The basin also appears to have received more sediment from the surrounding plateau through time, largely as a result of caldera-wall incision and drainage adjacent to intracaldera dome volcanoes. No evidence for surface drainage of the lake is indicated by the depositional record, although overflow may have occurred during exceptional highstand periods.

Given that the Creede basin was topographically-closed, the high-frequency lake-level variations (Fig. 13) are interpreted to have been controlled by climatic variables. Pseudomorphs after ikaite are present in basinal strata associated with highstands and lowstands; thus, temperature variations are unlikely to have been a primary control on lake level. We hypothesize that the climate experienced by Lake Creede was cold over the entire lake history, but was subjected to either (1) alternating wet and dry periods or (2) periodic changes in the seasonality of moisture. The importance of variations in precipitation on lake water-balance has been demonstrated through numerical modeling experiments (Phillips and others, 1992).

The depositional facies and carbonate mineralogy provide additional information regarding the structure and water chemistry of the lake. The alternating detrital and

carbonate lamina are characteristic of temperate, meromictic lakes (Anderson and others, 1985b). In the case of Lake Creede, waters of the hypolimnion were probably anoxic as indicated by depositional pyrite, preservation of lamina and organic materials, and pseudomorphs after ikaite (e.g., Jansen and others, 1987). Epilimnion water were likely oxygenated, and hosted the algal/bacterial and lacustrine shrimp populations.

The predominance of carbonate minerals and absence of sulfates is indicative of chemical evolution toward bicarbonate-rich waters (Eugster and Hardie, 1978). Some caution is required because anoxia in the hypolimnion would favor reduced, rather than oxidized, sulfur species; thus, sulfates might not be expected to precipitate. The absence of evaporitic minerals such as gaylussite or trona suggests that the lake waters did not reach hypersaline concentrations. This is further supported by the prevalence of pseudomorphs after ikaite throughout the section; ikaite is believed to react with hypersaline bicarbonate brines to form gaylussite (Bischoff and others, 1993b). The carbonate peloids, however, bear close resemblance to fecal pellets of modern brine shrimp from the Great Salt Lake, Utah (Eardley, 1938). The salinity and water chemistry limits for these animals are unknown, but their presence suggests at least brackish water. The apparent continuity of the carbonate record above 400 m in the section implies some degree of groundwater seepage (e.g., Wood and Sanford, 1990). Water-balance modeling of the basin suggests that a small quantity of groundwater seepage (ca. 1/200 of the input flux) could account for the predominance of calcite (or aragonite) in the upper part of the stratigraphy (Larsen and Crossey, 1994; Larsen, 1995).

The effects of contemporary volcanism on lake water chemistry are not known, but carbonate production was temporarily shut down in the open lake waters following major fallout events. Studies of modern lakes affected by eruptions indicate that short-term effects (10 years or so) include: (1) increase in the total dissolved solids, and (2) variation in the amount and type of aquatic biological activity (Larson, 1993; Kurenkov, 1966). The trace element composition and textural characteristics of Creede carbonates do not show variations that can be uniquely ascribed to eruption effects (Forsman and others, 1994). If biological and chemical changes similar to those described in modern settings occurred in Lake Creede, they must have dissipated by the time carbonate sedimentation resumed or were not preserved.

The abundance of carbonate minerals and travertine in the Creede Formation is anomalous compared to modern lake basins in volcanic regions. If the extensive carbonate deposits are interpreted to be related to low-temperature hydrothermal circulation, as has been previously suggested (Steven and Friedman, 1968; Rye and others, 1988; Larsen, 1994b), what is the source of the calcium? Steven and Friedman (1968) argued that the carbon stable isotope composition of the travertine could have been derived from decarbonation reactions during metamorphism of Mesozoic limestones that may underlie the San Juan volcanic field. Similar associations have been made between large travertine deposits adjacent to other calderas and subsurface limestone formations (Bargar, 1978; Goff and Shevenell,

1987). White and others (1980) showed experimentally, however, that calcium-rich waters can result during low-temperature, acidic alteration of crystalline rhyolitic tuff. A strontium isotope study of the Creede carbonates is being pursued to help clarify the origin of the calcium and constrain the hydrology of the spring system.

Pore Fluid Evolution

Mineral authigenesis associated with hydration and dissolution of volcanic glass can be explained by kinetics of dissolution and growth (Dibble and Tiller, 1981). Metastable zeolite phases form in preference to feldspar and quartz because their growth decreases the total free energy of the system faster than growth of the stable phases. Bulk equilibrium is not obtained during the dissolution and growth reactions. Observations in the Creede Formation that preclude bulk equilibrium during authigenesis include: 1) dissolution and alteration of framework mineral grains through most of the alteration history, 2) coexistence of poorly-crystalline smectite with discrete illite, and 3) the presence of randomly interstratified clay minerals. Permeability and duration of fluid flux are also important controls on authigenic and alteration reactions, especially in low-temperature hydrothermal systems (Browne, 1978). Thus, porous, coarse-grained units in the Creede Formation were most susceptible to rapid and extreme changes in fluid chemistry and temperature. Fine-grained units interbedded with the porous units may have experienced temperature effects but less fluid flow, as a result of thermal diffusion being greater than chemical advection or diffusion.

Thus, both diagenetic and alteration reactions in the Creede strata did not proceed under equilibrium conditions, but rather were strongly controlled by kinetics, diffusion, and fluid flow. Because of these conditions, the approach used to decipher the pore fluid evolution is more empirical than thermodynamic, although equilibrium relationships are considered where appropriate. This type of approach is also used because quality thermodynamic data are not available for many of the phases considered (erionite, mixed layer clay minerals).

The initial pore fluid in most of the Creede strata was derived from the fresh to brackish, mildly alkaline lake waters buried with the sediments. Initial reactions between the lake water with volcanic glass include hydration and dissolution. Glass hydration consumes hydrogen ions resulting in increased pH and reaction rate (Hay, 1966). Formation of smectites from glass dissolution (Table 4) is favored by interaction with low salinity, neutral to mildly alkaline fluids (Höller and Wirsching, 1978; Kawano and Tomita, 1992). The close paragenetic relationship of pyrite to early smectite further suggests that these reactions occurred under reducing conditions.

Clinoptilolite is thought to precipitate under a variety of conditions, but generally through interaction with mildly alkaline, brackish to saline waters containing relatively high ratios of alkali (and alkali earth) to hydrogen cations and high silica contents (Surdam and Sheppard, 1978; Boles and Wise, 1978; Bowers and Burns, 1990). An example of a possible reaction for the formation of smectite and clinoptilolite from volcanic glass is shown in Table 4. Mariner and Surdam (1970)

proposed that aluminous zeolites (e.g., erionite, phillipsite) form under more alkaline conditions than siliceous zeolites (e.g., clinoptilolite, mordenite) as a result of charged alumina species catalyzing the formation of aluminosilicate gels. The upsection increase in the abundance of erionite at Creede suggests that pore fluids in the upper part of the formation progressed to more alkaline compositions, possibly to pH values of 9 (e.g., Surdam and Eugster, 1976), than those in the lower parts. Furthermore, sodium and potassium are concentrated in solution through the formation of smectite and clinoptilolite from volcanic glass (Larsen, 1994b), conditions that should stabilize erionite (Surdam and Sheppard, 1978). In summary, the paragenetic relationships among the clay minerals and zeolites formed during burial diagenesis reflect a pore-fluid evolution from relatively fresh, mildly alkaline waters to brackish or saline, alkaline fluids.

Textural relationships in the Creede strata suggest that clinoptilolite reacted to form potassium feldspar + quartz (Table 4). The driving mechanism for this reaction is thought to be the silica saturation of the pore fluids (Bowers and Burns, 1990; Bish and Aronson, 1993). As cristobalite or opal C-T react to form quartz, the equilibrium dissolved silica content decreases to that of quartz; thus, destabilizing clinoptilolite. Temperature and time are indirect controls because they are the primary factors affecting the opal C-T to quartz reaction (Mizutani, 1970). It is unclear whether this reaction is favored by other changes in pore fluid chemistry or salinity (e.g., Kastner and others, 1977; Isaacs, 1982). Decreased alkali ion activities and salinity are supported by the observation of late smectite growth on clinoptilolite and potassium feldspar in some samples.

The chemical conditions necessary for formation of analcime (i.e., relatively high sodium concentrations and alkaline conditions (Boles, 1972; Höller and Wirsching, 1978)) are interpreted to have developed as hydrothermal fluids and diagenetic pore fluids mixed during the Antlers Park hydrothermal event. Chlorite and mixed-layered chlorite-smectite clays form when smectite is reacted with magnesium and iron in hydrothermal environments (Inuoe, 1987), but also form during diagenesis of lacustrine clays subjected to Mg-rich, alkaline fluids (April, 1981). The reaction of clinoptilolite to analcime is interpreted to have been directly coupled with the chlorite-smectite reaction (e.g., Table 4), because it would provide magnesium and a small amount of iron. Analcime does not partition either of these elements (Gottardi and Galli, 1985). Additional iron may have been provided by dissolution of pyrite; it is notably absent in many samples bearing abundant chlorite-smectite mixed-layered clay. Excess potassium and silicon produced by the formation of analcime and mixed-layered chlorite-smectite may have contributed to formation of potassium feldspar and quartz.

Textural relationships in samples from above 400 m indicate that the bulk of the silica precipitated following the zeolites and crystallized metastably from solutions supersaturated with respect to amorphous silica and opal C-T. These conditions arise when solutions are subjected to rapid changes in temperature, solution volume, or solution chemistry (Williams and others, 1985). Precipitation of the silica phases is interpreted to have occurred as hydrothermal fluids from the vein-

hosted Creede hydrothermal system mixed with diagenetic pore waters in the Creede Formation and lost heat to sedimentary framework materials. Precipitation of potassium feldspar and illite may have been promoted by input of potassium because it was a major constituent in the hydrothermal fluids (Barton and others, 1977).

Precipitation of coarse, low-magnesium calcite cements is favored by low degrees of supersaturation and slow-moving fluids (Given and Wilkinson, 1985). Furthermore, the fact that clinoptilolite and calcium-bearing primary minerals are replaced but analcime is preserved, suggests that the fluids were calcium-poor and silica deficient. It is unlikely that these waters would have evolved from the diagenetic and hydrothermal pore fluid mixtures. They are interpreted to have invaded the Creede strata at a later point, either directly following the hydrothermal events or possibly during later hydrologic events.

Relationship to the Creede Hydrothermal System

Ore deposition in the Creede mineral district is interpreted to have occurred at about 25 Ma (Bethke and others, 1976), approximately 1.8 million years after the beginning of Creede Formation sedimentation. Investigations of the mineral district clearly indicate that fluids entered the Creede Formation through the Bachelor paleovalley and faults that intersect the northern part of the Creede moat basin (Steven and Eaton, 1975; Rice, 1984). Recent hydrologic modelling by Hayba (1993) demonstrated the conceptual feasibility of the Bethke (1987) model for the Creede hydrothermal system. Barton and others (1977) used mineral equilibria and fluid inclusion data to characterize the fluids associated with mineralization in the OH vein as relatively sulfate-rich, with a salinity of 1 molal (Na/K ratio of 9), temperature of 250°C, and pH of 5.4. Robinson (1981) obtained homogenization temperatures of 238°C and salinities of 9.5 weight % NaCl equivalent in fluid inclusions from the southern Amethyst vein. Fluid conditions were estimated from analysis of mineral equilibria and fluid inclusions (in barite) in the Bachelor paleovalley (Rice, 1984): sulfate-rich fluid, salinities between 1.1 and 2.2 molal, temperatures ranging from 155 to 195°C, and pH of 5.8.

Considering Rice's fluid inclusion data and mineralogical relationships, the lateral thermal gradient between the Bachelor paleovalley and the moat strata during mineralization was at least 50°C/km. Extrapolation of Rice's lateral thermal gradient to the intersection of the Bachelor paleovalley and the moat basin suggests that a maximum temperature of 100°C occurred along the north-central moat margin during alteration. This maximum temperature is consistent with the absence of ordered mixed-layered illite-smectite, analcime, or other higher temperature zeolites, and the change from quartz to cristobalite/opal C-T silicification (e.g., Keller and Isaacs, 1985). The results of the current study extend the zone of hydrothermal interaction across the Creede moat basin along trend with the NNW-trending fault system (Fig. 25). Some comments and speculations regarding the role of the Creede Formation in the Creede hydrothermal system are discussed below.

The character of alteration suggests that hydrothermal fluids entered the Creede Formation via three avenues: 1) southern extensions of faults in the Creede mineral district, 2) coarse-grained conglomerates of the Creede Formation in the Bachelor paleovalley, and 3) porous, coarse-grained strata and travertine around the margin of the Creede caldera moat (Fig. 25). In order for these fluids to enter the Creede Formation, the diagenetic pore waters must have been at least partially displaced. Steven and Eaton (1975) proposed that the coarse-grained strata around the margin would have allowed the diagenetic fluids to descend through the Creede Formation, enter into bedrock faults, and recharge hydrothermal circulation. The distribution of silica phases, potassium feldspar, and illite in the upper part of the stratigraphy is in part consistent with this interpretation. The relationship of alteration to the NNW-trending faults through the Creede Formation, however, suggests that the faults also provided an avenue for descent of diagenetic fluids. Focusing of fluids along the faults may have been aided by the topographic expression of the structural graben in the northern part of the moat (Fig. 25). Poor vertical connectivity between permeable units and the stratiform permeability structure, however, would preclude efficient vertical displacement of diagenetic pore waters and promote fluid mixing. Presuming this to have been the case, one might expect to find some mineralogical remnant (formation of zeolites where none had existed or a second generation of zeolite) of the passage of the highly evolved diagenetic fluids through conduits of fluid flow. Little direct evidence for this is observed. Mineralogical investigation of authigenic phases in the NNW-trending fault zones that dissect the Creede Formation may provide more clues to the fluid-flow history.

It is clear from the discussion above that hydrothermal fluid flow in the Creede Formation was greatly influenced by both faults and sedimentary facies relationships. These controls are interpreted to have resulted in extensive lateral flow away from the area of most intense alteration bordering the Creede mineral district. Similar types of lateral flow systems are identified by reversals in downhole thermal gradients (Goff and others, 1988) in many hydrothermal systems, including the Valles caldera and Long Valley caldera systems (Sorey and others, 1991). In both of these systems, hot (> 200°C) fluids ascend to near the surface and flow laterally down-gradient in porous units and along faults. In the Creede Formation, the former presence of an inverted thermal gradient is suggested by the upsection increase in illite, illite interstratification in illite-smectite, potassium feldspar, and T_{max} pyrolysis temperatures in the north-central part of the moat. The lack of extensive overprinting from changes in the hydrology of the hydrothermal system, such as that observed at Long Valley (Flexser, 1991), suggests that the Creede event was of short duration. This conclusion is also consistent with the speculations of Barton and others (1977) and hydrothermal flow modeling of Hayba (1993).

If the Creede Formation diagenetic waters did partially supply the Creede Hydrothermal system, what type of fluids would these have been? Prolonged evaporative fractionation in the lake and isotopic equilibration with the tuffaceous sediments would undoubtedly have produced heavy oxygen isotopic compositions

as required by the hypothesized model by Bethke and Rye (1979). The magnitude of heavy isotope enrichment has yet to be fully evaluated by isotopic analysis of carbonate and silicate minerals, but the lake water may have had a $\delta^{18}O$ composition of as much as 2 ‰ (Rye and others, this volume). In terms of chemistry, the hydrochemical modeling (Larsen and Crossey, 1994; Larsen, 1995) and comparison to other burial diagenetic sequences suggest that the pore waters likely would have developed to a Na-HCO_3 fluid, rather than the Na-Cl observed in fluid inclusions from the mineral district. The chemical evolution of a descending Na-HCO_3 fluid in the Creede hydrothermal system has not been investigated, but is critical for addressing the problem further.

Fluid mixing and silica precipitation in the Creede Formation

The extensive cristobalite/opal C-T mineralization is interpreted to have resulted from mixing of hydrothermal and diagenetic waters, and conductive cooling of these mixtures. Quartz-saturated hydrothermal fluids that entered the Bachelor paleovalley would have mixed with cool, dilute meteoric waters prior to entering the moat basin. Considering the diagenetic conditions, pore waters in the Creede Formation were saturated with respect to amorphous silica and relatively cool (< 50°C in the upper 400 m). Equal proportion mixing of the diluted hydrothermal fluid and diagenetic pore fluid would result in compositions supersaturated with respect to cristobalite phases (Larsen, 1994a). Flow of fluids from the two-dimensional vein system to a three-dimensional porous media is interpreted to have involved greater conductive heat loss due to increased solid surface area, further driving solutions toward amorphous silica saturation. Similarly, flow from conglomeratic to fine-grained sandy porous media would have resulted in additional conductive heat loss.

The characteristics of the cristobalite/opal C-T alteration in the Creede strata and travertines are consistent with these interpretations. Drusy silica phases are most prominent in the most porous strata (deltaic, nearshore, and sublacustrine-fan facies; average intergranular volume = 26.3 %) and travertine, consistent with precipitation from highly supersaturated fluids (Barton and others, 1963). Less porous strata (turbiditic and suspension lamination facies; average intergranular volume = 10.5 %) contain silica phases with crystal forms or replacement textures, commonly associated with precipitation at lower degrees of supersaturation. Given that the porous, permeable units represented the stratigraphic avenues along which the hydrothermal fluids accessed less porous strata, flow through them would have involved the initial quenching of the fluids and precipitation from the greatest degrees of supersaturation. High permeability would also have allowed the hydrothermal fluids to transport silica and heat well into the center of the basin, provided diagenetic fluids could be displaced laterally or downward. Conversely, low permeability units surrounding permeable facies would have inhibit hydrothermal fluid transport, but silica precipitation would be driven more by conductive heat loss than advective transport and mixing.

Although conductive cooling appears to have been an important drive for authigenesis, its importance is difficult to quantify. Mixing expressions can be written for the fluid interaction if one assumes: 1) that hydrothermal fluids traveled via the Amethyst vein and Bachelor paleovalley to the upper part of the Creede Formation in the north-central part of the moat with a minimum amount of reaction and 2) that temperature changes were largely due to mixing. Such calculations provide an indication of the mixing proportions associated with maximum heat transport efficiency. The enthalpy of the saline hydrothermal solutions was calculated using a regression expression that Drummond (1981) derived using the steam tables of Haas (1976). The end-member solutions include: a) 238°C (T_1), 1.84 molal NaCl equivalent for the vein system (Robinson, 1981); b) 155°C (T_{m1}), 1.1 molal NaCl eq. for the Bachelor paleovalley (Rice, 1984); c) 38°C (T_3), 0.02 molal NaCl eq. for the Creede Formation diagenetic fluids (Larsen, 1994a), and d) 5°C (T_2), 0.001 molal NaCl eq. for dilute, meteoric water in the Bachelor paleovalley. The maximum temperature of a fluid mixture is 100°C, as discussed in the previous section. The salinity of the 100°C fluid is unknown but the enthalpy calculation is relatively insensitive to minor variations in salinity at that temperature (Haas, 1976). For simple mixing and heat transfer:

$$H_1 \times V_1 + H_2 \times V_2 = H_m \times V_{tot}, \text{ or}$$

$$H_1 \times R_1 + H_2 \times (1-R_1) = H_m, \text{ where } R_1 = V_1/V_{tot}, R_2 = V_2/V_{tot} \text{ and } R_1 + R_2 = 1$$

$$R_1 = (H_m - H_2)/(H_1 - H_2)$$

H represents molar enthalpy, V represents molar volume, the subscripts 1 and 2 refer to hydrothermal and meteoric or diagenetic contributions, and subscript m refers to the mixture.

For mixing in the Bachelor paleovalley, H_1 = 17,210 J/mol (238°C), H_2 = 63 J/mol (5°C), and H_{mpv} = 11,356 J/mol (155°C): R_1 = 0.66 and R_2 = 0.34.

For mixing in the lacustrine Creede Formation, H_{mpv} = 11,356 J/mol (155°C), H_3 = 2,720 J/mol (38°C), and H_{mcf} = 7,542 J/mol (100°C): R_{mpv} = 0.56 and R_3 = 0.44.

Thus, under these ideal conditions the proportion of hydrothermal fluid within mixtures in the lacustrine Creede Formation was less than 0.37 ($R_1 \times R_{mpv}$). Using the total dissolved solids concentration of the diagenetic fluids (0.1 weight % NaCl equivalent) and Robinson's fluid inclusion salinity (9.5 weight % NaCl equivalent), similar expressions can be applied to fluid-mixture salinity. The 1:2 mixture of hydrothermal and diagenetic fluids results in a fluid concentration of 35,000 mg/L (NaCl equivalent), assuming no loss of mass by reaction. This calculation is not meant to indicate true fluid compositions, but rather to demonstrate that fluid mixing could be associated with a many-fold increase in the fluid salinity within the Creede Formation.

CONCLUSIONS

The Creede Formation provides a well-preserved record of sedimentation in a caldera lake within the ancient Creede caldera. The sedimentary facies are dominated by relatively deep-water (lacustrine-profundal) turbiditic and suspension

lamination deposits; however, lacustrine-margin and alluvial deposits are present around the margin of the basin. In addition, lacustrine travertine formed extensive accumulations along the ring-fracture zone and other fractures. Deposition is inferred to have occurred in a relatively-deep, basin-filling lake that experienced climatically-induced, alternating highstand and lowstand conditions.

The clastic sediment was largely derived from contemporaneous intracaldera volcanism and, to a lesser degree, from the caldera-wall erosion. Volcanic eruptions are interpreted to have produced rapid aggradation of ash-rich sediment in the lake, sediment progradation from basin-margin drainages, and possibly chemical and biological changes in the lake waters. Development of intracaldera volcanoes and basin-margin incision are believed to have increased water- and sediment-discharge from the surrounding plateau through time. Sedimentation and erosional patterns suggest that the basin geometry evolved from being narrow and deep to broad and shallow through the depositional history.

Stratigraphic and sedimentological data suggest that the lake evolved into a permanently stratified lake, with cold, bicarbonate-rich waters. Waters in the epilimnion were likely fresh and oxidated, but those in the hypolimnion were anoxic and concentrated. The ultimate extent of evaporative concentration of the lake is unknown, but no evidence for hypersaline conditions is observed. The abundance of depositional carbonate at Creede is, however, anomalous among volcanic lakes and requires further study.

Following deposition, the tuffaceous deposits across the basin experienced smectite-zeolite-potassium feldspar burial diagenesis under a moderately high geothermal gradient. The effects of two low-temperature hydrothermal alteration events were locally superimposed on the diagenetic assemblage. The Antlers Park event resulted in replacement of the clay and siliceous zeolite diagenetic assemblage by analcime and chlorite-smectite mixed-layered clay in the northwestern part of the basin. The Creede hydrothermal event resulted in silica-potassium feldspar-illite alteration of deposits above 400 m in the formation.

Alteration associated with the Creede hydrothermal system is interpreted to have formed as silica-saturated hydrothermal fluids entering the Creede Formation from the north mixed with diagenetic pore waters and conductively cooled in the porous sedimentary framework. The hydrothermal fluids are interpreted to have flowed laterally into coarse-grained facies in the Creede Formation from NNW-trending faults in the northern part of the moat basin. Fluid movement within the Creede Formation implies partial displacement of original diagenetic water. The sodium-bicarbonate diagenetic waters may have in part supplied the Creede hydrothermal system; however, questions regarding the chemistry and degree of concentration of these waters have yet to be resolved.

ACKNOWLEDGMENTS

This research was supported by National Science Foundation grants (EAR-9116021 and 9005344) to L. J. Crossey and institutional funding from the University of New

Mexico Department of Earth and Planetary Sciences and Graduate Student Association. Gary A. Smith introduced us to many of the field-related problems in the Creede Formation and contributed many ideas to the manuscript. Undergraduate and graduate assistants Johan Forsman, David Hicks, Chris Inoue, Jennifer Loomis, Shanda Norris, and David Schwarting contributed effort in field and laboratory work. Mike Spilde at the UNM electron microprobe facility assisted with scanning electron microscope and microprobe chemical analyses. John Husler, staff chemist at UNM, guided some of the geochemical analyses. Mark Miller at the UNM Earth and Planetary Sciences X-ray diffraction laboratory helped to solve some problems encountered during X-ray diffraction.

Accommodations for field work at Creede were provided by the United States Geological Survey and Homestake Mining Company. Much insight was gained through discussions with the CSDP on-site science crew (Phil Bethke, Wayne Campbell, Dan Hayba, Jeff Hulen, and Randy Streufert) at Creede in 1991. The United States Geological Survey (Denver) Core Repository provided assistance with core description and sampling. The following are acknowledged for helpful discussions: Steve Altaner, Paul Barton, Wolfgang Elston, Dave Finkelstein, Richard Hay, Grant Heiken, Marvin Lanphere, Joel Leventhal, Martin Nelson, Phil Nelson, Richard Reynolds, Joe Rosenbaum, Bob Rye, Tom Steven, and Crayton Yapp. We thank Joel Leventhal of the United States Geological Survey for anhydrous pyrolysis data.

REFERENCES

Allen, J. R. L., 1984, Sedimentary Structures, their character and physical basis, volume I: Developments in Sedimentology 30: Amsterdam, Elsevier, 593 p.

Anderson, R. Y., Nuhfer, E. B., and Dean, W. E., 1985a, Sedimentation in a blast-zone lake at Mount St. Helens, Washington - implications for varve formation: Geology, v. 13, p. 348-352.

Anderson, R. Y., Dean, W. E., Bradbury, P. J., and Love, D., 1985b, Meromictic lakes and varved lake sediments in North America: United States Geological Survey Bulletin 1607, 19 p.

April, R. H., 1981, Trioctahedral smectite and interstratified chlorite/smectite in Jurassic strata of the Connecticut Valley: Clays and Clay Minerals, v. 29, p. 31-39.

Arguden, A. T., and Rodolfo, K. S., 1990, Sedimentologic and dynamic differences between hot and cold laharic debris flows of Mayon volcano, Philippines: Geologic Society of America Bulletin, v. 102, p. 865-876.

Axelrod, D. I., 1987, The Late Oligocene Creede Flora, Colorado: Berkeley, University of California Press, 234 p.

Ballance, P. F., and Gregory, M. R., 1991, Parnell Grits-large subaqueous volcaniclastic gravity flows with multiple particle-support mechanisms: *in* Fisher, R. V. and Smith, G. A., eds., Sedimentation in Volcanic Settings:

Society of Economic Paleontologists and Mineralogists Special Publication 45, p. 189-200.

Bargar, K. E., 1978, Geology and thermal history of Mammoth Hot Springs, Yellowstone National Park, Wyoming: United States Geological Survey Bulletin 1444, 51 p.

Barton, P. B., Bethke, P. M., and Roedder, E., 1977, Environment of ore deposition in the Creede Mining District, San Juan Mountains, Colorado: Part III. Progress toward interpretation of the chemistry of the ore-forming fluid for the OH vein: Economic Geology, v. 72, p. 1-24.

Barton, P. B., Jr., Bethke, P. M., and Toulmin, P., 3rd, 1963, Equilibrium in Ore Deposits: International Mineralogical Association, Papers, Third General Meeting: Mineralogical Society of America Special Paper 1, p. 171-185.

Bethke, P. M., 1987, The Creede, Colorado ore-forming system: a summary model [abs.] Geological Society of America, Abstracts with Programs, v. 19, p. 260.

Bethke, P. M., and Rye, R. O., 1979, Environment of ore deposition in the Creede Mining District, San Juan Mountains, Colorado: Part IV. Source of fluids from oxygen, hydrogen, and carbon isotope studies: Economic Geology, v. 74, p. 1832-1851.

Bethke, P. M., Barton, P. B., Jr., Lanphere, M. A., and Steven, T. A., 1976, Environment of ore deposition in the Creede Mining District, San Juan Mountains, Colorado: II. Age of mineralization: Economic Geology, v. 71, p. 1006-1011.

Bischoff, J. L., Fitzpatrick, J. A., and Rosenbauer, R. J., 1993a, The solubility and stabilization of ikaite ($CaCO_3 \cdot 6H_2O$) from 0 to 25°C: Environmental and paleoclimatic implications for thinolitic tufa: Journal of Geology, v. 101, p. 21-33.

Bischoff, J. L., Stine, S., Rosenbauer, R. J., Fitzpatrick, J. A., and Stafford, T. W., 1993b, Ikaite precipitation by mixing of shoreline springs and lake water, Mono Lake, California: Geochimica et Cosmochimica Acta, v. 57, p. 3855-3866.

Bish, D. L., and Aronson, J. L., 1993, Paleogeothermal and paleohydrologic conditions in silicic tuff from Yucca Mountain, Nevada: Clays and Clay Minerals, v. 41, p. 148-161.

Blair, T. C., and MacPherson, J. G., 1994, Alluvial fans and their natural distinction from rivers based on morphology, hydraulic processes, sedimentary processes, and facies assemblages: Journal of Sedimentary Research, v. A64, p. 450-489.

Bodine, M. W., Jr., Hay, R. L., Madsen, B. M., and Altaner, S. P., 1987, Lacustrine volcaniclastic sediments in the Creede Formation, San Juan Mountains, CO [abs.]: Geological Society of America, Rocky Mountain Section, Abstracts with Programs, v. 19, p. 261.

Boles, J. R., 1972, Composition, optical properties, cell dimensions, and thermal stability of some heulandite group zeolites: The American Mineralogist, v. 57, p. 1463-1493.

Boles, J. R., 1971, Synthesis of analcime from natural heulandite and clinoptilolite: The American Mineralogist, v. 56, p. 1724-1734.

Boles, J. R., and Wise, W. S., 1978, Nature and origin of deep-sea clinoptilolite: *in* Sand, L. B., and Mumpton, F. A., eds., Natural Zeolites, Occurrence, Properties, Use: Pergamon Press, Oxford, p. 235-243.

Bowers, T. S., and Burns, R. G., 1990, Activity diagrams for clinoptilolite: Susceptibility of this zeolite to further diagenetic reactions: American Mineralogist, v. 75, p. 601-619.

Browne, P. R., 1978, Hydrothermal alteration in active geothermal fields: Annual Reviews of Earth and Planetary Science, v. 6, p. 229-250.

Broxton, D. E., Bish, D. L., and Warren, R. G., 1987, Distribution and chemistry of diagenetic minerals at Yucca Mountain, Nye County, Nevada: Clays and Clay Minerals, v. 35, p. 89-110.

Bull, W. B., 1972, Recognition of alluvial-fan deposits in the stratigraphic record: *in* Rigby, K. J. and Hamblin, W. K., eds., Recognition of Ancient Sedimentary Environments: Society of Economic Paleontologists and Mineralogists Special Publication 16, p. 68-83.

Casanova, J., 1986, East African Rift stromatolites: *in* Frostick, L. E., Renaut, R. W., Reid, I., and Tiercelin, J. J., eds., Sedimentation in the African Rifts: Oxford, Blackwell, p. 201-210.

Chafetz, H. S., and Folk, R. L., 1984, Travertines: Depositional morphology and the bacterially constructed constituents: Journal of Sedimentary Petrology, v. 54, p. 289-316.

Chung, F. H., 1974a, Quantitative interpretation of x-ray diffraction patterns of mixtures. II. Adiabatic principle of x-ray diffraction analysis of mixtures: Journal of Applied Crystallography, v. 7, p. 526-531.

Chung, F. H., 1974b, Quantitative interpretation of x-ray diffraction patterns of mixtures. I. Matrix-flushing method for quantitative multicomponent analysis: Journal of Applied Crystallography, v. 7, p. 519-525.

Cohen, A. S., and Thouin, C., 1987, Nearshore carbonate deposits in Lake Tanganyika: Geology, v. 15, p. 414-418.

Dibble, W. E., Jr., and Tiller, W. A., 1981, Non-equilibrium water/rock interactions -- I. Model for interface-controlled reactions: Geochimica et Cosmochimica Acta, v. 45, p. 79-92.

Drummond, S. E., Jr., 1981, Boiling and mixing of hydrothermal fluids: chemical effects on mineral precipitation [Ph. D. thesis]: State College, Pennsylvania, Pennsylvania State University, 380 p.

Eardley, A. J., 1938, Sediments of Great Salt Lake, Utah: American Association of Petroleum Geologists Bulletin, v. 22, p. 1305-1411.

Eugster, H. P., and Hardie, L. A., 1978, Saline lakes: *in* Lerman, A., Ed., Lakes: Chemistry, Geology, Physics: New York, Springer-Verlag, p. 237-294.

Finkelstein, D. B., Altaner, S. P., and Hay, R. L., 1994, Silicate diagenesis of tuffs and their geochemical implications for pore fluids in the Oligocene Creede Formation, southwestern Colorado [abs.]: Geological Society of America, Abstracts with Programs, v. 26, p. A-398.

Fisher, R. V., 1983, Flow transformations in sediment gravity flows: Geology, v. 11, p. 273-274.
Fisher, R. V., and Schmincke, H. -U., 1984, Pyroclastic Rocks: Berlin, Springer-Verlag, 472 p.
Flexser, S., 1991, Hydrothermal alteration and past and present thermal regimes in the western moat of Long Valley caldera: Journal of Volcanology and Geothermal Research, v. 48, p. 303-318.
Forsman, J., Larsen, D., and Crossey, L. J., 1994, Carbonate geochemistry of moat sediments of the Creede caldera, CO [abs.]: Geological Society of America, Abstracts with Programs, v. 26, p. A-400.
Gilbert, G. K., 1890, Lake Bonneville: Monograph of the United States Geological Survey 1, 438 p.
Giresse, P., Maley, J., and Kelts, K., 1991, Sedimentation and paleoenvironment in crater lake Barombi Mbo, Cameroon, during the last 25,000 years: Sedimentary Geology, v. 71, p. 151-175.
Given, R. K., and Wilkinson, B. H., 1985, Kinetic control of morphology, composition, and mineralogy of abiotic sedimentary carbonates: Journal of Sedimentary Petrology, v. 55, p. 109-119.
Glicken, H., 1991, Sedimentary architecture of large volcanic-debris avalanches: *in* Fisher, R. V. and Smith, G. A., eds., Sedimentation in Volcanic Settings: Society of Economic Paleontologists and Mineralogists Special Publication 45, p. 99-106.
Gloppen, T. G., and Steel, R. J., 1981, The deposits, internal structure, and geometry of six alluvial fan-fan delta bodies (Devonian-Norway) - A study in the significance of bedding sequences in conglomerates: *in* Etheridge, F. G. and Flores, R. M., eds., Recent and Ancient Nonmarine Depositional Environments: Models For Exploration: Society of Economic Paleontologists and Mineralogists Special Publication 31, p. 49-69.
Goff, F., and Shevenell, L., 1987, Travertine deposits of Soda Dam, New Mexico, and their implication for the age and evolution of the Valles caldera hydrothermal system: Geological Society of America Bulletin, v. 99, p. 292-302.
Goff, F., Shevenell, L., Gardner, J. N., Vuataz, F. D., and Grigsby, C. O., 1988, The hydrothermal outflow plume of Valles Caldera, New Mexico, and a comparison with other outflow plumes: Journal of Geophysical Research, v. 93, p. 6041-6058.
Goldsmith, J., Graf, D., and Heard, H., 1961, Lattice constants of the calcium-magnesium carbonates: American Mineralogist, v. 46, p. 453-457.
Gottardi, G., and Galli, E., 1985, Natural Zeolites: Heidelberg, Springer-Verlag, 385 p.
Guo, L., and Riding, R., 1992, Microbial micritic carbonates in uppermost Permian reefs, Sichuan Basin, southern China: some similarities with Recent travertines: Sedimentology, v. 39, p. 37-53.

Haas, J. L., Jr., 1977, Thermodynamic properties of the coexisting phases and thermochemical properties of the H_2O component in boiling NaCl solutions: United States Geological Bulletin 1421-A (revised), 73 p.

Halfman, J. D., and Johnson, T. C., 1988, High-resolution record of cyclic climatic change during the past 4 ka from Lake Turkana, Kenya: Geology, v. 16, p. 496-500.

Harms, J. C., and Fahnestock, R. K., 1965, Stratification, bed forms, and flow phenomena (with an example from the Rio Grande): *in* Middleton, G. V., ed., Primary sedimentary structures and their hydrodynamic interpretation: Society of Economic Paleontologists and Mineralogists Special Publication 12, p. 84-115.

Hawkins, D. B., Sheppard, R. A., and Gude, 3rd, A. J., 1978, Hydrothermal synthesis of clinoptilolite and comments on the assemblage Phillipsite-Clinoptilolite-Mordenite: *in* Sand, L. B., and Mumpton, F. A., eds., Natural Zeolites, Occurrence, Properties, Use: Oxford, Pergamon Press, p. 337-344.

Hay, R. L., 1966, Zeolites and Zeolitic Reactions in Sedimentary Rocks: Geological Society of America Special Paper 85, 130 p.

Hay, R. L., 1963, Stratigraphy and zeolitic diagenesis of the John Day Formation of Oregon: University of California Pubs. Geol. Sci., v. 42, p. 199-262.

Hayba, D. O., 1993, Numerical hydrologic modeling of the Creede epithermal ore-forming system, Colorado [Ph.D. thesis]: Urbana, Illinois, University of Illinois, 186 p.

Heiken, G., and Krier, D. J., 1987, Moat deposits of the Creede caldera, CO: Los Alamos Laboratory, LA-10943-MS, 36 p.

Henley, R. W., and Ellis, A. J., 1983, Geothermal systems ancient and modern: a geochemical review: Earth-Science Reviews, v. 19, p. 1-50.

Höller, H., and Wirsching, U., 1978, Experiments on the formation of zeolites by hydrothermal alteration of volcanic glasses: *in* Sand, L. B., and Mumpton, F. A., eds., Natural Zeolites, Occurrence, Properties, Use: Oxford, Pergamon Press, p. 329-336.

Hulen, J. B., 1992, Field Geologic Log Summaries for Coreholes CCM-2 and CCM-1: Creede Scientific Drilling Project (USGS-NSF-DOE): Salt Lake City, DOE/ER/14207-1, 24 p.

Iijima, A., 1985, Application of zeolites to petroleum exploration: *in* Kallo, D., and Sherry, H. S, eds., Occurrence, Properties, and Utilization of Natural Zeolites: Budapest, Akademiai Kiado, p. 29-37.

Iijima, A., 1978, Geological occurrences of zeolite in marine environments: *in* Sand, L. B., and Mumpton, F. A., eds., Natural Zeolites, Occurrence, Properties, Use: Oxford, Pergamon Press, p. 175-198.

Inoue, A., 1987, Conversion of smectite to chlorite by hydrothermal and diagenetic alterations, Hokuroku Kuroko mineralization area, northeast Japan: *in* Schultz, L. G., van Olphen, H., and Mumpton, F. A., eds., Proceedings of the International Clay Conference, Denver, 1985, p. 158-164.

Isaacs, C. M., 1982, Influence of rock composition on kinetics of silica phase changes in the Monterey Formation, Santa Barbara area, California: Geology, v. 10, p. 304-308.

Jansen, J. H. F., Woensdregt, C. F., Kooistra, M. J., and van der Gaast, S. J., 1987, Ikaite pseudomorphs in the Zaire deep-sea fan: An intermediate between calcite and porous calcite: Geology, v. 15, p. 245-248.

Jones, J. B., and Segnit, E. R., 1972, Genesis of cristobalite and tridymite at low temperatures: Journal of the Geological Society of Australia, v. 18, p. 419-422.

Kastner, M., Keene, J. B., and Gieskes, J. M., 1977, Diagenesis of siliceous oozes -- I. Chemical controls on the rate of opal-A to opal-CT transformation -- an experimental study: Geochimica et Cosmochimica Acta, v. 41, p. 1041-1059.

Kawano, M., and Tomita, K., 1992, Formation of allophane and beidellite during hydrothermal alteration of volcanic glass below 200°C: Clays and Clay Minerals, v. 40, p. 666-674.

Kelts, K., and Hsü, K. J., 1978, Freshwater carbonate sedimentation: *in* Lerman, A., ed., Lakes: Chemistry, Geology, Physics: New York, Springer-Verlag, p. 295-324.

Keller, M. A., and Isaacs, C. M., 1985, An evaluation of temperature scales for silica diagenesis in diatomaceous sequences including a new approach based on the Miocene Monterey Formation, California: Geo-Marine Letters, v. 5, p. 31-35.

Khoury, H. N., and Eberl, D. D., 1979, Bubble-wall shards altered to montmorillonite: Clays and Clay Minerals, v. 27, p. 291-292.

Kisch, H. J., 1983, Mineralogy and petrology of burial diagenesis (burial metamorphism) and incipient metamorphism in clastic rocks: *in* Larsen, G, and Chilingar, G. V, eds., Diagenesis in Sediments and Sedimentary Rocks, 2: Amsterdam, Elsevier Scientific Publishing, p. 289-511.

Komar, P. D., 1976, Beach Processes and Sedimentation: Englewood Cliffs, New Jersey, Prentice-Hall, 429 p.

Komar, P. D., 1974, Oscillatory ripple marks and the evaluation of ancient wave conditions and environments: Journal of Sedimentary Petrology, v. 44, p. 169-180.

Kurenkov, I. I., 1966, The influence of volcanic ashfall on biological processes in a lake: Limnology and Oceanography, v. 11, p. 426-429.

Lanphere, M. A., 1994, Duration of sedimentation of the Creede Formation [abs.]: Geological Society of America, Abstracts with Programs, v. 26, p. A-400.

Larsen, D., 1995, Hydrochemical modeling of an ancient caldera lake: The Oligocene Creede Formation, Colorado. First SEPM Congress on Sedimentary Geology, Congress Program and Abstracts, vol. 1, p. 81-82.

Larsen, D., 1994a, Depositional Environments and Diagenesis in the Creede Formation, San Juan Mountains, Colorado [Ph.D. thesis]: Albuquerque, University of New Mexico, 315 p.

Larsen, D., 1994b, Origin and paleoenvironmental significance of calcite pseudomorphs after ikaite in the Oligocene Creede Formation, Colorado: Journal of Sedimentary Research, v. A64, p. 593-603.

Larsen, D., and Crossey, L. J., 1994, Analysis of sedimentation, hydrology, and diagenesis within an ancient caldera lake basin: The Oligocene Creede Formation, Colorado, U.S.A. [abs.]: Geological Society of America, Abstracts with Programs, v. 26, p. A-400.

Larsen, D., and Nelson, P. H., 1995, Stratigraphy and geophysical characteristics of the Oligocene Creede Formation in two cored boreholes: United States Geological Survey Open-File Report 94-260P, 24p.

Larson, D., 1993, The Recovery of Spirit Lake: American Scientist, v. 81, p. 166-177.

Leventhal, J., Daws, T., and Bostick, N., 1994, Organic geochemical studies to understand ore genesis at Creede: United States Geological Survey Open File Report 94-260J, 19p.

Liou, J. G., 1971, Analcime equilibria: Lithos, v. 4, p. 389-402.

Lipman, P. W., 1984, The roots of ash-flow tuff calderas in western North America: windows into the tops of granitic batholiths: Journal of Geophysical Research, B10, v. 89, p. 8801-8841.

Lipman, P. W., Sawyer, D. A., and Hon, K., 1989, Central San Juan caldera cluster: *in* Chapin, C. E., and Zidek, J., eds., Field excursions to volcanic terranes in the western United States, Volume 1: Southern Rocky Mountain region: New Mexico Bureau of Mines and Mineral Resources, Memoir 46, p. 330-350.

Lowe, D. R., 1982, Sediment gravity flows: II. Depositional models with special reference to the deposits of high-density turbidity currents: Journal of Sedimentary Petrology, v. 52, p. 279-297.

Lowe, D. R., 1979, Sediment gravity flows: their classification and some problems of application to natural flows and deposits: *in* Doyle, L. J. and Pilkey, O. H., eds., Geology of Continental Slopes: Society of Economic Paleontologists and Mineralogists Special Publication 27, p. 75-82.

Ludlam, S. D., 1969, Fayetteville Green Lake, New York. III. The laminated sediments: Limnology and Oceanography, v. 14, p. 849-857.

Mariner, R. H., and Surdam, R. C., 1970, Alkalinity and formation of zeolites in saline alkaline lakes: Science, v. 170, p. 977-980.

Marland, G., 1975, Stability of calcium carbonate hexahydrate (ikaite): Geochimica et Cosmochimica Acta, v. 39, p. 83-91.

McCrink, M. T., 1982, Diagenesis in the Creede Formation, San Juan Mountains, Creede, Colorado [M.Sc. thesis]: Socorro, New Mexico, New Mexico Institute of Mining and Technology, 113 p.

Middleton, G. V., 1970, Experimental studies related to problems of flysch sedimentation: *in* Lajoie, J., ed. Flysch Sedimentology in North America: Geological Association of Canada Special Paper 7, p. 253-272.

Mitsui, K., and Taguchi, K., 1977, Silica mineral diagenesis in neogene tertiary shales in the Tempoku district, Hokkaido, Japan: Journal of Sedimentary Petrology, v. 47, p. 158-167.

Mizutani, S., 1970, Silica minerals in the early stage of diagenesis: Sedimentology, v. 15, p. 419-436.

Moore, D. M., and Reynolds R. C., Jr., 1989, X-ray Diffraction and the Identification and Analysis of Clay Minerals: New York, Oxford University Press, 332 p.

Nelson, A. R., 1992, Lithofacies analysis of colluvial sediments - an aid in interpreting the recent history of Quaternary normal faults in the Basin and Range province, western United States: Journal of Sedimentary Petrology, v. 62, p. 607-621.

Nelson, C. H., 1967, Sediments of Crater Lake, Oregon: Geological Society of America Bulletin, v. 78, p. 833-848.

Nelson, C. H., Bacon, C. R., Robinson, S. W., Adam, D. P., Bradbury, J. P., Barber, J. H., Schwartz, D., and Vagenas, G., 1994, The volcanic, sedimentologic, and paleolimnologic history of the Crater Lake caldera floor, Oregon: Evidence for small caldera evolution: Geological Society of America Bulletin, v. 106, p. 684-704.

Nelson, C. H., Meyer, A. W., Thor, D., and Larsen, M., 1986, Crater Lake, Oregon: A restricted basin with base-of-slope aprons of nonchannelized turbidites: Geology, v. 14, p. 238-241.

Nelson, C. H., and Nilsen, T. H., 1984, Modern and Ancient Deep-Sea Fan Sedimentation: Society of Economic Paleontologists and Mineralogists Short Course Notes No. 14, 404 p.

Newhall, C. G., Paull, C. K., Bradbury, J. P., Higuera-Gundy, A., Poppe, L. J., Self, S., Bonar Sharpless, N., and Ziagos, J., 1987, Recent geologic history of Lake Atitlan, a caldera lake in western Guatemala: Journal of Volcanology and Geothermal Research, v. 33, p. 81-107.

Newman, A. D., and Brown, G., 1987, The chemical constitution of clays.: *in* Newman, A. C. D., ed., Chemistry of Clays and Clay Minerals: London, Longman, p. 1-128.

Osborne, R. H., Licari, G. R., and Link, M. H., 1982, Modern lacustrine stromatolites, Walker Lake, Nevada: Sedimentary Geology, v. 32, p. 39-61.

Papike, J. J., 1988, Chemistry of the rock-forming silicates: multiple-chain, sheet, and framework structures: Reviews of Geophysics, v. 26, p. 407-444.

Pharo, C. H., and Carmack, E. C., 1979, Sedimentation processes in a short residence-time intermontane lake, Kamloops Lake, British Columbia: Sedimentology, v. 26, p. 523-541.

Phillips, F. M., Campbell, A. R., Kruger, C., Johnson, P., Roberts, R., and Keyes, E., 1992, A reconstruction of the response of the water balance in western United States lake basins to climate change: Socorro, New Mexico, New Mexico Water Resources Research Institute Report 269, 154 p.

Picard, M. D., and High, L. R., Jr., 1973, Sedimentary structures of ephemeral streams: Developments in Sedimentology 17: Amsterdam, Elsevier, 223 p.

Pollastro, R. M., 1993, Considerations and applications of the illite/smectite geothermometer in hydrocarbon-bearing rocks of Miocene to Mississippian age: Clays and Clay Minerals, v. 41, p. 119-133.

Popp, B. N., and Wilkinson, B. H., 1983, Holocene lacustrine ooids from Pyramid Lake, Nevada: *in* Peryt, T., ed., Coated Grains: Heidelberg, Springer-Verlag, p. 142-153.

Poppe, L. J., Paull, C. K., Newhall, C. G., Bradbury, J. P., and Ziagos, J., 1985, A geophysical and geological study of Laguna De Ayarza, a Guatemalan caldera lake: Journal of Volcanology and Geothermal Research, v. 25, p. 125-144.

Ratté, J. C., and Steven, T. A., 1967, Ash flows and related volcanic rocks associated with the Creede caldera, San Juan Mountains, Colorado: United States Geological Survey Professional Paper 524-H, p. H1-H58.

Reading, H. G., 1986, Sedimentary Environments and Facies: Oxford, Blackwell Scientific, 615 p.

Rice, J. A., 1984, Controls on silver mineralization in the Creede Formation, Creede, Colorado [M.Sc. thesis]: Fort Collins, Colorado, Colorado State University, 113 p.

Robinson, R. W., 1981, Ore mineralogy and fluid inclusion study of the southern Amethyst vein system, Creede mining district, Colorado [M. Sc. thesis]: Socorro, New Mexico, New Mexico Institute of Mining and Technology, 85 p.

Rust, B. R., 1978, Depositional models for braided alluvium: *in* Miall, A. D., ed., Fluvial Sedimentology: Canadian Society for Petroleum Geologists, Calgary, p. 605-626.

Rye, R. O., Bethke, P. M., and Finkelstein, D. B., 1995, Stable isotope geochemistry of the Creede Formation and implications for the origin of fluids responsible for hydrothermal vein minerals in the Creede mining district: United States Geological Survey, Open-File Report 94-260G.

Rye, R. O., Plumlee, G. S., Bethke, P. M., and Barton, P. B., 1988, Stable isotope geochemistry of the Creede, Colorado hydrothermal system: United States Geological Survey Open-File Report 88-356, 40 p.

Scholl, D. W., and Taft, W. H., 1964, Algae, contributors to the formation of calcareous tufa, Mono Lake, California: Journal of Sedimentary Petrology, v. 34, p. 309-319.

Shearman, D. J., McGugan, A., Stein, C., and Smith, A. J., 1989, Ikaite, $CaCO_3 \cdot 6H_2O$, precursor of the thinolites in the Quaternary tufas and tufa mounds of the Lahontan and Mono Lake Basins, western United States: Geological Society of America Bulletin, v. 101, p. 913-917.

Shearman, D. J., and Smith, A. J., 1985, Ikaite, the parent mineral of jarrowite-type pseudomorphs: Proceedings of the Geologists Association, v. 96, p. 305-314.

Sheppard, R. A., and Gude, 3rd, A. J., 1968, Distribution and genesis of authigenic silicate minerals in tuffs of Pleistocene Lake Tecopa, Inyo County, California: United States Geological Survey Professional Paper 597, 38 p.

Smith, G. A., 1986, Coarse-grained nonmarine volcaniclastic sediment: terminology and depositional processes: Geological Society of America Bulletin, v. 97, p. 1-10.

Smith, G. A., and Lowe, D. R., 1991, Lahars: volcano-hydrologic events and deposition in the debris flow-hyperconcentrated flow continuum: *in* Fisher,

R. V. and Smith, G. A., eds., Sedimentation in Volcanic Settings: Society of Economic Paleontologists and Mineralogists Special Publication 45, p. 59-70.
Smoot, J. P., 1983, Depositional subenvironments in an arid closed basin; the Wilkins Peak Member of the Green River Formation (Eocene), Wyoming, U.S.A.: Sedimentology, v. 30, p. 801-827.
Smoot, J. P., and Lowenstein, T. K., 1991, Depositional environments of nonmarine evaporites: *in* Melvin, J. L., ed., Evaporites, Petroleum and Mineral Resources: Developments in Sedimentology 50, Amsterdam, Elsevier, p. 189-347.
Sorey, M. L., Suemnicht, G. A., Sturchio, N. C., and Nordquist, G. A., 1991, New evidence on the hydrothermal system in Long Valley caldera, California, from wells, fluid sampling, electrical geophysics, and age determinations of hot-spring deposits: Journal of Volcanology and Geothermal Research, v. 48, p. 229-263.
Steiner, A., 1968, Clay minerals in hydrothermally altered rocks at Wairakei, New Zealand: Clays and Clay Minerals, v. 16, p. 193-213.
Steven, T. A., 1968, Critical review of the San Juan peneplain, southwestern Colorado: United States Geological Survey Professional Paper 594-I, 19 p.
Steven, T. A., and Eaton, G. P., 1975, Environment of ore deposition in the Creede Mining District, San Juan Mountains, Colorado: Part I. Geologic, hydrologic, and geophysical setting: Economic Geology, v. 70, p. 1023-1037.
Steven, T. A., and Friedman, I., 1968, The source of travertine in the Creede Formation, San Juan Mountains, Colorado: United States Geological Survey Professional Paper 600-B, p. 29-36
Steven, T. A., and Lipman, P. W., 1976, Calderas of the San Juan Volcanic Field, southwestern Colorado: United States Geological Survey Professional Paper 958, 35 p.
Steven, T. A., and Ratté, J. C., 1965, Geology and Structural Control of Ore Deposition in the Creede District, San Juan Mountains, CO: United States Geological Survey Professional Paper 487, 90 p.
Sturm, M., and Matter, A., 1978, Turbidites and varves in Lake Brienz (Switzerland): deposition of clastic detritus by density currents: *in* Matter, A. and Tucker, M. E., eds., Modern and Ancient Lake Sediments: Oxford, Blackwell, p. 145-166.
Surdam, R. C., and Eugster, H. P., 1976, Mineral reactions in the sedimentary deposits of the Lake Magadi region, Kenya: Geological Society of America Bulletin, v. 87, p. 1739-1752.
Surdam, R. C., and Sheppard, R. A., 1978, Zeolites in saline, alkaline-lake deposits: *in* Sand, L. B., and Mumpton, F. A., eds., Natural Zeolites, Occurrence, Properties, Use: Oxford, Pergamon Press, p. 145-174.
Swirydczuk, K., Wilkinson, B. H., and Smith, G. R., 1980, The Pliocene Glenns Ferry Oolite-II: Sedimentology of Oolitic Lacustrine Terrace Deposits: Journal of Sedimentary Petrology, v. 50, p. 1237-1248.
Tucker, M. E., and Wright, V. P., 1990, Carbonate Sedimentology: Oxford, Blackwell, 482 p.

Utada, M., 1985, Occurrence and genesis of hydrothermal zeolites and related minerals from the Kuroko-type mineralization areas in Japan: *in* Kallo, D., and Sherry, H. S, eds., Occurrence, Properties, and Utilization of Natural Zeolites: Budapest, Akademiai Kiado, p. 39-48.

Walton, A. W., and Palmer, B. A., 1988, Lahar facies of the Mount Dutton Formation (Oligocene-Miocene) in the Marysvale volcanic field, southwestern Utah: Geological Society of America Bulletin, v. 100, p. 1078-1091.

Waresback, D. B., and Turbeville, B. N., 1990, Evolution of a Plio-Pleistocene volcanogenic-alluvial fan: The Puye Formation, Jemez Mountains, New Mexico: The Geological Society of America Bulletin, v. 102, p. 298-314.

Waples, D. W., 1985, Geochemistry in Petroleum Exploration: Boston, International Human Resources Development Corporation, 180 p.

Weirich, F. H., 1989, The generation of turbidity currents by subaerial debris flows, California: Geological Society of America Bulletin, v. 101, p. 278-291.

White, A. F., Claasen, H. C., and Benson, L. V., 1980, The effect of dissolution of volcanic glass on the water chemistry in a tuffaceous aquifer, Ranier Mesa, Nevada: Geochemistry of water: United States Geological Survey Water-Supply Paper 1535-Q, 34 p.

Williams, L. A., Parks, G. A., and Crerar, D. A., 1985, Silica diagenesis, I. solubility controls: Journal of Sedimentary Petrology, v. 55, p. 301-311.

Wolfe, J. A., and Schorn, H. E., 1989, Paleoecologic, paleoclimatic, and evolutionary significance of the Oligocene Creede flora, Colorado: Paleobiology, v. 15, p. 180-198.

Wood, W. W., and Sanford, W. E., 1990, Ground-water control on evaporite deposition: Economic Geology, v. 85, p. 1226-1235.

Figure Captions

Fig. 1. Generalized geologic map of the Creede caldera and Creede Formation. The locations of measured sections and core sites used in Figure 2 are shown. Sections and localities discussed in the text are also shown.

Fig. 2. Correlation chart of sections and cores in the Creede Formation. Numbers beneath sections indicate the height in the total section relative to core CCM-2. The sections are aligned to the I tuff because it more closely represents a horizontal surface than the base of the Creede Formation.

Fig. 3. A. Laminated siltstone facies in core CCM-2 (562.2-562.5 ft.) interpreted as suspension fallout. cl indicates carbonate lamina; dl indicates detrital lamina; p is a flattened pumice; pai is a pseudomorph after ikaite. B. Graded tuffaceous sandstone facies in core CCM-1 (634.2-634.5 ft.) interpreted as lacustrine turbidites (lt). c is a concretion.

Fig. 4. A. Calcite pseudomorphs after ikaite in a sample taken from a travertine body west of AP-1 (Fig. 1). Radiating orientations of pseudomorphs and ribbed internal structure are similar to Quaternary-age pseudomorphs from western Great Basin, U.S.A. (Shearman and others, 1989). B. Photomicrograph of half of a pseudomorph from a mudstone bed, section AP-1 (Fig. 1). Sand-size hexagonal, rounded, and rhombic calcite grains lie within calcite cement. This replacement texture is typical of pseudomorphs after ikaite (Larsen, 1994b). Scale bar is 0.5 mm; plane-polarized light.

Fig. 5. A. Graded, massive, pebbly sandstone facies interpreted as a sediment-gravity-flow bed (sgf). Scale bar is 15 cm. ic indicates intraclasts; f indicates flame structures at the base of the bed. B. Large-scale cross-bedded calcareous sandstone facies (lccs) interpreted as wave-formed terrace foresets. Increments on staff are 10 cm. C. Horizontal-bedded sandstone (hbs) and low-angle cross-bedded sandstone (lcs) facies interpreted as braided-stream deposits. D. Light-colored, fine-grained tuff facies in core CCM-1 interpreted as fallout tuff (H tuff). The sample on the right is from near the base of a 3-m thick unit, where the beds are turbiditic in character. The middle sample is from the middle of the unit and is crudely bedded to massive. The sample on the left is from the top of the unit and shows convolute bedding (cb). E. Travertine mound showing laminated and stromatolitic travertine facies (lt+st) and massive travertine with pseudomorphs after ikaite (mt+pai). Increments on staff are 10 cm. F. Photomicrograph of travertine showing clumped micritic (cm) and radial-fibrous calcite (rfc) components. Note the fine organic filaments throughout the radial-fibrous calcite. Scale bar is 10 μm; plane-polarized light.

Fig. 6 A. Slump deposits (Sl) composed of suspension lamina and turbiditic facies overlain by undeformed suspension lamina and turbiditic facies (L & T). B. Partial stratigraphic column of section WR-3 showing interbedded suspension lamina, turbiditic, and pebbly sediment-gravity-flow facies.

Fig. 7. Sketch and partial stratigraphic column of section AP-1 (west of CCM-1) showing lacustrine-fan deposits interbedded with lacustrine-profundal deposits.

Fig. 8. Partial stratigraphic column of section CE-3 showing interbedded coarse-grained, lithic-rich sediment-gravity-flow, turbidite, and suspension lamina deposits.

Fig. 9. Fining-upward sections containing fan-delta/alluvial-fan, nearshore, and shoreline deposits. A. Partial stratigraphic column of section 4UR-2 showing sediment-gravity-flow-dominated alluvial-fan/fan-delta deposits capped by nearshore facies association. B. Part of section NPR-2 showing sheetflood-dominated alluvial-fan/fan-delta deposits with braided-stream and wave-worked-terrace deposits.

Fig. 10. Sketch showing relationship between wave-worked-terrace and stream deposits west of the town of Creede. Note deltaic and shoreline deposits overlie nearshore facies.

Fig. 11. Sketch of a fining-upward, alluvial-valley sequence in the Bachelor paleovalley (upper) and rose diagram of channel orientations (lower).

Fig. 12. Sketches showing the distribution of depositional environments during (A) highstand and (B) lowstand lake conditions.

Fig. 13. Sketch showing volcanic, lake-level, and basin-fill history. Dashed part of lake-level history is derived solely from sequences in Bachelor paleovalley and is not corrected relative to CCM-2 stratigraphy. Basin history cross-section represents a schematic north-south cross-section through site CCM-2. Ts is Snowshoe Mountain Tuff, Tov is older volcanic rocks.

Fig. 14. A. Photomicrograph of a fine- to very coarse-grained calcareous sandstone with plagioclase (Pl) and biotite (B) crystals and ash-flow tuff fragments (A-fT) cemented by early calcite and gothic-arch calcite (G-a C); sample LG-1-1. Scale bar is 500 μm. B. Photomicrograph of pyroclasts (Pu) in a silt to medium-grained tuffaceous sandstone; sample WR-1-5. Pipe-vesicle pumice is on left, whereas that on the right is more coarsely vesicular. Scale bar is 50 μm.

Fig. 15. A. Crystal-vitric-lithic ternary diagram. B. Mafic-plagioclase-sanidine & quartz ternary diagram. The mafics include biotite, Fe-Ti oxides, hornblende, and pyroxene. C. Crystal composition of Creede Formation facies and sediment source rocks. Lines connect end-member compositions of ash-flow tuff lithologies. Samples outlined represent compositions that cannot be derived solely by mixing of source rock crystal fragments. The weighting of the sanidine and pyroxene apices serves to increase the sensitivity of the plot and to provide separation between the various ash-flow tuff units. Because of their minor and trace abundance in the Creede strata, relative errors on the pyroxene and sanidine values range from 40 to 100 %.

Fig. 16. Paragenetic sequence of authigenic phases and alteration events.

Fig. 17. A. Photomicrograph of travertine with clotted micrite (CM), radial-fibrous calcite (R-f C), gothic-arch calcite (G-a C), and pore-filling chalcedony; sample CW-1-1. Scale bar is 100 μm. B. Scanning electron microscope (SEM) image of early smectite (S) that lines glassy (Gl) pumice vesicle walls; sample WW-C-1. C. Photomicrograph of a dissolved glass shard filled with pore-lining early smectite (ES), clinoptilolite (Cl), late smectite (LS), and late calcite (C); sample 2R157-A1.0. Authigenic potassium feldspar (Kf) lines pore with remnant clinoptilolite on lower side of shard. Scale bar is 50 μm. D. SEM image of erionite (Er) embedded in and overlying clinoptilolite crystals; sample WC-1-15. E. SEM image of cristobalite (Cr) lepispheres overlying clinoptilolite (Cl); sample 4UR-1-1. F. Photomicrograph of analcime (A) filling a dissolved shard cavity lined with clinoptilolite (Cl) remnants; sample AP-1-1. Scale bar is 25 μm. G. SEM image of clinoptilolite (Cl) serving as a host for growth of authigenic potassium feldspar (Kf); sample WR-3-5. H. SEM image of a pyroxene or amphibole dissolution pore with remnant apatite (Ap) crystals, and partially filled with clinoptilolite (Cl), cristobalite (Cr), and illite (Il); sample LG-K-2. Scale bar is 5 μm.

Fig. 18. A. X-ray diffraction patterns of oriented, Mg- and ethylene glycol-saturated, < 2 μm-fraction mounts illustrating variability in smectite characteristics. B. X-ray diffraction pattern of non-heated (25°C) and heated (450°C) oriented, < 2 μm-fraction mount illustrating Na-K clinoptilolite behavior. C. X-ray diffraction patterns of oriented, Mg- and ethylene glycol-saturated, < 2 μm-fraction mounts illustrating some of the late-paragenetic clay minerals. Peaks are labeled with the d-spacing and mineral identification (Ch - chlorite, Cl - clinoptilolite, Cor - corrensite, Cr - cristobalite, Er - erionite, Il - illite, I/S - illite-smectite mixed-layered clay, K - kaolinite, Ks - K-feldspar, Q - quartz, Sm - smectite).

Fig. 19. A) Percent of interstratified illite in illite-smectite mixed-layered clay and B) delta 2-theta (2θ) values of smectite (< 15 % interstratified illite) from samples

in the northwestern (NW), north-central (NC), and northeastern (NE) parts of the moat. Values are plotted against height in the formation relative to core CCM-2, except for NW where height is relative to core CCM-1.

Fig. 20. A. Backscattered electron image of drusy, banded cristobalite/opal C-T (Cr/O) abruptly terminating against clinoptilolite (Cl), with smectite (S) underlying both phases; sample DLCR-61B. Scale bar is 50 μm. B. Backscattered electron image of chlorite-smectite mixed-layered clay (Ch-S) replacing clinoptilolite (Cl); sample NPR-2-1. Scale bar is 25 μm.

Fig. 21. Tmax values (°C) from anhydrous pyrolysis of organic materials plotted against height in formation for A) core CCM-1 and adjacent sections and B) core CCM-2 and adjacent sections.

Fig. 22. Authigenic mineral distribution in cores and stratigraphic sections. Sample density is > 1 sample per 35 m in the cores and > 1 sample per 10 m in the sections. The distribution of the authigenic mineral associations is also indicated.

Fig. 23. Map distribution of authigenic mineral associations.

Fig. 24. Sketch of a conceptual model for burial diagenesis and superimposed hydrothermal alteration in the Antlers Park area.

Fig. 25. Block diagram showing a conceptual model for diagenesis and hydrothermal alteration (related to the Creede hydrothermal system) in the north-central part of the Creede moat basin. The arrow represents the inferred direction of hydrothermal fluid flow from the hydrothermal system.

TABLE 1: DESCRIPTIONS AND INTERPRETATIONS OF STRATIFIED AND TRAVERTINE DEPOSITIONAL FACIES IN THE CREEDE FORMATION

Facies	Description	Interpretation and modern analogs
Laminated siltstone	Sandy tuffaceous siltstone and carbonate siltstone. Laminae are 0.2 to 10 mm thick and lack grading. Carbonate constituents include micrite, elongate micritic peloids, and calcite pseudomorphs after ikaite. Pyrite commonly lines the lower contact of and is dispersed within lamina. Soft-sedimentary deformation structures (slumps, folds, injection structures, and faults) are present in all siltstone facies.	suspension fallout sedimentation; comparable modern deposits found in Fayetteville Green Lake, NY (Ludlam, 1969), Kamloops Lake, B.C. (Pharo and Carmack, 1979), and Lake Zurich, Switzerland (Kelts and Hsü, 1978). Offset of pyritic laminae by syndepositional faults implies some of the pyrite formed during early diagenesis.
Graded tuffaceous sandstone	Silt to very-coarse-grained, pebbly, laminated and bedded, graded, tuffaceous sandstone. Beds are generally less than 6 cm thick but beds up to 1.5 m are observed. Internal stratification is not prominent in outcrop, but Bouma subdivisions T_a, T_b, T_c, T_d, and T_e are observed in core. Distribution normal grading is ubiquitous. Pumice lapilli, intraclasts, and less-abundant lithic pebbles are generally only present at the base of beds. The bases of beds are usually flat, although loading and flame structures are present where beds overlie laminated facies.	Turbidite deposition based on the grading characteristics (Lowe, 1982), presence of Bouma subdivisions (Middleton, 1970), and intercalation with laminated facies. Graded, structureless turbidites known from numerous modern lakes (Ludlam, 1969; Pharo and Carmack, 1979; Anderson and others, 1985a). Particularly tuffaceous, graded beds with flat bases could also be thin, sublacustrine, fallout tuffs.
Cross-laminated tuffaceous sandstone	Very-fine- to very-coarse-grained, moderately-sorted, wave-ripple and pinch-and-swell cross-laminated sandstone. Descriptive characteristics of the bedforms are presented in Table 3.	Wave-rippled beds have symmetrical, bifurcating crests typically formed under oscillatory flow conditions. Pinch-and-swell beds may form by both wave-related (Smoot and Lowenstein, 1991) or density-current-related (Sturm and Matter, 1978) processes. Sporadic occurrence and relationship to other wave-worked facies suggests an origin due to periodic storm-wave activity
Horizontal-bedded and laminated sandstone	Very-fine- to very-coarse-grained, pebbly, moderately- to poorly-sorted, laminated and bedded sandstone. The moderately-sorted sandstones are generally finer grained and tuffaceous. The poorly sorted sandstones are coarser grained, and contain lithic and pyroclastic grains.	Moderately-sorted units are comparable to sands deposited as sand sheets under upper-flow-regime conditions (Harms and Fahnestock, 1965; Allen, 1984). Poorly-sorted units most likely represent sheetflood deposits laid down in either subaerial or shallow, lacustrine settings, analogous to those described by Blair and MacPherson (1994) and Smoot (1983).
Cross-bedded pebbly sandstone	Fine- to very-coarse-grained, pebbly, moderately- to poorly-sorted, scour-and-fill, low-angle-trough, and planar-cross-bedded sandstone. Beds are composed of lithic and pyroclastic grains, but lack intraclasts.	Scour-and-fill and low-angle-trough cross-beds are similar to low-angle cross-stratified deposits laid down during high-discharge events in shallow, braided streams (Picard and High, 1973). Planar-cross-bedded sandstones likely represent avalanche-face deposition on broad barforms, probably under lower-flow-regime conditions (Harms and Fahnestock, 1965).
Large-scale, planar-cross-bedded pebbly sandstone and conglomerate	Coarse- to very-coarse-grained, moderately-sorted, cross-bedded sandstone and pebble conglomerate in sets up to 1.1 m thick. These facies are usually calcareous; lithic and pyroclastic grains have micritic or oolitic coatings and are cemented with sparry calcite.	Similar deposits are described in lake-margin settings where detritus worked by stream and wave processes cascades down lakeward-dipping foresets (Gilbert, 1890; Smoot and Lowenstein, 1991).
Crudely-bedded, pebble to cobble conglomerate	Sandy, pebble to cobble, poorly-sorted, horizontal-bedded and cross-bedded conglomerate. Individual tabular beds are less than 0.5 m thick, but channel-fill cross-beds are up to 1.0 m thick	Similar deposits are described by Rust (1978) and Gloppen and Steel (1981), and attributed to thalweg or barform deposition in high-gradient channels.
Graded, massive, sandstone and conglomerate	Silt- to very-coarse-grained, very-poorly sorted, pebble sandstone and pebble to boulder conglomerate. Beds are generally tabular and 5 to 50 cm thick, but some channel-fill beds are observed. The bases of beds are commonly flat or undulatory, but loading deformation is present where beds overlie laminated facies.	See below

TABLE 1 (CONT.): DESCRIPTIONS AND INTERPRETATIONS OF STRATIFIED AND TRAVERTINE DEPOSITIONAL FACIES IN THE CREEDE FORMATION

Facies	Description	In
	A) Matrix-supported beds are commonly somewhat pumiceous or contain much intraclast material. Where they are intercalated with laminated facies, they have a distinct grading pattern: coarse-tail reverse grading at the base, coarse-tail normal grading in the middle, and distribution-normal grading in the upper part of the bed.	A) The lack of internal bedding, density grading of clasts, bedding-parallel orientation of flat clasts, and convex-up bed profiles indicate deposition by debris-flow (Lowe, 1979; Smith, 1986; Smith and Lowe, 1991).
	B) Clast-supported conglomerates are chiefly composed of lithic material. Grading is not well-developed, but coarse-tail reverse grading is present in some beds.	B) The lack of internal bedding, weakly developed grading, and protrusion of boulders above the beds surface are also attributed to deposition by debris-flow (Gloppen and Steele, 1981; Walton and Palmer, 1988; Smith and Lowe, 1991). Debris-flows with these characteristics result from high-discharge events in volcanic settings (Arguden and Rodolfo, 1990).
Massive breccia	Sandy, pebble to boulder, very-poorly-sorted, breccia in crude tabular beds up to 2.5 m thick. In a given bed, the clasts are composed of angular to subangular lithic fragments dominantly derived from a single caldera-wall-rock lithology.	The crude bedding, very-poor sorting, and monolithologic character are consistent with colluvial depositional processes on or adjacent to steep slopes (Nelson, 1992). Facies near the base of the Creede Formation possess fractured clasts and blocks up to 35 m across, features typical of landslide or debris-avalanche deposits (Glicken, 1991). These facies lack a significant primary pyroclastic component and probably originated from caldera-wall collapse following caldera formation.
Massive travertine	Micrite, radial-fibrous calcite, and various recrystallization and secondary-mineral phases. The micrite ranges in texture from massive to clotted. Radial-fibrous calcite and micrite combine to form cylindrical structures up to 2.5 mm long and 0.25 mm across. Dark, organic blebs and filaments are present in both the micrite and fibrous calcite; filaments tend to be randomly oriented in the micrite, but oriented length-parallel in the fibrous calcite	The micrite and radial-fibrous calcite resemble precipitates associated with algal (Scholl and Taft, 1964) and bacterial processes (Chafetz and Folk, 1984; Casanova, 1986; Guo and Riding, 1992) in modern spring environments.
Laminated travertine	Micritic to peloidal laminae oriented from horizontal to vertical, the latter being specifically associated with fissure ridges and travertine mound margins. Whereas the horizontal laminae are often graded and interlaminated with tuffaceous material, the vertical laminae show no grading and have indistinct parting. Travertine laminae are observed to grade laterally into laminated siltstone facies.	The vertical and, in part, the horizontal laminae are interpreted as precipitates of algal or bacterial carpets that lined travertine mounds. The graded laminae probably represent re-sedimented material, deposited either within or adjacent to the mounds. Similar facies are also known from largely subaerial deposits at Soda Dam, New Mexico (Goff and Shevenell, 1987) and Mammoth Hot Springs, Wyoming (Bargar, 1978).
Stromatolitic travertine	Facies include laminated travertine that form micro-mound structures (< 1 cm diameter), digitate stromatolites, and oncolites.	Modern lacustrine stromatolites are either directly or indirectly attributed to microbial and/or algal processes (Osborne and others, 1982; Casanova, 1986).
Travertine-cemented sandstone, conglomerate, and breccia	Beds of detrital clasts (lithic, pyroclastic, and travertine) cemented by banded and micritic calcite. Facies are found around the basin margin in crude beds that dip steeply (15 to 30°) away from the moat margin.	Interpreted to represent colluvial and alluvial deposits that were laid down and subsequently cemented in spring environments.

TABLE 2: ORGANIC ANALYSES AND MAGNESIUM CONTENTS OF CALCITE IN STRATIFIED AND TRAVERTINE FACIES

Sample*	Facies	Ht. in Fm. (m)	Wt. % $CaCO_3$	Mole % Mg	Wt. % TOC†	HI§	OI#
2R127-A8.7	lam. siltstone	214.5	33	1.6	N.D.	N.D.	N.D.
2R103-B2.7	lam. siltstone	287.0	17	0.7	2.02**	508	27
2R71-B3.2	lam. siltstone	377.7	26	1.8	1.02**	219	45
DLCR-20	lam. siltstone	416.9	0	N.D.	2.40	119	123
WR-1-11	lam. siltstone	432.8	29	1.2	0.27	329	114
2R50-B1.6	lam. siltstone	438.9	63	2.1	1.76**	525	69
2R34-B0.9	lam. siltstone	478.8	8	N.D.	3.20**	674	64
2R20-B3.1	lam. siltstone	517.7	N.D.	N.D.	1.14**	281	71
2R19-A4.8	lam. siltstone	520.3	N.D.	4.0	N.D.	N.D.	N.D.
NPR-2-3	lam. siltstone	557.3	69	1.8	N.D.	N.D.	N.D.
DLCR-27	lam. travertine	578.0	N.D.	1.1	N.D.	N.D.	N.D.
DLCR-31	lam. siltstone	580.0	80	0.4	0.15	201	128
NPR-M-5	calc. sandstone	N.D.	N.D.	2.3	N.D.	N.D.	N.D.
DLCR-61D	calc. sandstone	N.D.	N.D.	3.3	N.D.	N.D.	N.D.
CW-O-2	lam. siltstone	649.0	76	0.2	0.43	249	125
DLCR-46	lam. siltstone	660.0	N.D.	0.9	N.D.	N.D.	N.D.
Travertine							
LG-I-1	lam. travertine	N.D.	N.D.	0.8	N.D.	N.D.	N.D.
DLCR-35	massive travertine	N.D.	N.D.	1.4	N.D.	N.D.	N.D.
DLCR-37B	massive travertine	N.D.	N.D.	0.7	N.D.	N.D.	N.D.

* 2R-samples are from core CCM-2, others are from surface localities. Excluding the travertine samples, samples are listed in stratigraphic sequence relative to the base of the Formation in CCM-2.

† TOC is the total organic carbon content.

§ HI (Hydrogen Index) is the milligrams of volatile hydrocarbon generated during pyrolysis normalized to the grams of TOC; it represents pre-existing hydrocarbons within the sample.

OI (Oxygen Index) is the milligrams of CO_2 generated during pyrolysis normalized to the grams of TOC; it is a measure of the oxygen content of the kerogen.

** Organic analysis was performed on a carbonate-rich extract from the rock.

TABLE 3: DESCRIPTION AND INTERPRETATION OF FACIES ASSOCIATIONS

Description*	Interpretation
Lacustrine Facies Associations	
Laminated siltstone, graded tuffaceous sandstone, graded massive sandstone and conglomerate, pinch-and-swell sandstone	Lacustrine-profundal
Graded massive sandstone and conglomerate, crudely-bedded conglomerate, graded tuffaceous sandstone, scour-and-fill sandstone, laminated siltstone	Lacustrine-fan
Massive travertine, laminated travertine, stromatolitic travertine, all with pseudomorphs after ikaite	Lacustrine-travertine
Lacustrine-margin and Alluvial Facies Associations	
Graded massive conglomerate and sandstone, horizontal-bedded and scour-and-fill-cross-bedded sandstone, laminated siltstone	Debris-apron
Horizontal-bedded and laminated sandstone, cross-bedded pebbly sandstone, wave-ripple cross-laminated, laminated siltstone with desiccation cracks, graded massive conglomerate and sandstone	Ephemeral-lake
Wave-ripple cross-laminated sandstone, horizontal-bedded and laminated sandstone, graded massive sandstone, planar-cross-bedded sandstone, laminated siltstone	Nearshore
Calcareous large-scale-planar-cross-bedded pebbly sandstone and conglomerate,, horizontal-bedded and scour-and-fill sandstone, crudely-bedded conglomerate	Shoreline
Horizontal-bedded and **cross-bedded pebbly sandstone, crudely-bedded conglomerate,** graded tuffaceous sandstone, laminated siltstone	Gilbert-type-delta
Horizontal-bedded and pebbly cross-bedded sandstone, crudely-bedded conglomerate, graded massive conglomerate, laminated sandstone and siltstone	Alluvial-fan/Fan-delta
Massive breccia, crudely-bedded conglomerate, pebbly cross-bedded and horizontal-bedded sandstone, wave-ripple cross-laminated and laminated sandstone	Alluvial-valley
Massive breccia, graded massive sandstone, and laminated sandstone	Talus-and-landslide
Laminated travertine, travertine-cemented clastic beds, massive travertine	Lacustrine-margin-travertine

* Bold type indicates the major facies in the association.

TABLE 4: POSSIBLE ALTERATION REACTIONS BETWEEN GLASS AND AUTHIGENIC PHASES IN THE CREEDE FORMATION

1)* Glass{1.28 SiO_2, 0.003 TiO_2, 0.143 Al_2O_3, 0.011 FeO, 0.003 MgO, 0.016 CaO, 0.03 Na_2O, 0.048 K_2O}†
+ 0.0323 Ca^{+2} + 0.0012 Ti^{+4} + 0.0520 Fe^{+2} + 0.0474 Mg^{+2} + 0.297 H_2O
$\Rightarrow$ 0.210$(Ca_{0.23}, Na_{0.02}, K_{0.25})(Al_{1.36}, Ti_{0.02}, Fe^{+2}_{0.30}, Mg_{0.24})Si_4O_{10}(OH)_2$ (smectite)§
+ 0.0558 Na^+ + 0.0435 K^+ + 0.441 SiO_2 + 0.174 H^+

2) Glass{1.28 SiO_2, 0.003 TiO_2, 0.143 Al_2O_3, 0.011 FeO, 0.003 MgO, 0.016 CaO, 0.03 Na_2O, 0.048 K_2O}
+ 0.0123 Ca^{+2} + 0.0076 Ti^{+4} + 0.107 Fe^{+2} + 0.0021 Mn^{+2} + 0.112 Mg^{+2} + 0.000114 BaO + 0.0002 O_2
+ 0.667 H_2O
$\Rightarrow$ 0.212$(Ca_{0.06}, Na_{0.11}, K_{0.39})(Al_{1.01}, Ti_{0.05}, Fe^{+2}_{0.55}, Mn_{0.01}, Mg_{0.53})Si_4O_{10}(OH)_2$ (smectite)# +
0.0114$(Ca_{1.37}, Na_{0.51}, K_{0.82}, Mg_{0.20}, Ba_{0.01})(Al_{6.30}, Fe^{+3}_{0.07})Si_{30.12}O_{72}\bullet 20H_2O$ (clinoptilolite)**
+ 0.0309 Na^+ + 0.0039 K^+ + 0.0896 SiO_2 + 0.454 H^+

3) 0.0114$(Ca_{1.37}, Na_{0.51}, K_{0.82}, Mg_{0.20}, Ba_{0.01})(Al_{6.30}, Fe^{+3}_{0.07})Si_{30.12}O_{72}\bullet 20H_2O$ (Clinoptilolite)+ 0.0622 K^+
$\Rightarrow$ 0.0715 $KAlSi_3O_8$ (potassium feldspar) + 0.1273 SiO_2 + 0.0156 Ca^{+2} + 0.0058 Na^+ + 0.0023 Mg^{+2} +
0.0001 Ba^{+2} + 0.0008 Fe^{+3} + 0.217 H_2O + 0.0191 H^+

4) 0.0114$(Ca_{1.37}, Na_{0.51}, K_{0.82}, Mg_{0.20}, Ba_{0.01})(Al_{6.30}, Fe^{+3}_{0.07})Si_{30.12}O_{72}\bullet 20H_2O$ (clinoptilolite) +
0.212$(Ca_{0.06}, Na_{0.11}, K_{0.39})(Al_{1.01}, Ti_{0.05}, Fe^{+2}_{0.55}, Mn_{0.01}, Mg_{0.53})Si_4O_{10}(OH)_2$ (smectite)
+ 0.0383 Na^+ + 0.0202 Fe^{+2} + 0.1707 Fe^{+3} + 0.00198 Mn^{+2} +0.0543 Mg^{+2} + 0.339 H_2O
$\Rightarrow$ 0.00492 $Na_{10\,79}(Fe^{+3}_{0\,10}, Al_{14\,60})Si_{34\,28}O_{96}$ (analcime)†† +
0.0684$(Ca_{0.11}, Na_{0.21}, K_{0.02})(Fe^{+2}_{2\,00}, Fe^{+3}_{2\,50}, Mn_{0\,06}, Mg_{2.47}, Al_{0.53})(Al_{2.6}, Ti_{0.07}, Si_{5.33})O_{20}(OH)_8$
(smectite-chlorite mixed-layered clay)§§ + 0.0208 Ca^{+2} + 0.0907 K^+ + 0.00581 Ti^{+4} + 0.658 SiO_2 + 0.000114 BaO + 0.555 H^+

* - Reactions written assuming conservation of aluminum in the solid phases.

† - Analytical totals for the glass range from 89.00 to 92.20 weight %. Composition is the average of 10 data points from sample 4UR-U-1.

§ - Analytical totals are between 60.00 and 80.00 %; thus, the analyses only approximate the composition of smectite. Composition is the average of 8 data points from sample 4UR-U-1.

- Analytical totals are between 65.00 and 80.00 %; thus the analyses only approximate the composition of smectite. Composition is the average of 8 data points from sample 2R3-A1.5.

** - Analytical totals are greater than 80.00 %. Composition is the average of 4 data points from sample 2R3-A1.5.

†† - Analytical total is 87.00 %. Composition is representative of the average of 11 analyses from sample 1R16-A1.5.

§§- Analytical total is 67.00 %; thus, the analysis only approximates the composition of smectite-chlorite mixed-layered clay. Note also that iron was partitioned into equal ferric and ferrous components as indicated in Newman and Brown (1987). Composition is representative of the average of 5 data points from sample 1R16-A7.0.

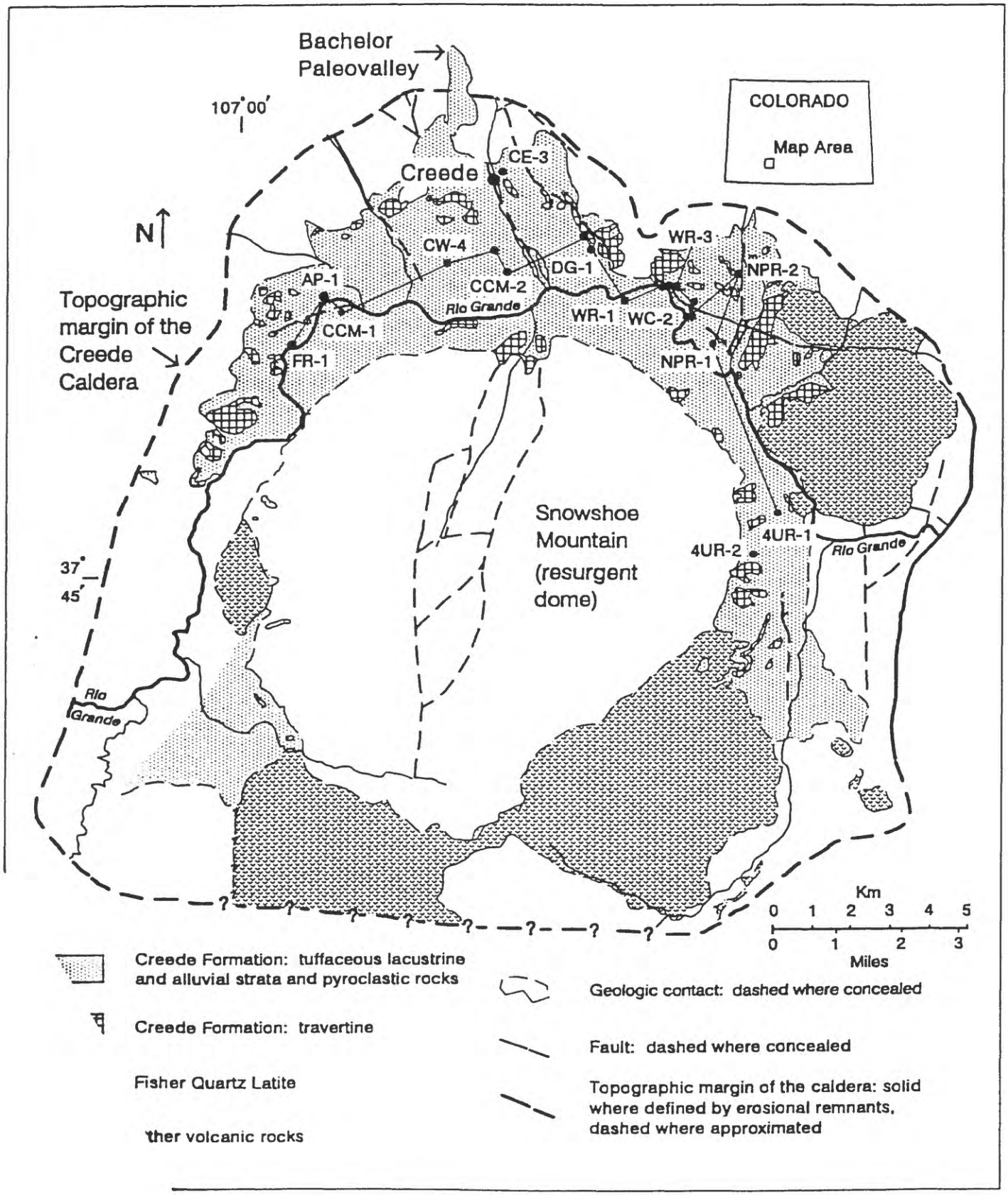
Bachelor
Paleovalley
107°00'
COLORADO
Map Area
Creede
CE-3
N
CW-4
WR-3
NPR-2
DG-1
AP-1
CCM-2
Rio Grande
Topographic
margin of the
Creede
Caldera
WR-1
WC-2
CCM-1
FR-1
NPR-1
Snowshoe
Mountain
(resurgent
dome)
4UR-1
4UR-2
Rio Grande
37°
45'
Rio
Grande
Km
0 1 2 3 4 5
0 1 2 3
Miles
Creede Formation: tuffaceous lacustrine and alluvial strata and pyroclastic rocks
Creede Formation: travertine
Fisher Quartz Latite
ther volcanic rocks
Geologic contact: dashed where concealed
Fault: dashed where concealed
Topographic margin of the caldera: solid where defined by erosional remnants, dashed where approximated

Figure 1

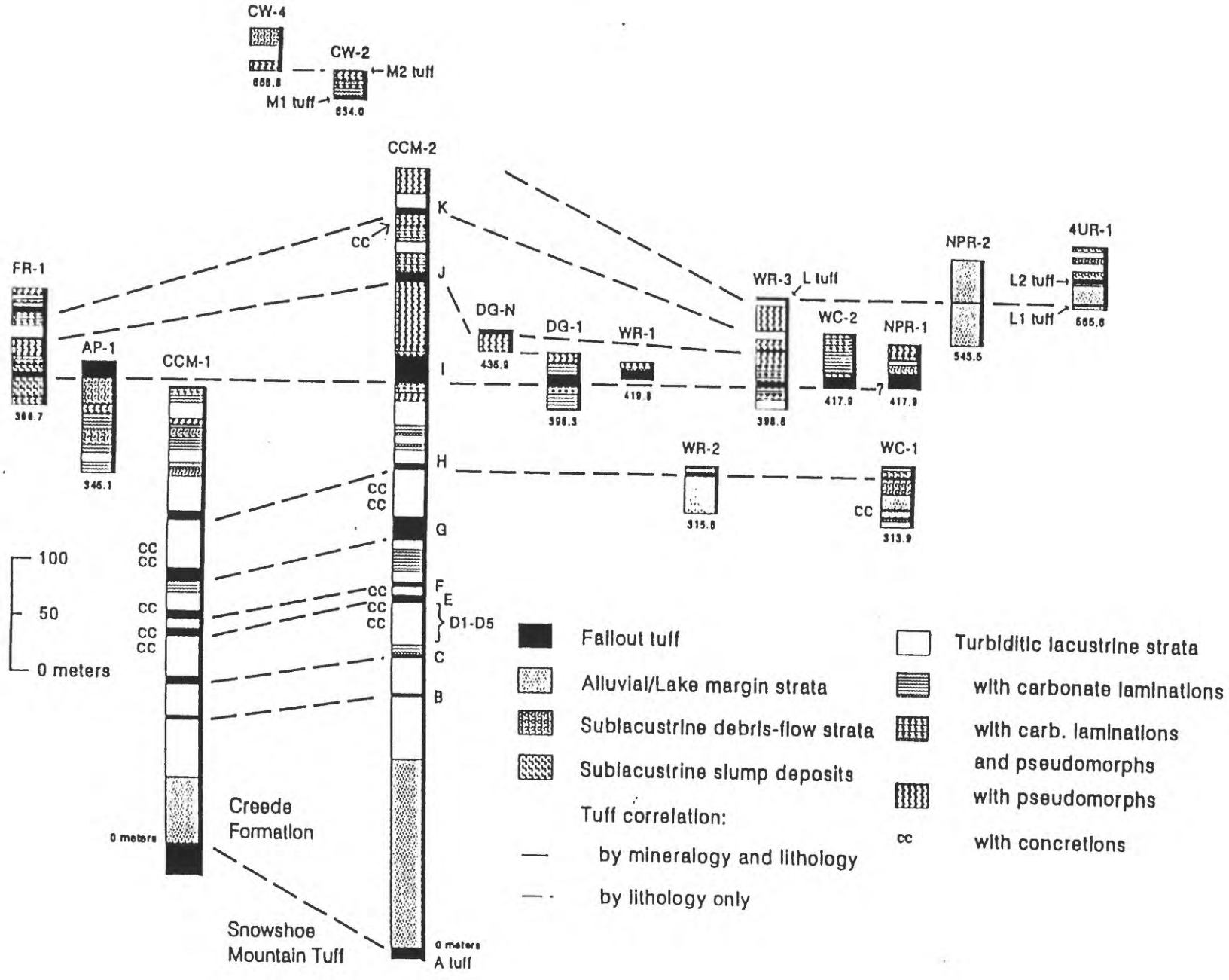
CW-4
CW-2
M2 tuff
M1 tuff
CCM-2
K
J
I
H
G
F
E
D1-D5
C
B
A tuff
CC
FR-1
AP-1
CCM-1
DG-N
DG-1
WR-1
WR-3
L tuff
WC-2
NPR-1
NPR-2
L2 tuff
L1 tuff
4UR-1
WR-2
WC-1
100
50
0 meters
Creede Formation
Snowshoe Mountain Tuff
Fallout tuff
Alluvial/Lake margin strata
Sublacustrine debris-flow strata
Sublacustrine slump deposits
Tuff correlation:
by mineralogy and lithology
by lithology only
Turbiditic lacustrine strata
with carbonate laminations
with carb. laminations and pseudomorphs
with pseudomorphs
with concretions

Figure 2

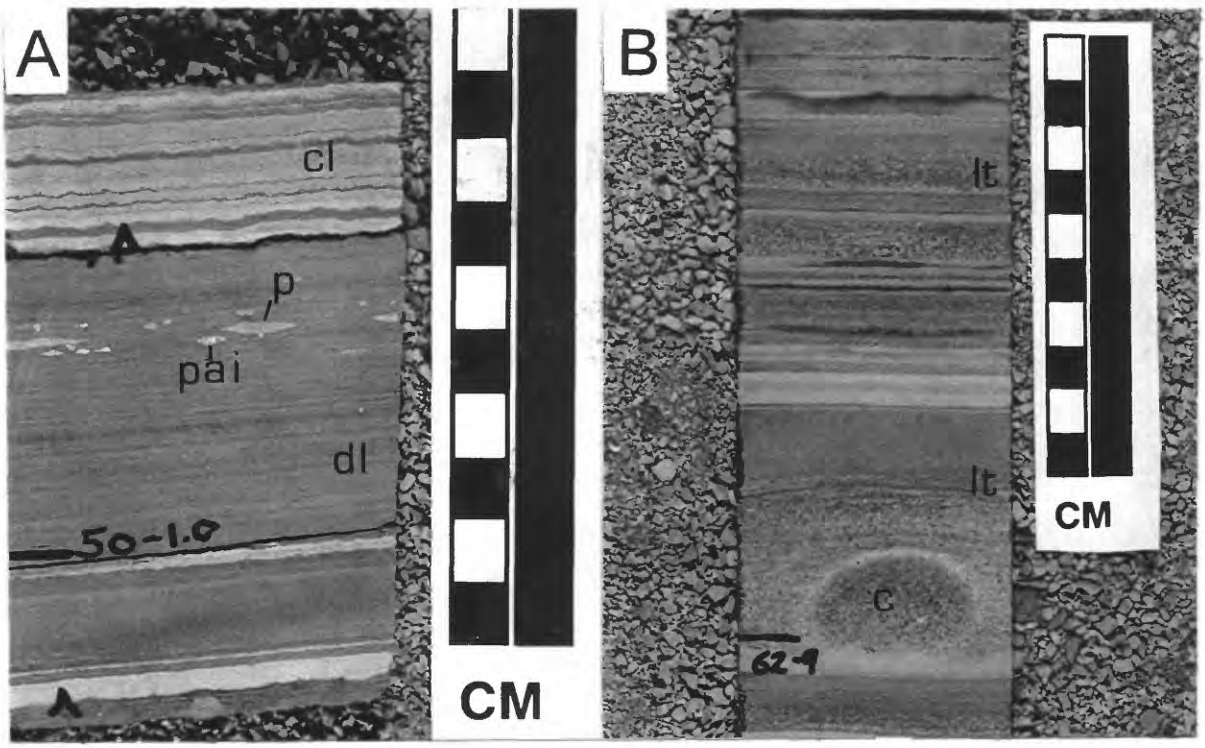

Figure 3

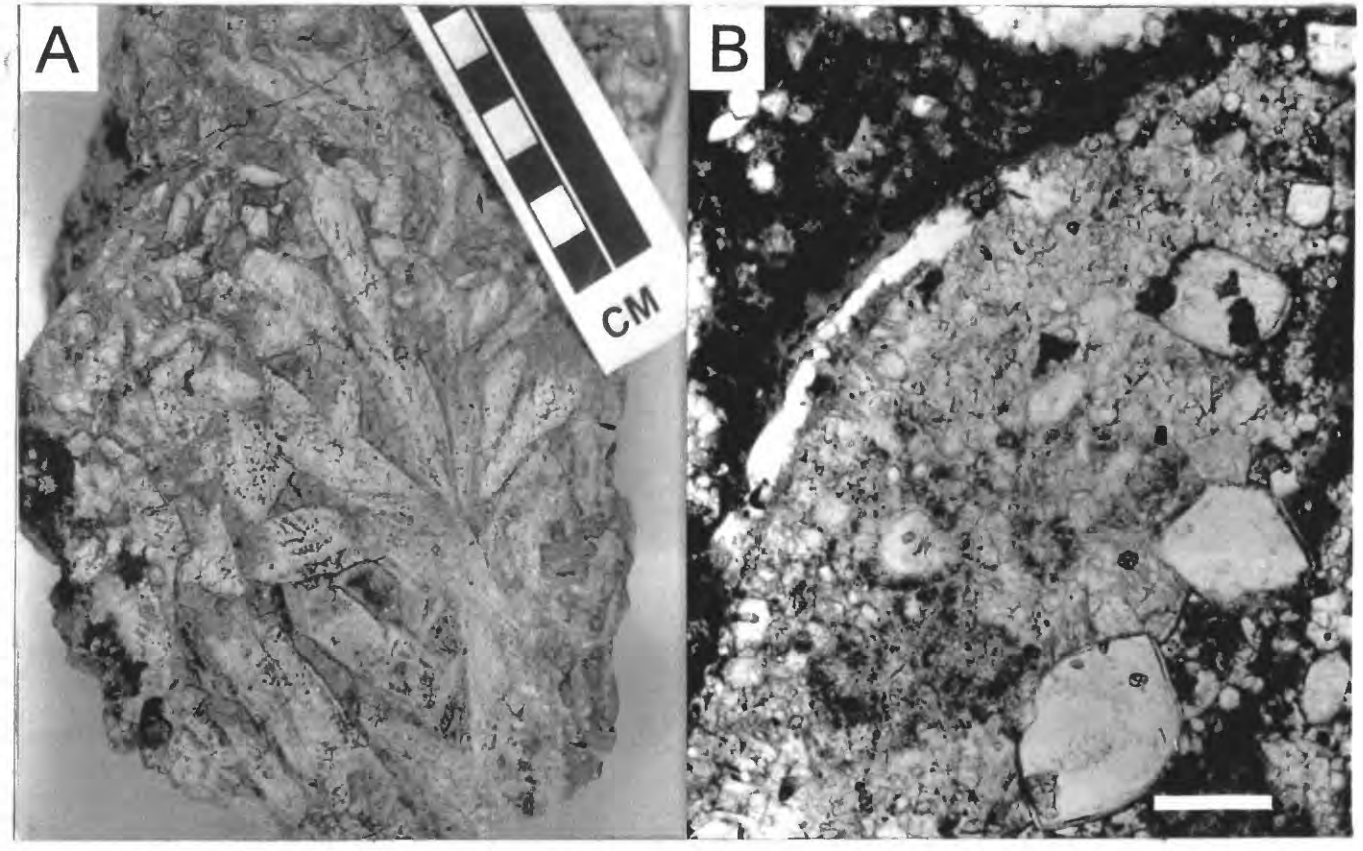

Figure 4

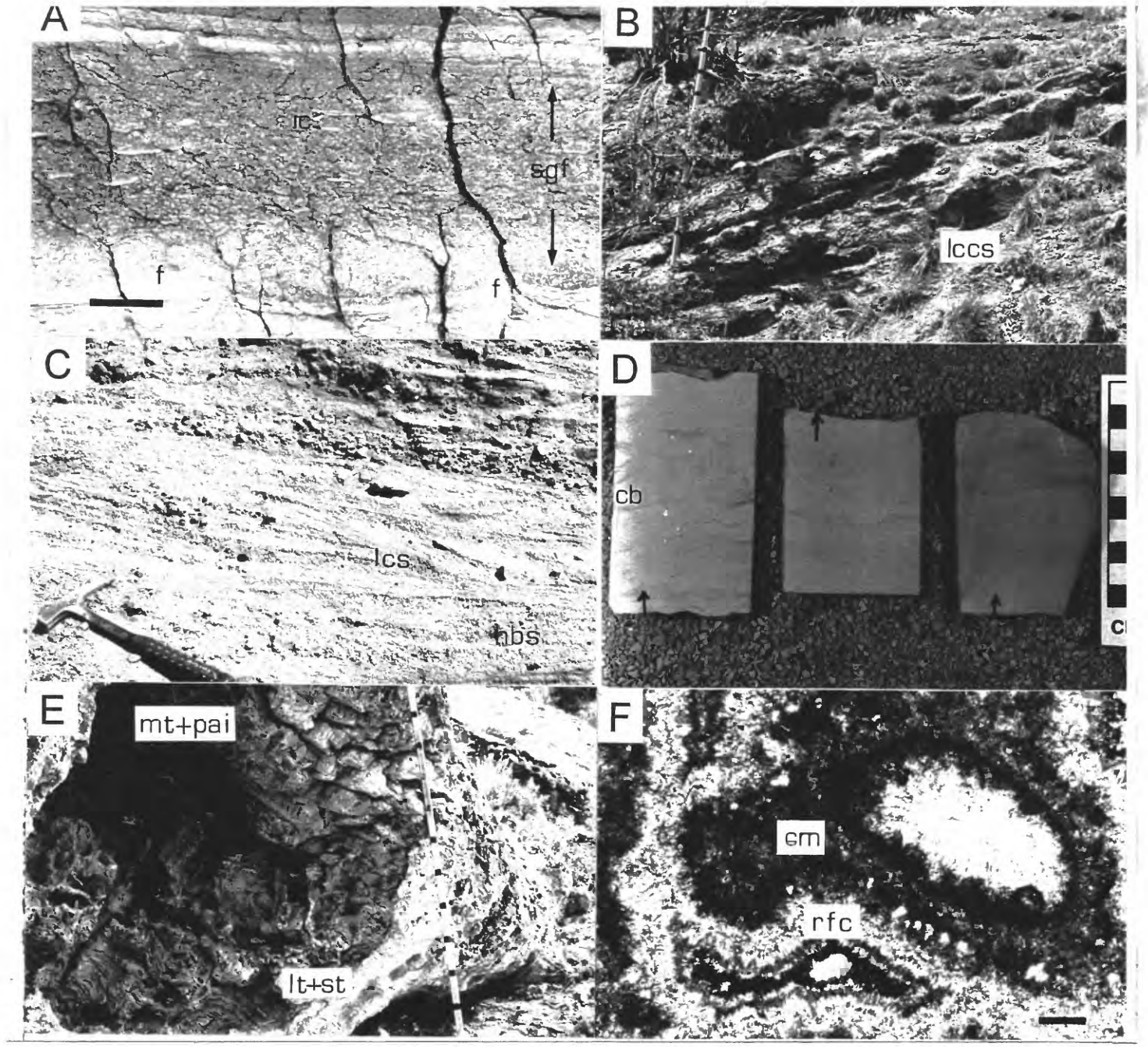

Figure 5

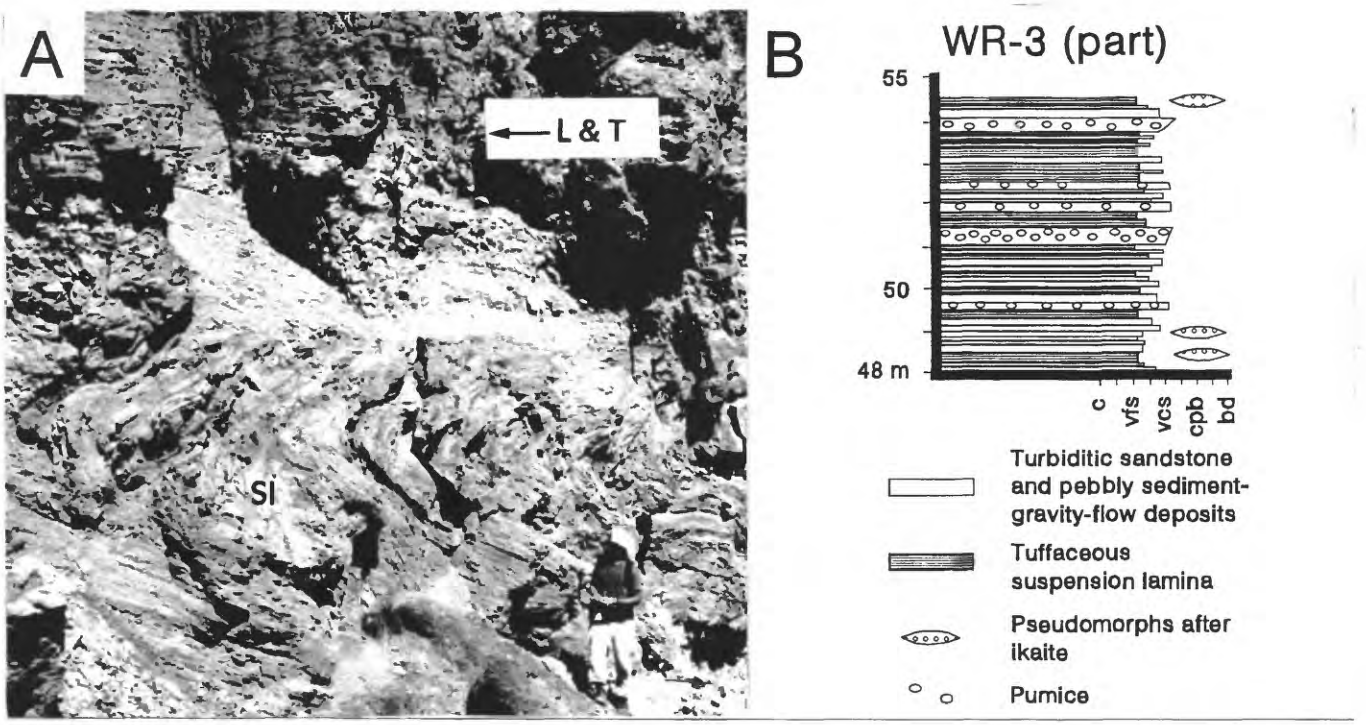
A
L & T
SI
B
WR-3 (part)
55
50
48 m
c
vfs
vcs
cpb
bd
Turbiditic sandstone and pebbly sediment-gravity-flow deposits
Tuffaceous suspension lamina
Pseudomorphs after ikaite
Pumice

Figure 6

AP-1 (part)
slump folds
Turbiditic sandstone and pebbly sediment-gravity-flow deposits
Tuffaceous suspension lamina
Carbonate and tuffaceous suspension lamina
Pseudomorphs After ikaite
Flame structure
Detrital rip-up clasts
Pumice
Lithic pebbles
38
35
30
25
20
16 m
slump folds
vfs
vcs
cpb
bd
slump folds and debris-flow deposit
Lacustrine Fan Lobe
Turbiditic and Suspension Lamina Deposits
20 m

Figure 7

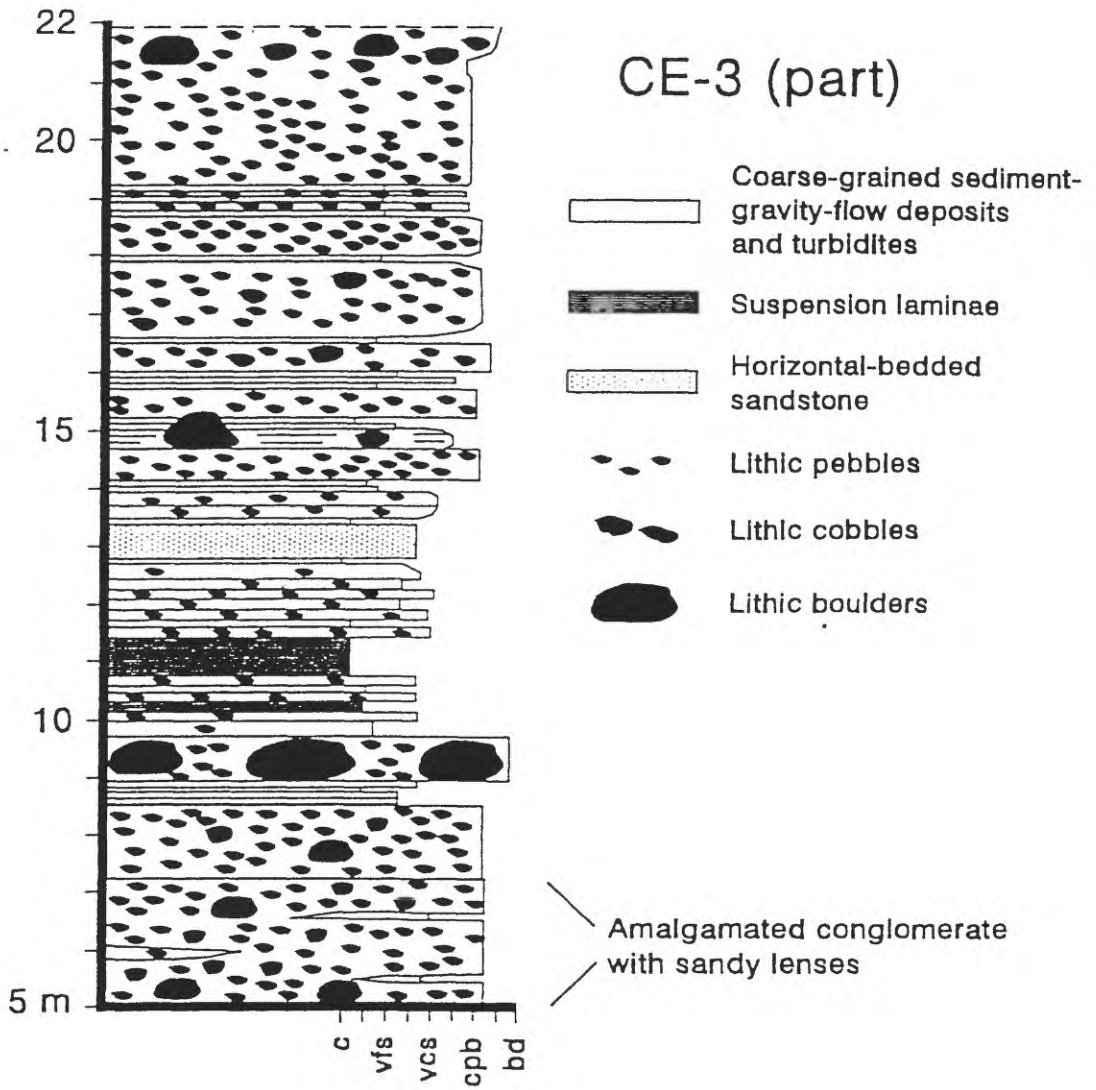
22
20
15
10
5 m
c
vfs
vcs
cpb
bd
CE-3 (part)
Coarse-grained sediment-gravity-flow deposits and turbidites
Suspension laminae
Horizontal-bedded sandstone
Lithic pebbles
Lithic cobbles
Lithic boulders
Amalgamated conglomerate with sandy lenses

Figure 8

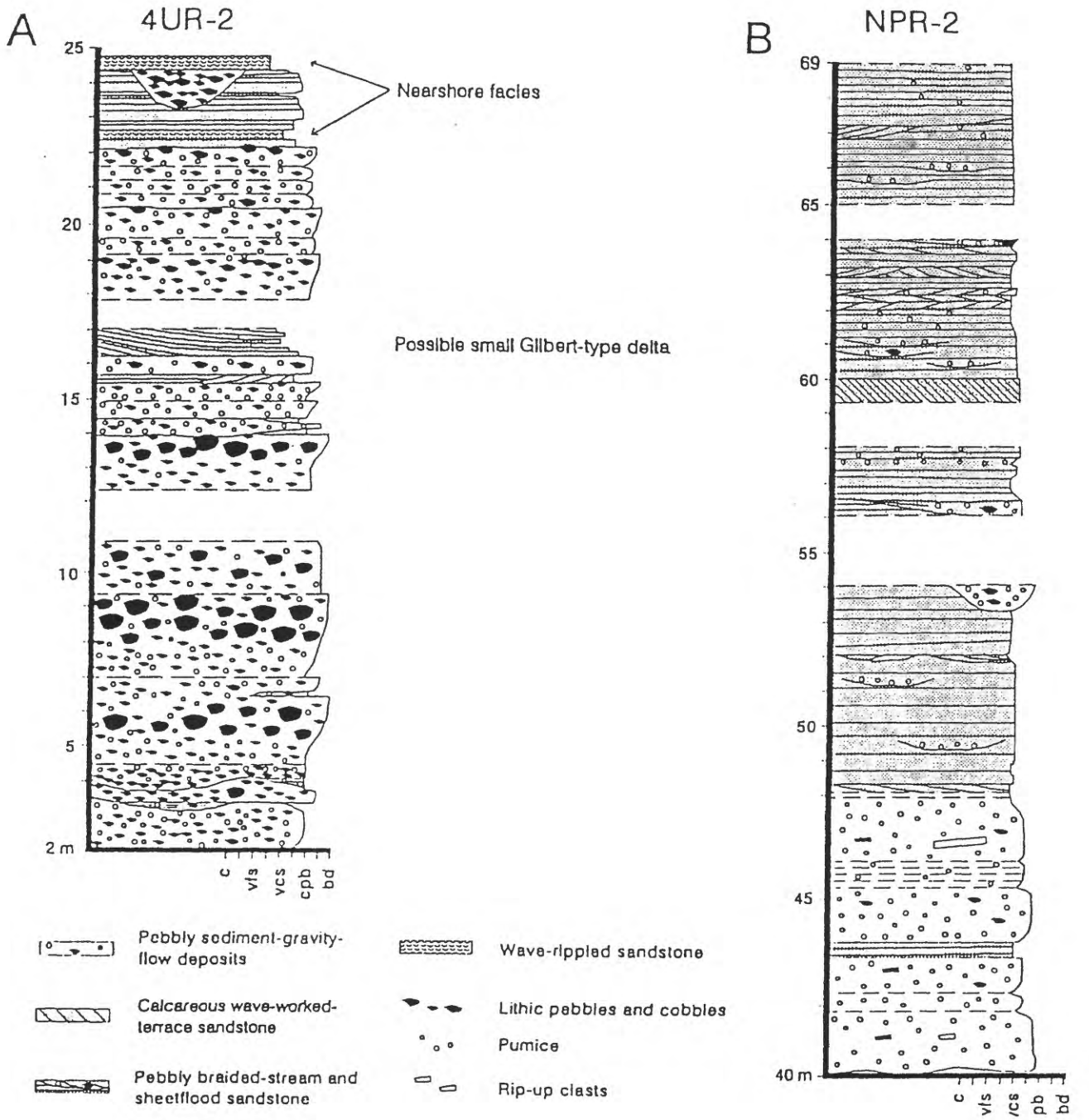
A
4UR-2
25
20
15
10
5
2 m
Nearshore facies
Possible small Gilbert-type delta
c
vfs
vcs
cpb
bd
Pebbly sediment-gravity-flow deposits
Calcareous wave-worked-terrace sandstone
Pebbly braided-stream and sheetflood sandstone
Wave-rippled sandstone
Lithic pebbles and cobbles
Pumice
Rip-up clasts
B
NPR-2
69
65
60
55
50
45
40 m
c
vfs
vcs
pb
bd

Figure 9

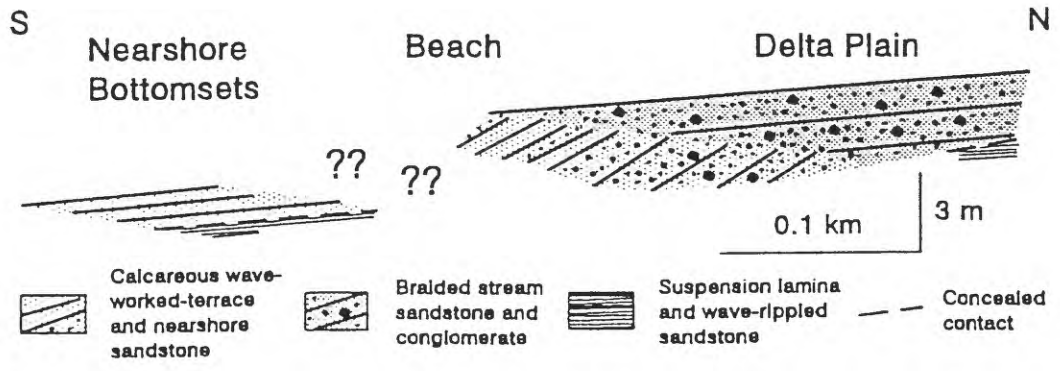
S
N
Nearshore
Bottomsets
Beach
Delta Plain
??
??
0.1 km
3 m
Calcareous wave-worked-terrace and nearshore sandstone
Braided stream sandstone and conglomerate
Suspension lamina and wave-rippled sandstone
Concealed contact

Figure 10

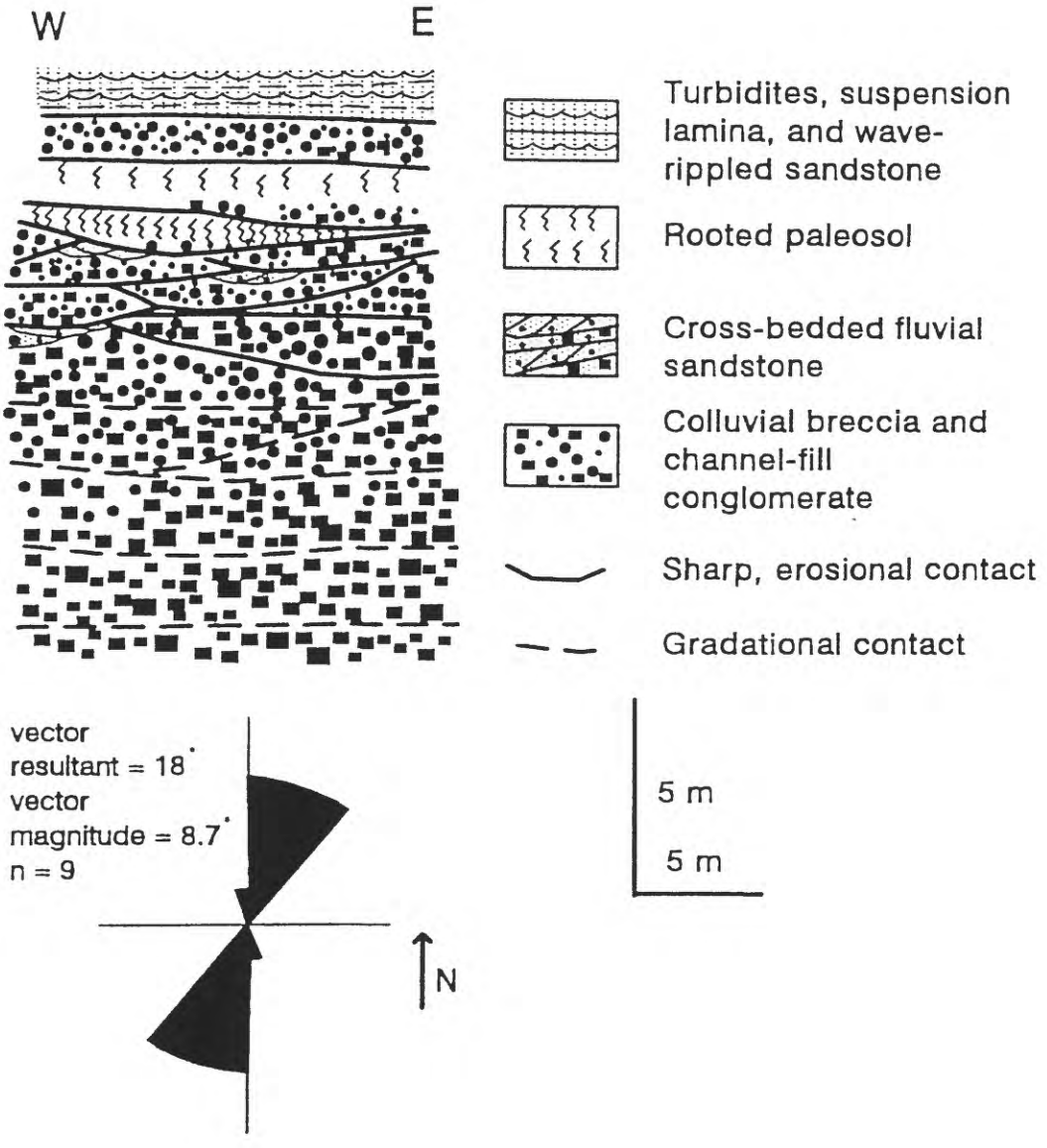
W
E
Turbidites, suspension lamina, and wave-rippled sandstone
Rooted paleosol
Cross-bedded fluvial sandstone
Colluvial breccia and channel-fill conglomerate
Sharp, erosional contact
Gradational contact
5 m
5 m
vector resultant = 18°
vector magnitude = 8.7°
n = 9
N

Figure 11

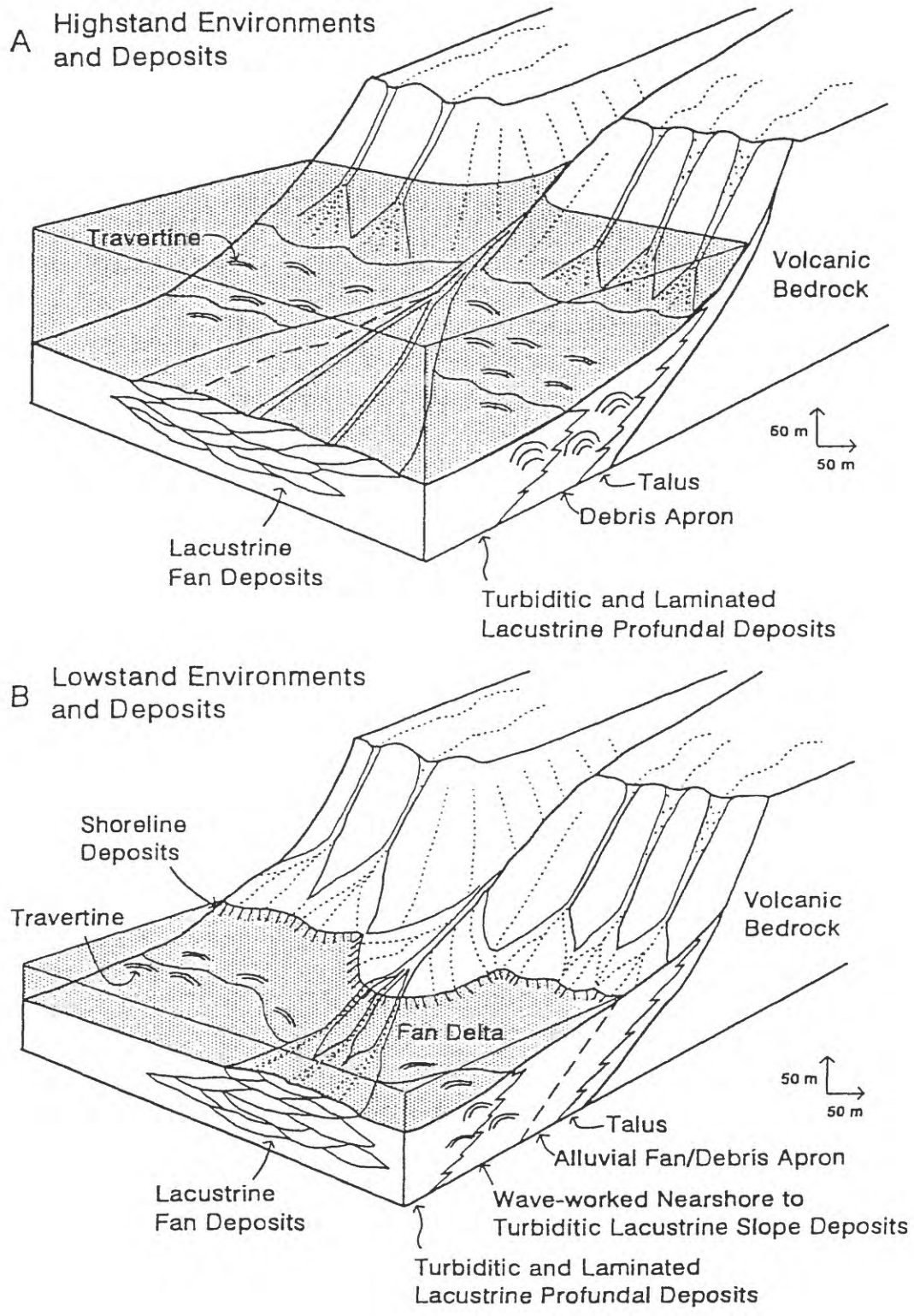
A Highstand Environments and Deposits
Travertine
Volcanic Bedrock
60 m
50 m
Talus
Debris Apron
Lacustrine Fan Deposits
Turbiditic and Laminated Lacustrine Profundal Deposits
B Lowstand Environments and Deposits
Shoreline Deposits
Travertine
Volcanic Bedrock
Fan Delta
50 m
50 m
Talus
Alluvial Fan/Debris Apron
Lacustrine Fan Deposits
Wave-worked Nearshore to Turbiditic Lacustrine Slope Deposits
Turbiditic and Laminated Lacustrine Profundal Deposits

Figure 12

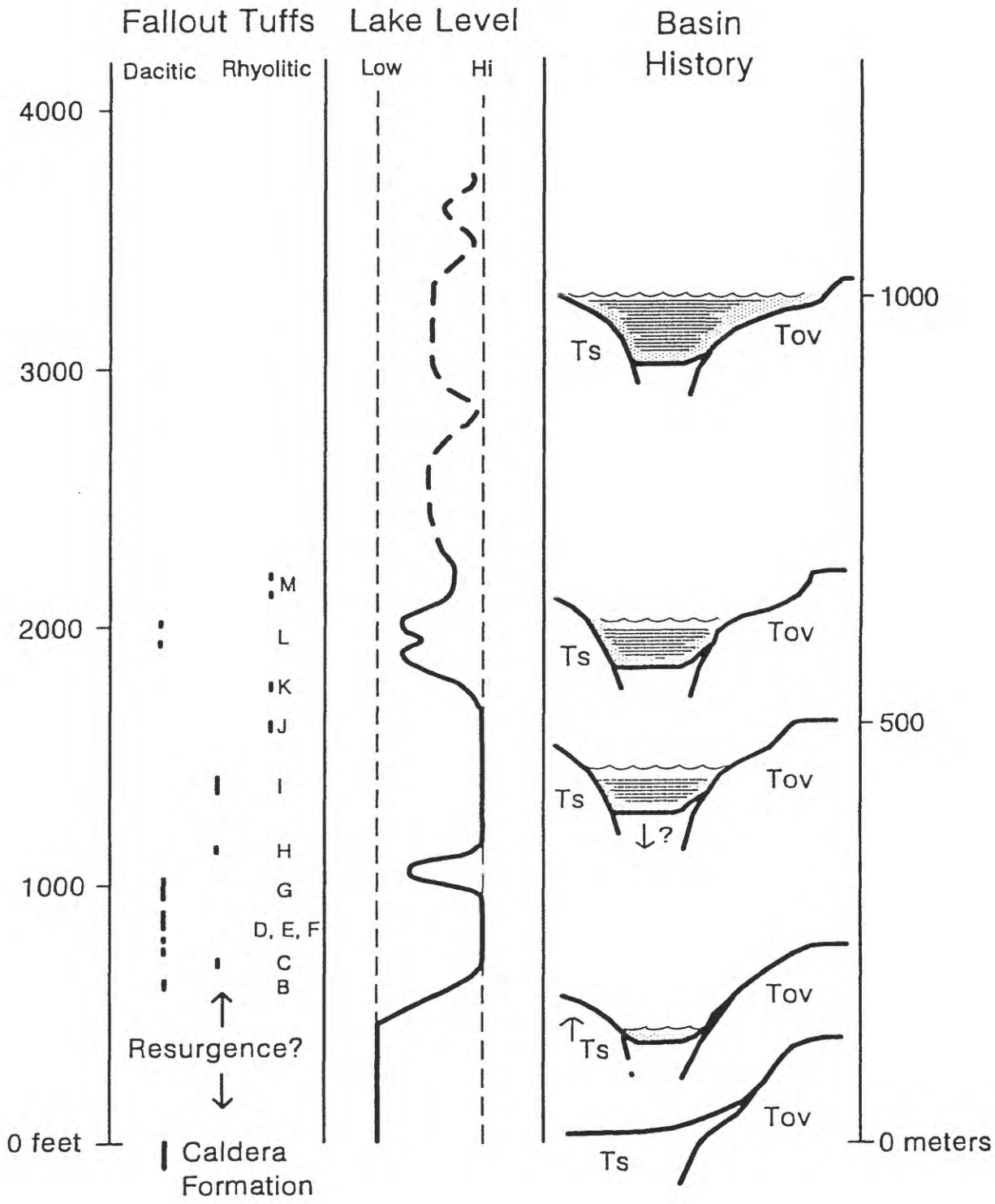
Fallout Tuffs
Lake Level
Basin History
Dacitic
Rhyolitic
Low
Hi
4000
3000
2000
1000
0 feet
M
L
K
J
I
H
G
D, E, F
C
B
Resurgence?
Caldera Formation
Ts
Tov
1000
500
0 meters
↓?

Figure 13

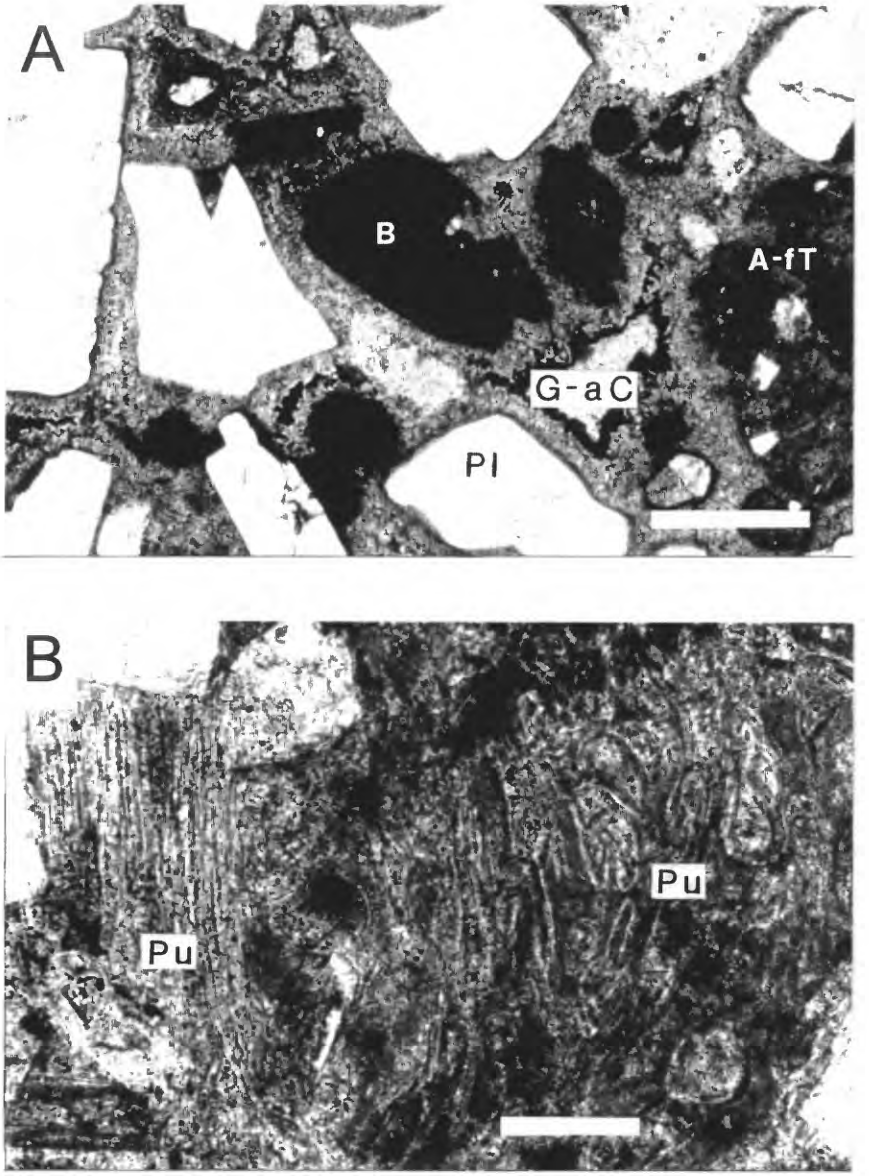

Figure 14

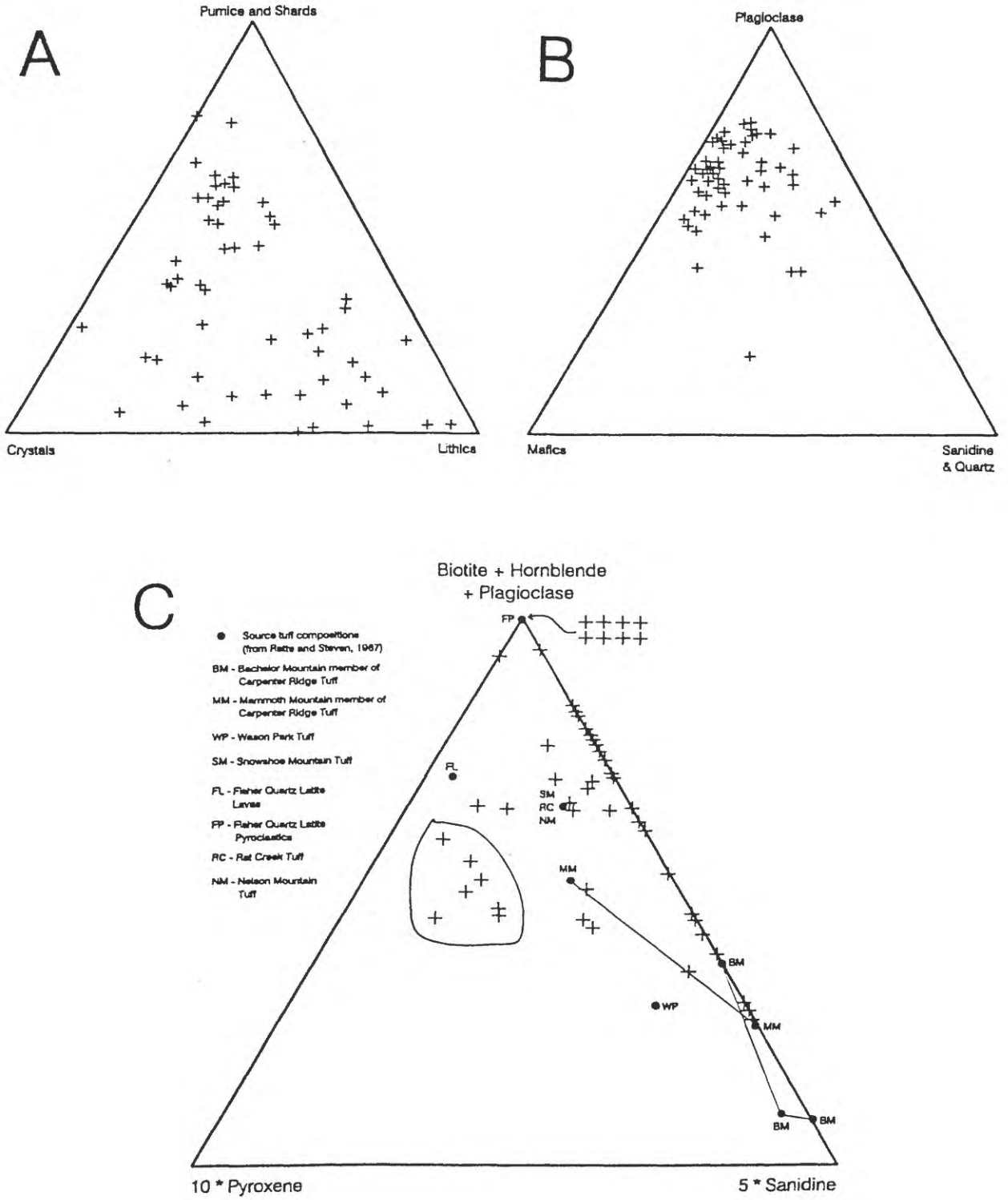
A
Pumice and Shards
Crystals
Lithics
B
Plagioclase
Mafics
Sanidine
& Quartz
C
Biotite + Hornblende
+ Plagioclase
Source tuff compositions
(from Ratte and Steven, 1967)
BM - Bachelor Mountain member of Carpenter Ridge Tuff
MM - Mammoth Mountain member of Carpenter Ridge Tuff
WP - Wason Park Tuff
SM - Snowshoe Mountain Tuff
FL - Fisher Quartz Latite Lavas
FP - Fisher Quartz Latite Pyroclastics
RC - Rat Creek Tuff
NM - Nelson Mountain Tuff
FP
FL
SM
RC
NM
MM
BM
WP
MM
BM
BM
10 * Pyroxene
5 * Sanidine

Figure 15

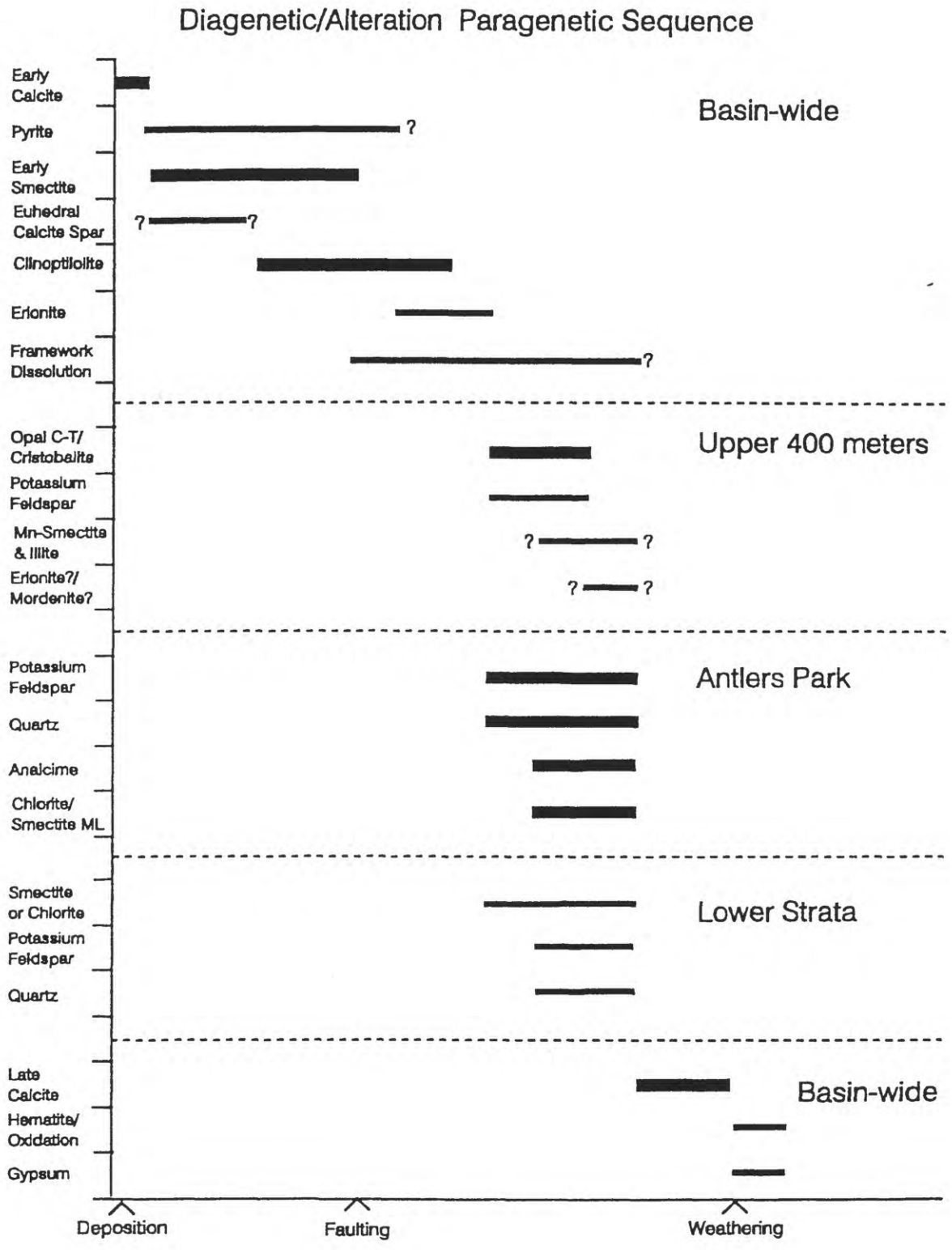
Diagenetic/Alteration Paragenetic Sequence
Early Calcite
Pyrite
Early Smectite
Euhedral Calcite Spar
Clinoptilolite
Erionite
Framework Dissolution
Basin-wide
Opal C-T/ Cristobalite
Potassium Feldspar
Mn-Smectite & Illite
Erionite?/ Mordenite?
Upper 400 meters
Potassium Feldspar
Quartz
Analcime
Chlorite/ Smectite ML
Antlers Park
Smectite or Chlorite
Potassium Feldspar
Quartz
Lower Strata
Late Calcite
Hematite/ Oxidation
Gypsum
Basin-wide
Deposition
Faulting
Weathering

Figure 16

A
CM
R-fC
B
S
GI
01000 15KU 50U
C
LS
C
Cl
ES
K-f
D
Cl
Cr
11508 15KU
E
Cr
Cl
11002 15KU 5U
F
A
Cl
G
Cl
Kf
H
Ap
Cl
Cr

Figure 17

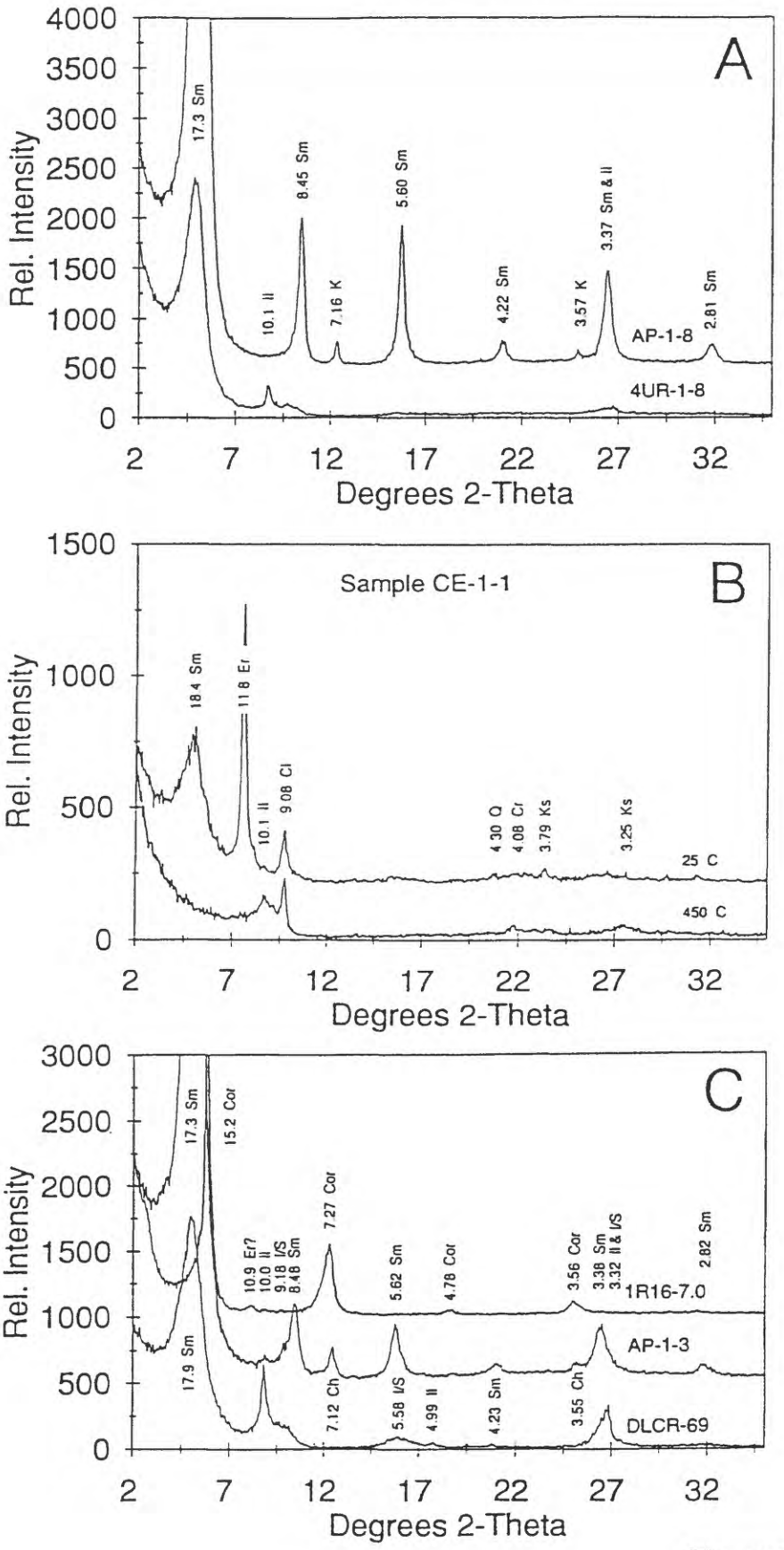
A
Rel. Intensity
Degrees 2-Theta
17.3 Sm
10.1 Il
8.45 Sm
7.16 K
5.60 Sm
4.22 Sm
3.57 K
3.37 Sm & Il
2.81 Sm
AP-1-8
4UR-1-8
B
Sample CE-1-1
18.4 Sm
11.8 Er
10.1 Il
9.08 Cl
4.30 Q
4.08 Cr
3.79 Ks
3.25 Ks
25 C
450 C
C
17.3 Sm
15.2 Cor
10.9 Er?
10.0 Il
9.18 I/S
8.48 Sm
7.27 Cor
5.62 Sm
4.78 Cor
3.56 Cor
3.38 Sm
3.32 Il & I/S
2.82 Sm
1R16-7.0
17.9 Sm
7.12 Ch
5.58 I/S
4.99 Il
4.23 Sm
3.55 Ch
AP-1-3
DLCR-69

Figure 18

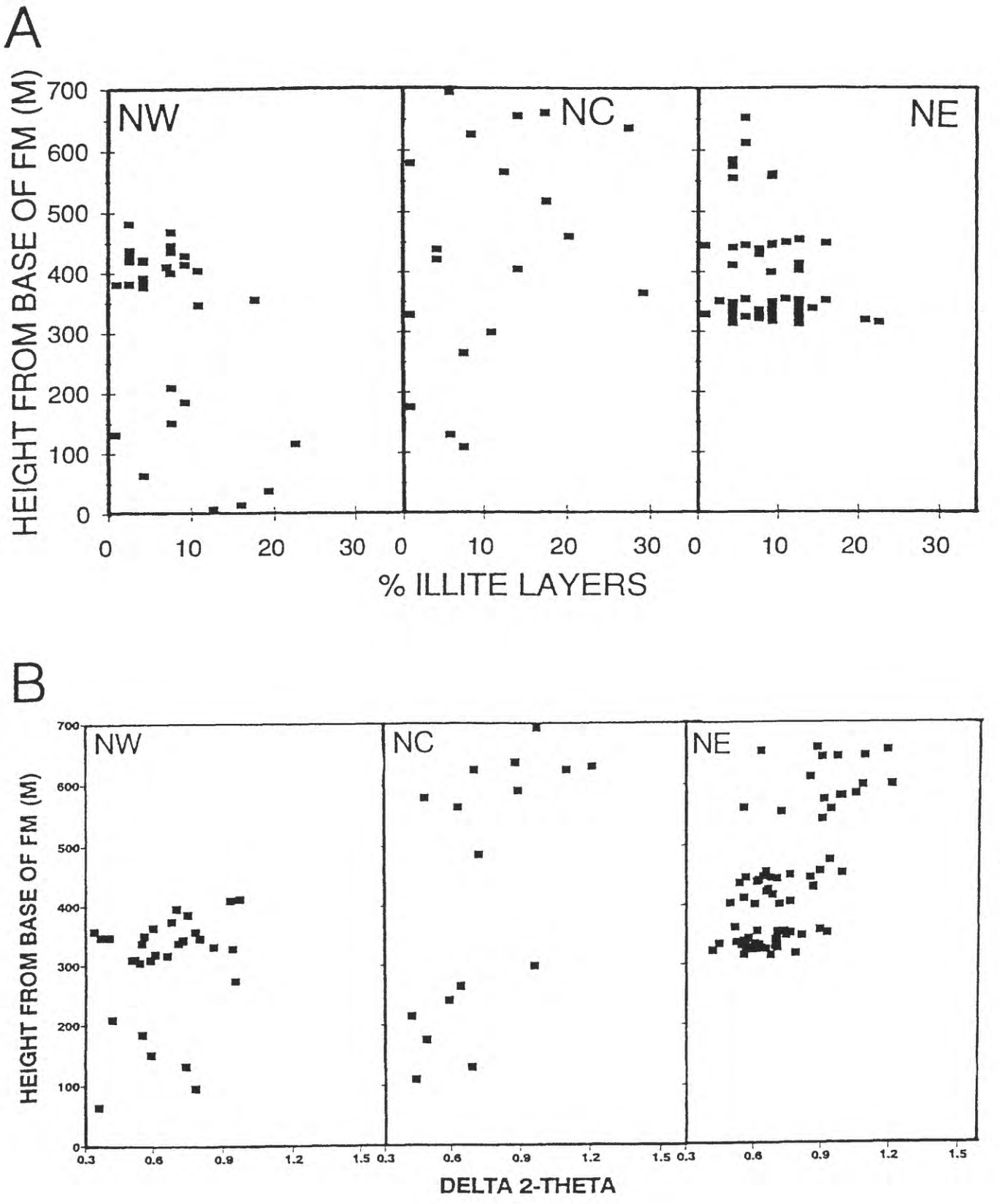
A
NW
NC
NE
HEIGHT FROM BASE OF FM (M)
0
100
200
300
400
500
600
700
0
10
20
30
% ILLITE LAYERS
B
NW
NC
NE
HEIGHT FROM BASE OF FM (M)
0.3
0.6
0.9
1.2
1.5
DELTA 2-THETA

Figure 19

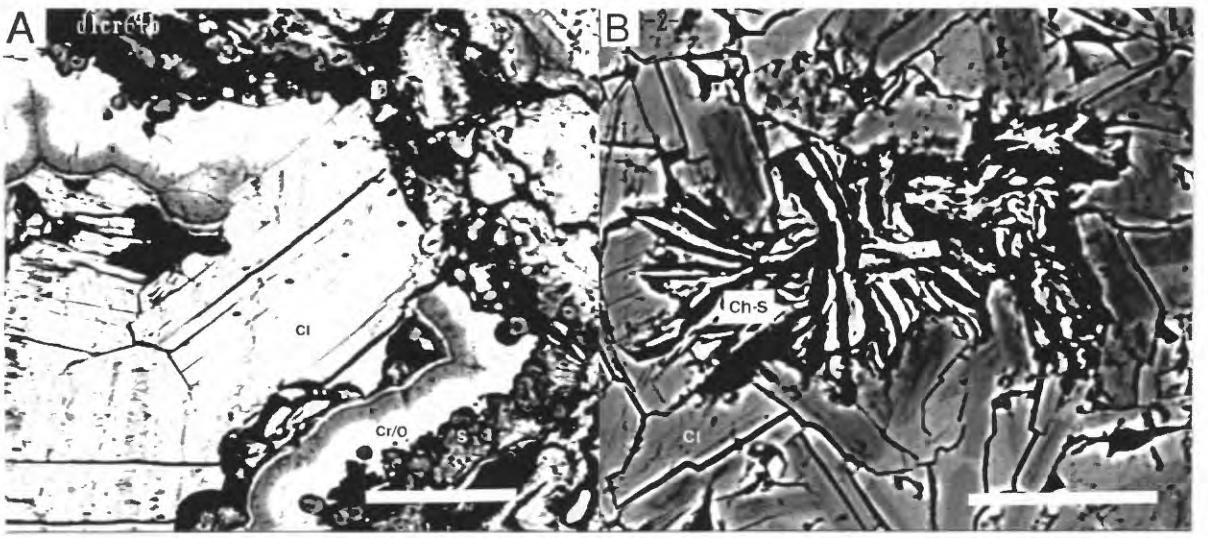

Figure 20

A
B
Height in Formation (M)
700
560
420
280
140
0
400
420
440
460
480
500
400
420
440
460
480
500
Tmax °C

Figure 21

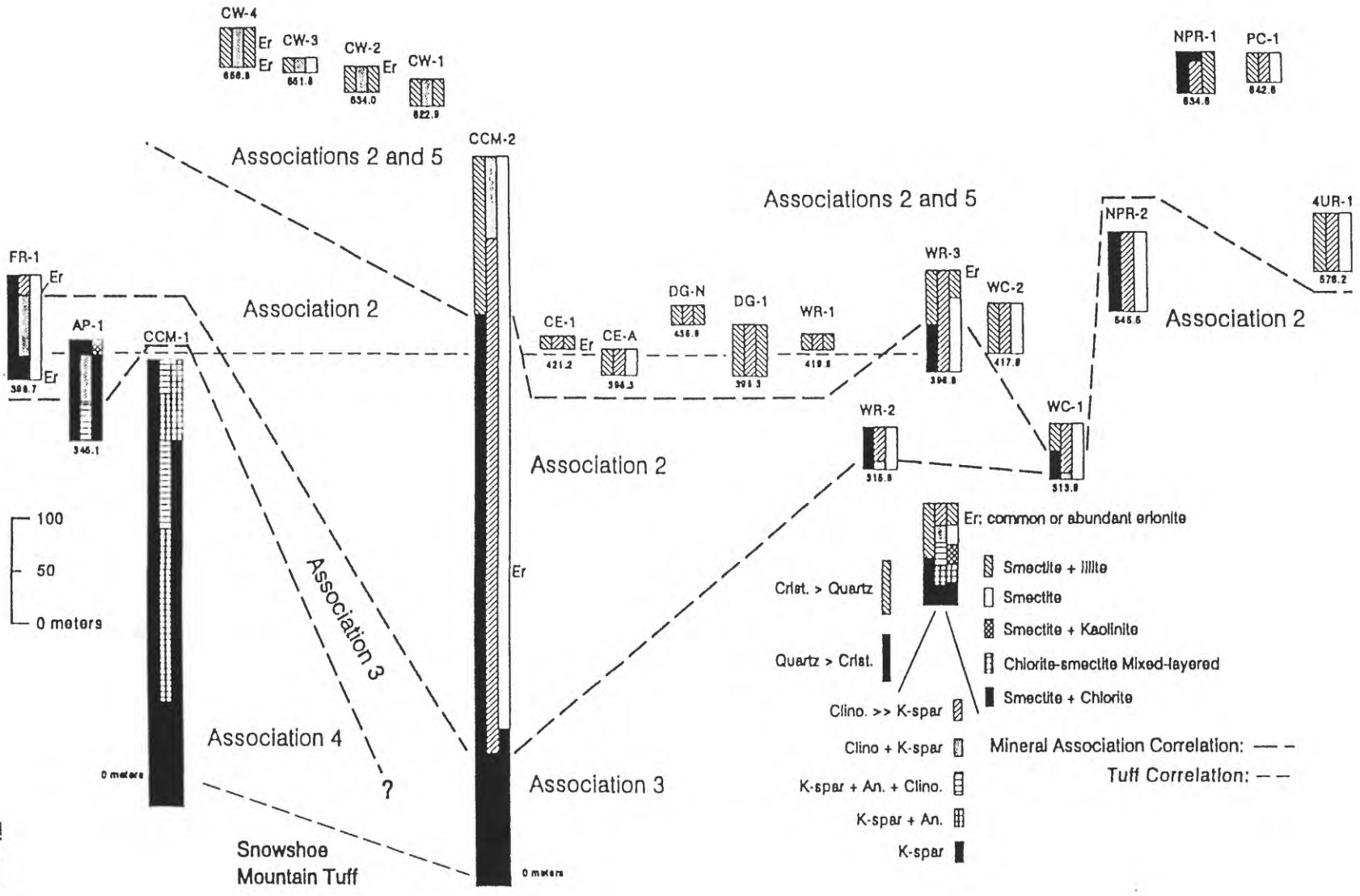
CW-4
CW-3
CW-2
CW-1
Er
NPR-1
PC-1
Associations 2 and 5
CCM-2
Associations 2 and 5
FR-1
AP-1
CCM-1
Association 2
CE-1
CE-A
DG-N
DG-1
WR-1
WR-3
WC-2
NPR-2
4UR-1
Association 2
WR-2
WC-1
Association 2
100
50
0 meters
Association 3
Association 4
Er
Association 3
?
Snowshoe
Mountain Tuff
Er: common or abundant erionite
Cryst. > Quartz
Quartz > Cryst.
Smectite + Illite
Smectite
Smectite + Kaolinite
Chlorite-smectite Mixed-layered
Smectite + Chlorite
Clino. >> K-spar
Clino + K-spar
K-spar + An. + Clino.
K-spar + An.
K-spar
Mineral Association Correlation:
Tuff Correlation:

Figure 22

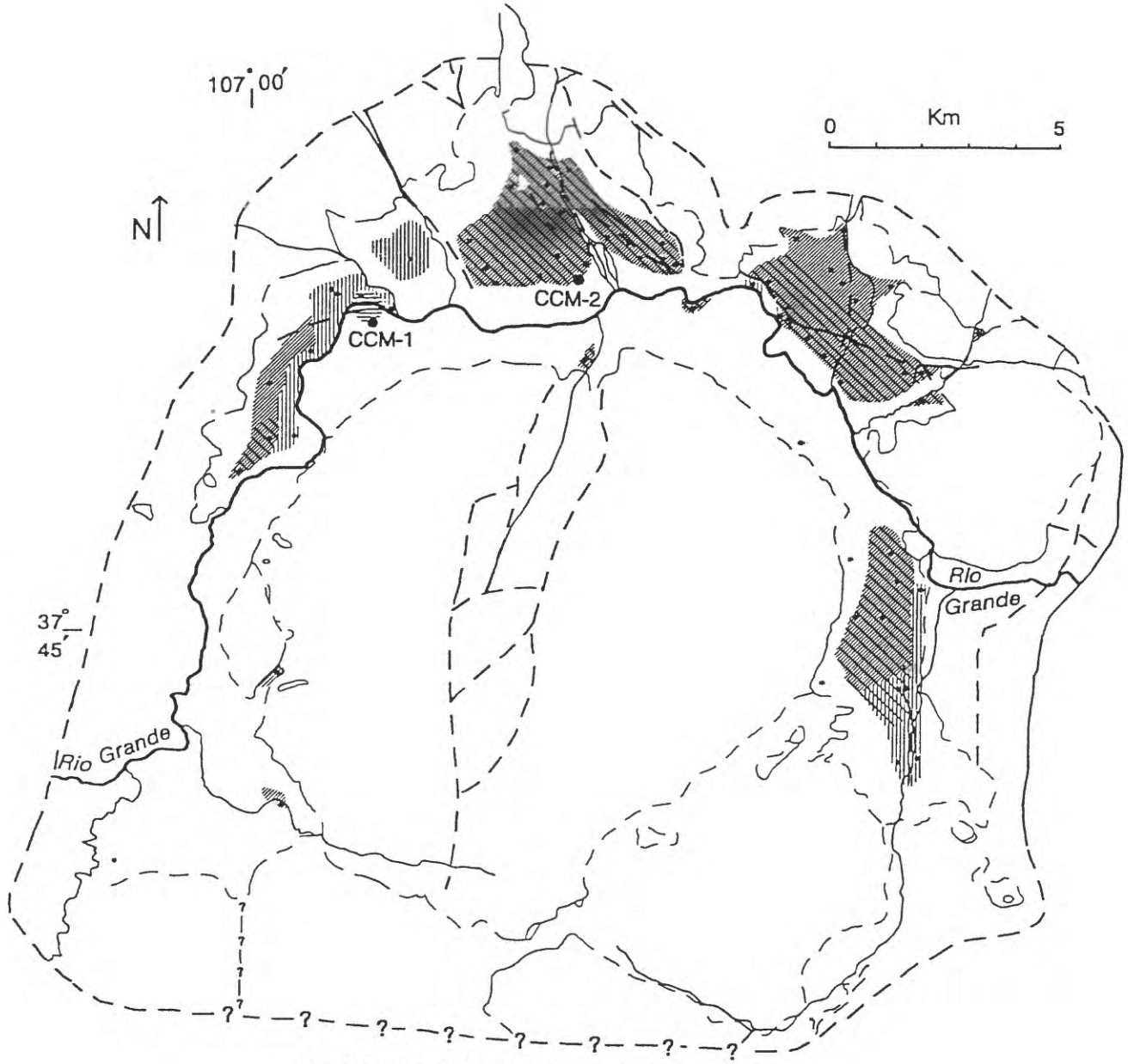
107° 00'
0 Km 5
N
CCM-2
CCM-1
Rio Grande
37° 45'
Rio Grande
Authigenic Mineral Associations
Volcanic glass-Smectite
Smectite-Potassium feldspar-Quartz-Clinoptilolite
Smectite-Clinoptilolite-Erionite
Cristobalite/Opal C-T-Illite-Potassium feldspar
Chlorite/Smectite ML clay-Chlorite-Analcime-Potassium feldspar-Quartz
fault contact, dashed where concealed.
sample location
geologic contact, dashed where concealed.

Figure 23

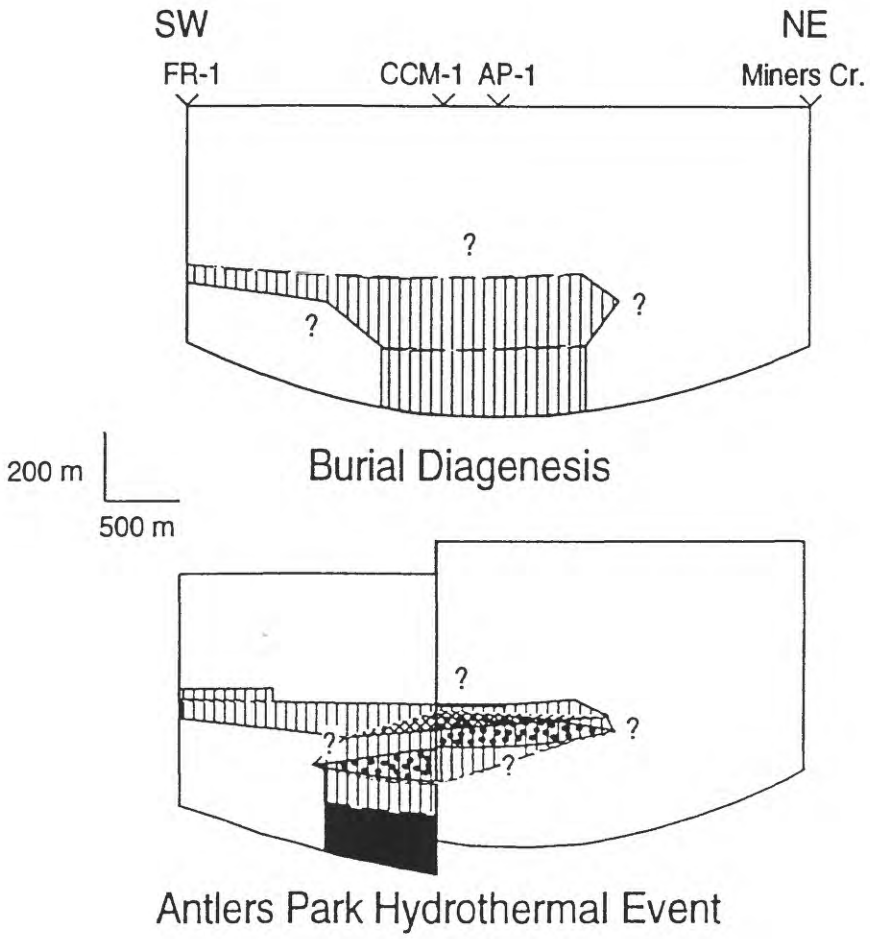
SW
NE
FR-1
CCM-1
AP-1
Miners Cr.
?
?
?
200 m
500 m
Burial Diagenesis
?
?
?
?
Antlers Park Hydrothermal Event
Smectite+Clinoptilolite+Erionite
Smectite-Kaolinite-Potassium feldspar-Quartz-Jarosite
Smectite-Potassium feldspar-Quartz-Clinoptilolite
Chlorite/Smectite ML clay-Chlorite-Analcime-Potassium feldspar-Quartz
Chlorite-Analcime-Potassium feldspar-Quartz
Sublacustrine Fan Deposits

Figure 24

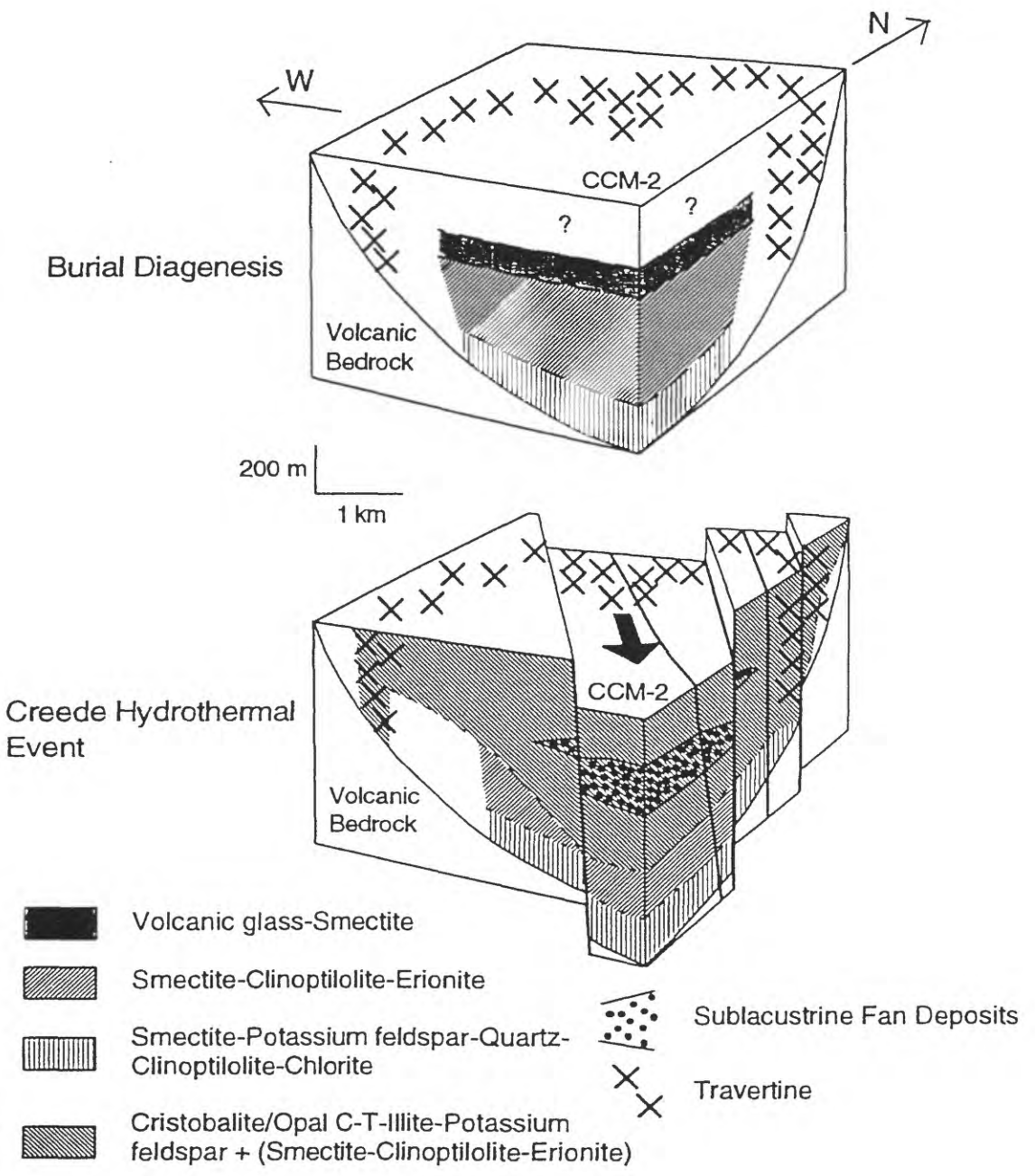
N
W
CCM-2
?
?
Burial Diagenesis
Volcanic
Bedrock
200 m
1 km
Creede Hydrothermal
Event
CCM-2
Volcanic
Bedrock
Volcanic glass-Smectite
Smectite-Clinoptilolite-Erionite
Smectite-Potassium feldspar-Quartz-
Clinoptilolite-Chlorite
Cristobalite/Opal C-T-Illite-Potassium
feldspar + (Smectite-Clinoptilolite-Erionite)
Sublacustrine Fan Deposits
Travertine

Figure 25